



TECHNISCHE  
UNIVERSITÄT  
WIEN  
Vienna University of Technology

## Master Thesis

# Characterization of Laser Scattering Detection System for Microfluidic 3D Cell Cultures

Submitted at the  
Institute for Technical Chemistry  
Vienna University of Technology

under the supervision of

Univ.Prof. Dipl.-Ing. Dr. Peter Ertl

by

Bilal Farooq  
Matriculation Number: 1242664

*To my*  
**Parents**

# Contents

<b>List of Figures</b> .....	<b>iv</b>
<b>List of Tables</b> .....	<b>viii</b>
<b>Acknowledgments</b> .....	<b>ix</b>
<b>Abstract</b> .....	<b>x</b>
<b>Kurzfassung</b> .....	<b>xi</b>
<b>1. Aim of Thesis</b> .....	<b>1</b>
<b>2. Introduction</b> .....	<b>2</b>
2.1 Tissue - As a Research and Diagnostic Tool .....	3
2.2 2D versus 3D - <i>In vitro</i> Models .....	5
2.3 Biosensors .....	12
2.4 Theory of Light Scattering .....	16
2.5 Light Scattering Detection .....	23
<b>3. Materials and Methods</b> .....	<b>26</b>
3.1 Light Scattering System .....	27
3.2 Microchip Fabrication .....	29
3.3 3D-Hydrogel Preparation .....	30
3.4 Preparation of Particles and Cells for Calibration.....	31
3.5 Cell Migration Assay .....	33
3.6 LS System Measurement and Data Generation.....	36
3.7 Statistical Analysis of LS System .....	37
<b>4. Results and Discussion</b> .....	<b>39</b>
4.1 Physical Characterization of Lab-on-a-Chip System .....	39
4.1.1 Calibration of Laser Power of LS System .....	39
4.1.2 Calibration of Temperature of LS System.....	41
4.1.3 Calibration of OPD Sensors of LS System .....	42
4.2 Preparation of Microchip .....	44
4.3 Performance Analysis of LS System .....	46
4.3.1 Ability to Determine Particle Size in LS.....	46
4.3.2 Influence of Particle Concentration in LS.....	49
4.3.3 Ability to Determine Particle Number in LS.....	53
4.3.4 Limit of Detection .....	56
4.3.5 Influence of Material Properties in LS .....	62
4.4 3D-Biosensing of 3D-Hydrogels using LS .....	64

4.5	3D-Biosensing of Dead Mouse Embryonic Fibroblasts with LS .....	68
4.6	3D-Biosensing of Dead Jurkat Cells with LS .....	70
4.7	Practical Application: Monitoring Cell Proliferation in Hydrogel.....	73
4.8	Practical Application: Monitoring Cell Migration in Hydrogel .....	76
<b>5.</b>	<b>Summary and Conclusion .....</b>	<b>79</b>
<b>6.</b>	<b>Bibliography.....</b>	<b>88</b>

## List of Figures

Figure 1: Schematic diagrams of (a) the 2D monolayer cell culture, (b) cell spheroids/aggregates grown on matrix, (c) cells embedded within matrix and (c) scaffold-free cell spheroids in suspension [29].	6
Figure 2: Effect of absorbance of water by polymer chains of hydrogels [39].	8
Figure 3: Hydrogel schematic microstructures based on the cross linking network, (a) an ideal cross-linked network representing tetra-functional network, (b) non-ideal cross linked network, (c) ideal cross-linked double network gel, (d) physically entangled network, (e) physical network with helix formation, (f) alginate like network with divalent $\text{Ca}^{+2}$ ions forming local bridges [38].	9
Figure 4: Direction of EM wave propagation perpendicular to electric and magnetic field [118].	18
Figure 5: Difference between (a) reflection, refraction, diffraction and (b) scattering phenomenon [121].	19
Figure 6: (a) Incident, scattered and transmitted intensities (b) scattering vector $q$ representation [122].	20
Figure 7: (a) A schematic of backward and forward scattering (b) Influence of backward and forward scattering in regime of Rayleigh and Mie scattering [125].	22
Figure 8: 488nm Laser system splitting into four channels by optical fibre cables	27
Figure 9: OPD layers with Indium-tin-oxide as bottom and Ca/Ag as top contact, PEDOT:PSS as hole conducting layer and rr-P3HT:PCBM as BHJ [192].	28
Figure 10: Workflow of laser scattering system	29
Figure 11: Chip preparation by mold.	29
Figure 12: Mould fabrication by using $\text{CO}_2$ Laser	30
Figure 13: Microfluidic chip preparation by hand cut design	30
Figure 14: Schematic of the steps involved in embedding cells in 3D-hydrogels.	33

Figure 15: Chip design for cell migration assay in hydrogel. ....	34
Figure 16: LS system equipped with 488nm laser source, detection station, shutter controller to operate laser and data collection equipment. ....	37
Figure 17: Characterization of (a) beam splitter and output power of laser, (b) laser power for the optical fibre light path.....	39
Figure 18: Temperature offset between water heating and chip heating system. ....	41
Figure 19: Characterization response of OPD's sensors without any illumination of light and with maximum illumination. ....	42
Figure 20: Microchip fabrication design.....	44
Figure 21: Schematic displaying characterisation of different particle sizes.....	46
Figure 22: Characterization curves of particles of (a) 46nm, (b) 794nm, (c) 5µm and (d) 10µm at different concentrations. The scattering effects were seen by varying the laser power from 7.5mW to 82.5mW.....	47
Figure 23: Characterization by utilizing concentrations of 125µg/mL, 250µg/mL, 500µg/mL and 1000µg/mL; particles of (a) 46nm, (b) 794nm, (c) 5µm and (d) 10µm were analysed at 7.5mW, 40mW and 82.5mW. The significance of the data was determined by using 2-way ANOVA test. * indicates significant difference of P<0.05, ** indicates significant difference of P<0.01 and *** indicates significant difference of P<0.001.....	50
Figure 25: OPD response by introducing (a) 1.25x10 <sup>5</sup> , (b) 2.5x10 <sup>5</sup> and (c) 5x10 <sup>5</sup> particles of 46nm, 794nm, 5µm and 10µm diameter in PBS (n = 3).....	53
Figure 26: Scattering behaviour of 1.25x10 <sup>5</sup> , 2.5x10 <sup>5</sup> and 5x10 <sup>5</sup> particles at (a) 7.5mW and (b) 82.5mW (n = 3).....	54
Figure 27: Scattering signal from 46nm, 794nm, 5µm and 10µm particles at 7.5mW, 40mW and 82.5mW. (a), (c), (e) and (g) represent curves with slopes and intercepts whereas (b), (d), (f) and (h) represent significance of number of particles with respect to zero number of particles. * indicates significant difference of P<0.05, ** indicates	

significant difference of $P < 0.01$ and *** indicates significant difference of $P < 0.001$ ( $n = 3$ ).....	58
Figure 28: Normalized OPD signal of (a) $5 \times 10^4$ and (b) $5 \times 10^5$ particles at powers 7.5mW, 40mW and 82.5mW. The signals were normalized according to the control group ( $n = 3$ ).....	60
Figure 29: Scattering behaviour of (a) amidine polystyrene latex and (b) sulfate polystyrene latex ( $n = 3$ ).....	62
Figure 30: Comparison of 60nm amidine polystyrene latex and sulfate polystyrene latex at power (a) 7.5mW and (b) 82.5mW ( $n = 3$ ). ....	63
Figure 31: Characterization of the scattering behaviour of 3D-hydrogels, matrigel, PEG-dextran and fibrin ( $n = 3$ ). ....	64
Figure 32: Scattering effects with $5 \times 10^5$ particles of 794nm diameter in matrigel, PEG-dextran and fibrin.....	65
Figure 33: Comparison between the scattering signal of $5 \times 10^5$ particles of diameter 794nm, hydrogels and similar particle in hydrogels at 82.5mW laser power .....	67
Figure 34: Difference between transparent, translucent and opaque materials. ....	67
Figure 35: Comparison of NIH-3T3 in PBS and hydrogels at three power levels .....	68
Figure 36: Scattering signals by embedding $1.25 \times 10^5$ , $2.5 \times 10^5$ and $5 \times 10^5$ Jurkat cells in (a) PEG-dextran and (b) matrigel. ** indicates significant difference of $P < 0.01$ and *** indicates significant difference of $P < 0.001$ . Indicated significance is in comparison to zero number of cells. ....	70
Figure 37: Comparison of scattering signal of NIH-3T3, Jurkat cells with particles of 794nm, $5 \mu\text{m}$ and $10 \mu\text{m}$ . ....	71
Figure 38: Normalised scattering response of 3000, 1500, 750 and 0 chondrocytes per $\mu\text{L}$ . The measurements were taken after injecting them into the microchips and then on 3 <sup>rd</sup> , 5 <sup>th</sup> and 7 <sup>th</sup> day ( $n = 3$ ). ....	74
Figure 39: Cell proliferation of 1500chondrocytes/ $\mu\text{L}$ in matrigel ( $n = 3$ ). ....	74

Figure 40: Microscopic images of Jurkat cells migration through 3% and 20% PEG-dextran. .... 77

Figure 41: Jurkat cell migration through 3% and 20% PEG-dextran hydrogel..... 78



## List of Tables

Table 1: Difference between 2D and 3D systems .....	6
Table 2: Some examples of physically and chemically cross linked hydrogels. ....	9
Table 3: Applications of matrigel, fibrin and polyethylene glycerol. ....	11
Table 4: Applications of optical detection methods in microfluidic systems.....	13
Table 5: Components utilized for manufacturing the LS detection system and for the characterization experiments. ....	27
Table 6: Specifications of particles utilized for characterization by concentration experiments.....	34
Table 7: Specification of particles and cells used in experiments. <sup>a</sup> represents volume of cell suspension before centrifugation and then re-suspended in a volume shown with <sup>b</sup> . ....	36
Table 8: Number of particles of 46nm, 794nm, 5 $\mu$ m and 10 $\mu$ m that can be significantly differentiated from a blank signal at 7.5mW, 40mW and 82.5mW. ....	57

## Acknowledgments

First of all, I am grateful to my supervisor Prof. Peter Ertl for his encouragement and providing me an opportunity to make this research work possible. Without his guidance and supervision, it would have been a difficult journey. Thanks to Mario Rothbauer, with whom I enjoyed the critical discussions very much. His forthcoming suggestions were always very fruitful.

Special thanks to Julie Rosser, Barbara Bachmann and Nejc Hren who introduced me to the cell culture at University of Veterinary Medicine, Vienna. Their help and advice enabled me to work with biological specimens.

I am grateful to Isabel Olmos Calvo for providing me the reagents for my experiments. I am really impressed by her helping attitude. Special thanks to Cristina Herráez Muñoz for a special discussion about understanding the system. Thanks is due to David Wartmann whose online conversation have always given me a new direction of research and encouraged me to think critically.

In the last, I would like to express my greatest gratitude to my whole family including my parents, wife and my siblings. Without their support and constant prayers this work wasn't possible.

## Abstract

Although lab-on-a-chip (LoC) enables the performance of experiments on a small scale using miniaturized devices, ability to detect dynamic cellular behaviour over long periods of time (e.g days or weeks) within 3D microenvironment is still in its infancy. The integration of optical detection techniques in microfluidic devices are often robust and sensitive for the assessment of cell cultures that are cultured in 3D environment. We have investigated, light scattering as a robust techniques capable of non-invasively and continuously determining cell morphology, proliferation, viability and migration of 3D cell cultures. Although light scattering has successfully been employed to study a variety of cellular responses of two-dimensional microfluidic cell cultures systems over recent years, its applications for 3D cell cultures systems has not been investigated in detail. 3D cell cultures system has the benefit that it mimics a suitable microenvironment for the growth of cells which usually reside in tissue surrounded by extracellular matrix. Their maturation into specialized cell types occurs in a more natural manner morphologically and physiologically compared to cells that are cultured in 2D cultures. In an attempt to show the potential benefit of laser scattering (LS) system for hydrogel-based microfluidic 3D cell culture analysis, the presented work investigates strengths, limitations and risk factors associated with the interpretation of data. Consequently, recently established, the LS system with the source wavelength of 488nm is characterized in detail by utilizing polystyrene particles of various sizes in PBS and in 3D-hydrogels. Additionally, LS is evaluated for cell culture analysis using mouse embryonic fibroblasts and Jurkat cells which are embedded in hydrogels. Results of the study revealed the feasibility of the LS system as reliable detection method for organ-on-a-chip applications. Practical application using chemotactic lymphocyte migration study revealed that LS is ideally suited to non-invasively and label free probe 3D-hydrogel based cell culture systems.

Keywords: Light Scattering, microparticles, nanoparticles, 3D-hydrogels, biosensor

## Kurzfassung

Obwohl Lab-on-a-Chip (LoC) die Durchführung von Experimenten im kleinen Maßstab unter Verwendung miniaturisierter Geräte ermöglicht, ist die Fähigkeit, dynamisches zelluläres Verhalten über lange Zeiträume (z. B. Tage oder Wochen) in der 3D-Mikroumgebung nachzuweisen, noch im Anfangsstadium. Die Integration optischer Detektionstechniken in mikrofluidische Geräte ist oft robust und empfindlich für die Bewertung von Zellkulturen, die in einer 3D-Umgebung kultiviert werden. Wir haben Lichtstreuung als robuste Techniken untersucht, die nicht-invasiv und kontinuierlich die Zellmorphologie, die Proliferation, die Lebensfähigkeit und die Migration von 3D-Zellkulturen bestimmen können. Obwohl Lichtstreuung in den letzten Jahren erfolgreich eingesetzt wurde, um eine Vielzahl von zellulären Reaktionen von 2-D mikrofluidischen Zellkultursystemen zu untersuchen, wurden ihre Anwendungen für 3D-Zellkultursysteme nicht im Detail untersucht. 3D-Zellkultursystem hat den Vorteil, dass es eine geeignete Mikroumgebung für das Wachstum von Zellen nachahmt, die sich gewöhnlich im Gewebe befinden, und von einer extrazellulären Matrix umgeben sind. In einem Versuch, den potenziellen Nutzen des Laserstreuensystems (LS) für die mikrofluidische 3D-Zellkulturanalyse auf Hydrogelbasis zu untersuchen, die vorliegende Arbeit die mit der Interpretation der Daten verbundenen Stärken, Einschränkungen und Risikofaktoren abzuschätzen. Infolgedessen wurde das LS-System mit der Quellenwellenlänge von 488nm durch die Verwendung von Polystyrolpartikeln verschiedener Größen in PBS und in 3D-Hydrogelen charakterisiert. Zusätzlich wird LS für die Zellkulturanalyse unter Verwendung von embryonalen Fibroblasten der Maus und Jurkat-Zellen, die in Hydrogele eingebettet sind, ausgewertet. Die Ergebnisse der Studie zeigten die Durchführbarkeit des LS-Systems als zuverlässiges Nachweisverfahren für Organ-on-a-Chip-Anwendungen. Die chemotaktische Lymphozytenmigrationsstudie ergab, dass LS gut für nicht-invasive und label-free 3D-Hydrogel-basierende Zellkultursysteme geeignet ist.

Schlüsselwörter: Lichtstreuung, Mikropartikel, Nanopartikel, 3D-Hydrogele, Biosensor

## **1. Aim of Thesis**

The 3D cell culture system has an advantageous factor as it closely mimics the physiological niche of the organ. In order to determine the behaviour of cells in 3D environment, cell analysis tools need to measure continuously, be non-invasive and label-free to detect cell-to-cell and cell-to-matrix interactions and the dynamic cellular responses. Therefore, optical detection technique is a novel tool to analyse 3D cellular activities. Consequently, the aim of this study was to optimize an optical biosensor that could be sensitive enough to determine the morphology, viability, proliferation and migration of cells cultured in 3D environment and determine the efficacy of the LS system. In order to address these tasks, particles and cells were exploited and LS system was characterized by varying different parameters such as size, concentration, material and 3D hydrogels in which they were embedded.

## 2. Introduction

Microfluidics is an interdisciplinary field of science that links engineering, chemistry and natural science. A common feature of all microfluidic devices is the microscaled channel network to utilize fluid dynamics on microscale that handles the liquid volume in micro, nano or pico range. Miniaturization shortens the time of experiment, requires low volume, minimizes the laboratory space consumption, gives efficient portability or wearability and is always cost effective [1]. In the early 1990s, the semiconductor micromachining paved the way for several microfluidic structures, so-called micro electro mechanical system (MEMS), including microvalves and micropumps for the purpose of precise handling of delicate sample volumes [2]. This in fact provided a platform for the development of micro-Total Analysis System ( $\mu$ -TAS), often also referred to as “Lab-on-a-chip systems” (LOC) that implements the analytical techniques on silicon and glass based microstructures for flow injection analysis [3, 4]. This technology enables the integration of one or several analysis systems on a single chip for chemical detection and utilization in biomedical, food, environment fields [5, 6] and fabrication of nanostructures especially in human diagnostics [7, 8]. The development of organ-on-a-chip systems may also replace clinical phase of human trials to predict efficacies of novel drugs. Among existing cell based *in vitro* methods, organ-on-a-chip has made a name for itself very rapidly. This state-of-the-art system mimics the structure and functionality of human organs without the need of using animal models [9]. This was basically introduced to replace animal studies for drug and toxicity testing. It successfully replicates the human physiology with the help of little micro engineered devices containing living cell types from various human organs and thus reconstitute the organ level functions [10]. Researchers can alter the chemical properties of the medium in which the organ cells are embedded in a chip and can also influence the forces involved in the fluid flow [11, 12]. So it has a better potential to mimic a human organ situation in a more refined way and is more predictive and practical as compared to an animal model [13]. This technology will not only help reduce and refine current research methods, but will also accelerate the research process, thereby delivering quicker results, enabling researchers to bring therapies to the patients in shorter amount of time by

omitting animal testing. The aim of this technology is to fabricate tissue artificially in the lab that closely mimics the natural environment, but the tissue of an organ is composed of mass of cells which are arranged in a specific configuration. To fabricate a tissue in laboratory has always been a quest of tissue engineers. In tissue engineering, a number of compatible techniques have been integrated with biomaterials to facilitate the fabrication of cell material composites. To date, different models have been developed that successfully explained the importance of 3D scaffolds for tissue engineering implants. However, multiple questions arise with the progress and improvement of the tissue-engineered constructs, which need to be answered. This is either done by *in vivo* testing or by creating *ex vivo* models which consume a large number of cells and other material which is mostly limited and unrealistic, giving results which are only one dimensional. Organs are made up of multiple cell types which are surrounded by supporting structures, microscale technology enables the mimicking of the natural structure and functionality of the whole organ on a microscopic level. Reconstructing the natural state on miniature level has the benefit of controlling the cellular microenvironment and offering cell-based and downstream assays for advanced applications [14].

## **2.1 Tissue - As a Research and Diagnostic Tool**

In the human body, cells are grouped together in a highly organised manner creating tissue, this in turn is sorted according to specific structure and function forming organs. Tissues makes our body, from bones to organ like heart and brain, even blood is considered a tissue. Apart from fulfilling functions inside the body, tissue extracted from donors can help save lives of recipients. Blood transfusion is one of the examples of life saving therapeutic uses of human tissue [15]. Red blood cells (RBC), white cells (WBC) and platelets are the main ingredients of blood that circulate in the plasma fluid [16]. Plasma also contains nutrients and proteins along with protective antibodies and promoting or inhibiting factors for blood clotting such as Factor VIII are used in the treatment of haemophilia [17] and albumin helps in the treatment of burn patients [18]. RBCs along with frozen plasma are used to replace lost blood. Freshly separated platelets are used for the treatment of leukaemias [19]. Research has proven that fetal nerve cells secrete neurotransmitter dopamine, which

could potential cure patients suffering from Parkinson's disease can be cured after transplantation, as they have a deficiency of the neurotransmitter dopamine [20]. Several symptoms of Down's syndrome and cystic fibrosis can be treated with the cells isolated from blood, bone marrow, amniotic fluid and chorionic villi [21, 22]. Apart from saving lives, different kinds of tissue can be isolated from patients or healthy donors to not only study the fundamental structure and function of various cell types in tissues, but to also find out about pathologies, to determine the correct therapy. Among non-therapeutic applications, tissues can help to develop forensic reports for the detection of crimes. Post-mortem reports of tissues enable the examiners to describe that either the cause of death was unnatural, natural, or violent [23].

Hence, human tissue has a number of applications in discoveries and developments of diagnostics and medicines. These may also be cultured to establish an analysis of the chromosomes or DNA for diagnostic purposes. Isolated tissues can be exposed and tested to the potential drug intended to be tested and before introduced commercially. So studies of tissues and of isolated cells have great importance in determining the fate of a newly introduced medicine and its toxicity on tissues, before the drug is tried on healthy volunteers [24]. To be able to culture tissues and cells outside the human body, it is important to understand the requirements of the biological material to be able to receive authentic data and prevent false results due to the change in cell structure and function due to extracorporeal cultivation.

Tissues and organs with different 3D structure require support to design a similar tissue from cells. The support is termed as scaffold, template or artificial ECM [25]. Biomaterials technology has a potential to mimic tissues *in vitro* that aims to partially eliminate *in vivo* testing. Viability, migration, growth, differentiation and apoptosis of cells in tissues can be controlled by controlling the cellular environment which may be comprised of many ECM [26]. ECM is an important feature of connective tissues that usually facilitates the cells by providing them a structural support. ECM generally includes the interstitial matrix which is always present between the cells and the basement membranes (BM) which are sheet-like scaffold and comprises proteoglycans, fibronectin, laminin and collagen IV [27]. The physical and chemical



features associated with BM help the cells to differentiate and self-recognize. Therefore, ECM contributes in providing support to the tissues, regulate intercellular communication and help them in segregation from one another. When the cells are isolated from the tissue, natural or synthetic ECM provides them a 3D natural environment that mimics the natural environment of the tissue [28].

## 2.2 2D versus 3D - *In vitro* Models

Recently developed 3D cell culture systems provided remarkable evidences, in contrast to the 2D culture systems and showed the actual microenvironment for the cells where they reside in tissues. Therefore, to develop *in vitro* cell-based system that can faithfully mimic the *in vivo* cell environment is more realistic to embed cells in an artificial 3D ECM. In drug discovery processes, cell-based assays are considered to be simple, fast, and cost-effective tools. [29]. In *in vivo* environment, cells experience a 3D environment as they are surrounded by other cells and different types of ECM, however 2D cell culture does not take into account the natural 3D environment of cells [30] and it may give misleading and non-predictive data [31]. 2D cell cultures have proven their importance and value in cell-based studies however, due to the monolayer of cells cultured on flat and rigid substrates, its limitations have to be taken into account while interpreting results its restrictions have been recognized so far. Cells in the 3D cultured system have different morphology and physiology from cells cultured in the 2D environment [32]. This additional dimension not only influences the structure of the cells but it also induces some physical constraints on the cells [33]. Due to the physical and spatial changes in 3D environment, signal transduction from the outside to inside of the cells is also affected which ultimately influences the gene expression and cellular behaviour.

In nephrotoxicology, the comparison between 2D and 3D models was studied by Romero et al. [34]. In order to observe the toxic effects of several drugs such as cisplatin, gentamicin and doxorubicin, NKI-2 cells, a proximal tubular cell line was immersed in matrigel and compared with a 2D cultured model. The results produced by the NKI-2 cells showed better expression of functional markers and were more sensitive to the nephrotoxicants. Effects of increasing drug, metabolism and toxicity

factors because of enhanced epithelial characteristics were shown by DesRochers in [35] by comparing 2D and 3D cultures. It was concluded from the experiments that the sensitivity of the 3D model due to repeated dosing, drug-induced toxicity was enhanced unlike the 2D model.

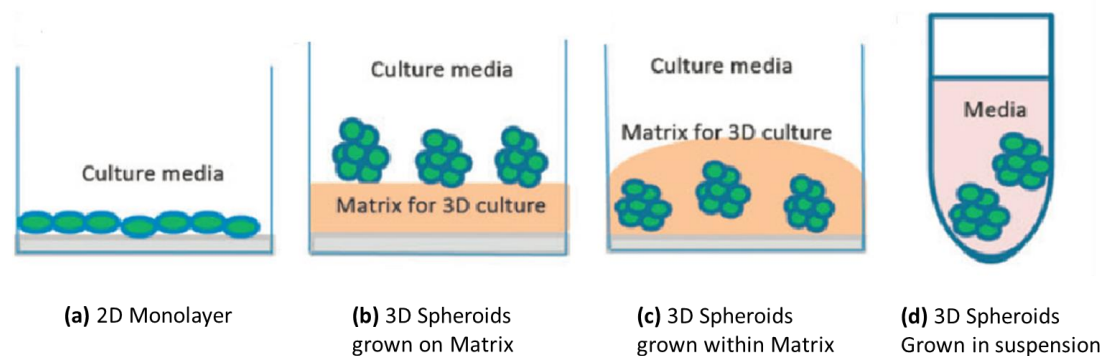


Figure 1: Schematic diagrams of (a) the 2D monolayer cell culture, (b) cell spheroids/aggregates grown on matrix, (c) cells embedded within matrix and (c) scaffold-free cell spheroids in suspension [29].

2D Cell Culture System	3D Cell Culture System
Cell-to-cell interaction is on edges only, mostly in contact with the bottom surface	Philological cell-to cell interaction
Contact with ECM is mostly on the surface	Cells interact with ECM
No gradient is present	Diffusion gradient of drugs, oxygen, nutrients and wastes
Co-culture is unstable to establish a microenvironment	Co-culture of multiple cell mimics the microenvironment
Anti-cancer drug resistance is not observed	Shows resistance to anti-cancer drug as <i>in vivo</i> tumor
More cells are likely to be in the same stage of cell cycle due to being equally exposed to the medium	Spheroids contain proliferating, quiescent, hypoxic and necrotic cells

Table 1: Difference between 2D and 3D systems.

Although, 2D cell-based models have made a good contribution in understanding the concepts of drug handling and its toxicity, 3D cell cultured systems shown in Figure 1 are exhibiting a promising contribution in biomedical applications such as drug discovery due to refined cell-cell structures, cell-ECM interactions and constructing structures that closely resemble the natural architecture of *in vivo* tissues. Therefore, the objective of 3D *in vitro* technology is to establish robust, simple, inexpensive and portable models that could be commercialized. In contrast to 2D cell culture where the cells generate adherent 2D monolayer, 3D cell culture has a benefit to mimic their original environment more naturally and the cells grow in complex 3D microenvironment [36]. Hydrogels among the other candidates of tissue engineered scaffolds have received a huge attention by scientists for the purpose of mimicking 3D cultures. Hydrogels are widely used for cell cultured system and tissue-engineering techniques due to their favourable hydration and nutrient transport properties. Hydrophilic gels having simple or complex 3D network of polymer chains are referred to as hydrogel and water acts as a dispersion medium [37]. When one or more monomers react then a water swollen gel is formed which is in fact a cross linkage of polymer chains and these chains remain insoluble in water because of the complex cross linkage of polymer network [38]. A volume swelling coefficient,  $Q$  of hydrogels is defined as

$$Q = \frac{V_{Swollen}}{V_{Dry}} \quad 2.1$$

where  $V_{Swollen}$  is the volume of polymers in swollen state and  $V_{Dry}$  is the volume of polymers without imbibing the water. The swelling coefficient of hydrogel is an important factor that explains the mechanical and transport properties of the hydrogel. The swelling coefficient varies widely based on the polymer chemistry of the hydrogel. It is also related to the polymer volume fraction in the swollen state i.e.

$V_{Swollen}$

$$V_{Swollen} = \frac{V_{Polymer}}{V_{Polymer} + V_{Water,Initial} + V_{Water,Imbibed}} \quad 2.2$$

From the above relation it is clear that there are two contributions to the overall water content. First one is the initial volume of water in the system and the other is the additional volume of water which is imbibed during the swelling phase. As the cross linking density increases, mesh size of polymer chains decreases and swelling ratio also decreases.

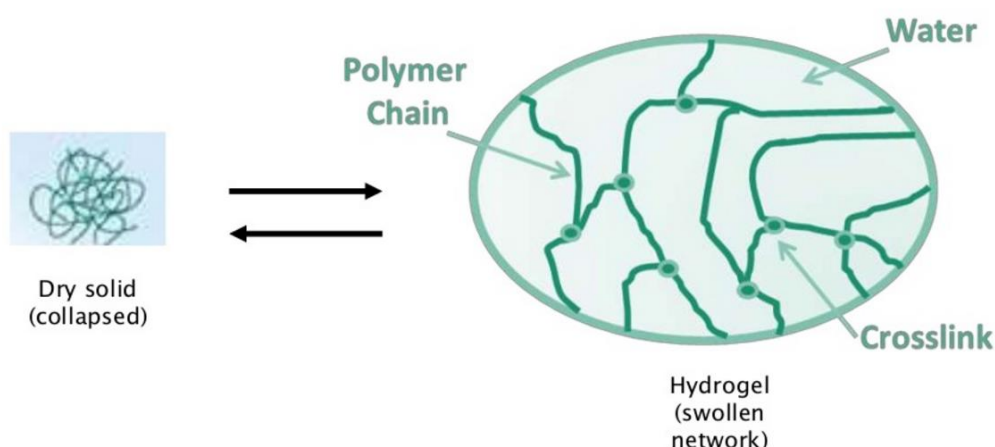


Figure 2: Effect of absorbance of water by polymer chains of hydrogels [39].

The Newtonian behaviour is exhibited by the polymers which are slightly soluble in water and there is no complex entanglement between polymer chains but as the cross linker is introduced, a linkage developed between polymeric chains and the network becomes viscoelastic or it shows completely elastic behaviour [40]. The cross linking network can be introduced either by physical or by chemical means. In chemically cross linked network, polymer chains are bonded by covalent bonds whereas, in physically cross linked networks, physical interactions exist. Hence, chemically cross linked hydrogels are relatively immobile compared to physically cross linked gels. Some examples of physically and chemically cross linked network of hydrogels are shown in Table 2.

Physically Cross Linked Hydrogels	Chemically Cross Linked Hydrogels
Cross linking by hydrogen bonding [41]	Cross linking by high energy radiation [42]
Cross linking by amphiphilic graft and block polymers [43]	Cross linking by condensation reaction [44]
Cross linking by ionic interaction [45]	Cross linking by free radical polymerization [41]
Cross linking by crystallization [46]	Cross linking using enzymes [47]
Cross linking by protein interactions [48]	Cross linking with aldehydes [49]

Table 2: Some examples of physically and chemically cross linked hydrogels.

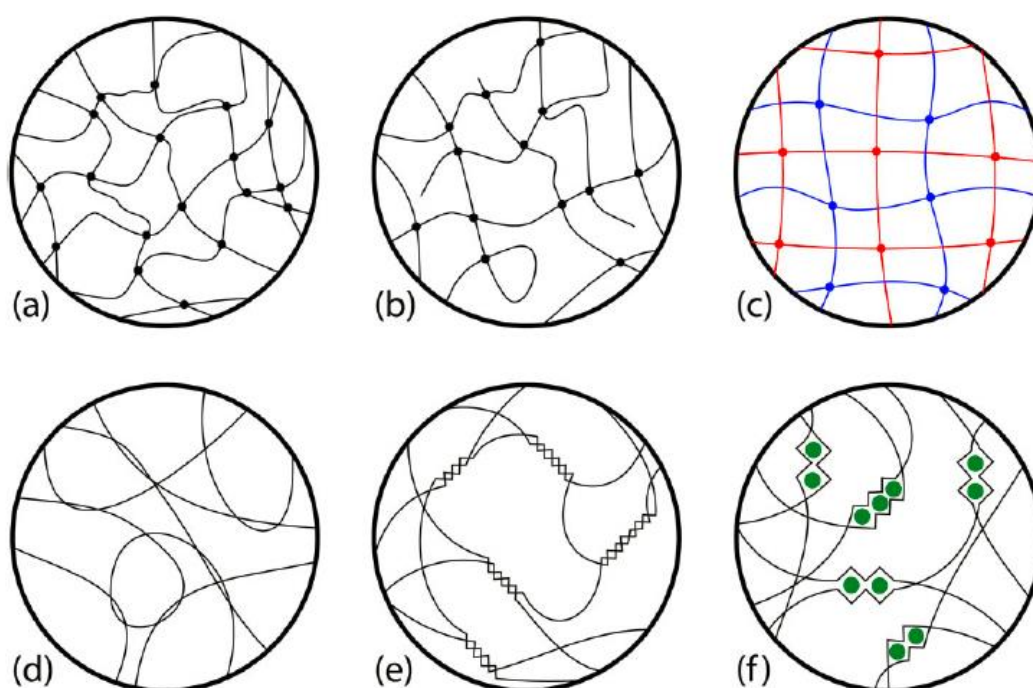


Figure 3: Hydrogel schematic microstructures based on the cross linking network, (a) an ideal cross-linked network representing tetra-functional network, (b) non-ideal cross linked network, (c) ideal cross-linked double network gel, (d) physically entangled network, (e) physical network with helix formation, (f) alginate like network with divalent  $\text{Ca}^{+2}$  ions forming local bridges [38].

Hydrogels can either be naturally occurring like collagen, fibrin and matrigel or they can also be synthetic such as polyethylene glycol (PEG) [50]. However, synthetic hydrogels are widely used as compared to natural hydrogels due to their high strength, water absorptive capacity, dependence on pH value, stable against sharp temperature variations and a well-defined duration. In synthetic hydrogels there is a possibility of modification of the polymer chains which governs that its biocompatibility, biodegradability and functionality can be controlled [51]. By introducing a variation in chemical composition or in any synthesis factor like crosslinking method or agent and synthesis method or condition, a biomaterial can be modified. Lability is synthetically introduced in the hydrogels that helps in biodegradation and the instability between the networks can be removed by hydrolysis releasing the cells for further analysis [52]. Synthetization can either be a single step process or it can be a multistep process [53]. Polymerization is an example of single step process however among the multistep synthetic processes, cross linking by crystallization, ionic interaction [45], antigen-antibody interaction [54] or by proteins interaction are the important examples.

Since the proliferation of a variety of cells are supported by ECM, matrigel is a natural hydrogels that acts as an ECM which is a mixture of proteins that are extracted from Englebreth-Holm-Swarm tumour cells in mice [55, 56]. Matrigel regulates the differentiation of various cell lines and is used to check tumour cell's invasive activity [57]. Endothelial cell's proliferation in matrigel and forming capillary like structure with lumen has been studied by Kubota et al. [58]. Fibrin gel is also a good choice for microenvironment as it naturally self-assembles into a scaffold in the last step of the blood coagulation cascade, where the enzyme thrombin becomes activated which converts plasma protein fibrinogen into fibrin clot. It acts like a cement and stops the blood flowing out of the body and creates cell binding sites for cell attachment which facilitates tissue regeneration [59]. Fibrin can be adapted during wound healing by interfering in the gelation time by changing the concentration of thrombin and fibrinogen [60]. Lower concentration of thrombin produces thick fibres in the clots with few branch points and having large pores. Fibrin gel has viscoelastic properties and, therefore serves as an effective scaffold

for cartilage [61], nervous and cardiovascular tissue engineering [62]. Chondrocytes injected with fibrin gel in the forehead and interocular areas of rabbits showed successful regeneration of damaged cartilage tissue [63]. For applications of drug delivery, PEG-based synthetic hydrogels can be characterized by their biocompatibility, solubility and lack of toxic influence [64]. Being stimulus sensitive, PEG drug release system reacts as a physical, chemical or biological agent [65]. Hydrogels having such properties of drug release systems are known as “smart” or “intelligent gels”. Physical stimulus can be temperature variation, light or acoustic factors, pressure, magnetic or electrical field, whereas the chemical and biological stimulus may include pH changes, specific ions, and molecular recognition events [66]. Out of these, chemically cross-linked PEG hydrogels are utilised in the manufacturing of synthetically and biologically active hydrogel scaffolds for functional tissue production.

<b>Matrigel</b>	<b>Fibrin</b>	<b>PEG</b>
Low concentration of gel enhances the development of human blastocyst and hatching <i>in vivo</i> [67].	Fibrin sealants are the most effective and degradable tissue adhesives [68].	Release of lysozyme from PEG/PBT by controlling the copolymer composition [69]
Formation of human cancer cell lines as xenografts model [70].	Injecting mixtures of bone marrow cells and fibrin into infarcted myocardium enhanced the formation of neovascularization [71].	Promising features as drug carriers for colon-specific drug delivery [72].
When biopsy sample of human colon carcinoma, was dispersed and coinjected with matrigel, growth of tumor enhanced [73].	Fibrin as a cell carrying microbeads show good viability of the cells [74].	Hydrogel based scaffolds enhances the angiogenic responses and helps in skin regeneration in burn cases [75].

Table 3: Applications of matrigel, fibrin and polyethylene glycerol.

Since hydrogels have 3D polymers that can swell by absorbing water and without dissolving in it, it resembles a biological tissue [38]. These characteristics are ideal to embed cells in them and use different detection system to analyse their structure, function and interaction with the ECM. The swelling behaviour of the polymer chains the detection, whatever detection technology is used. Number of detection schemes have been introduced to examine the cellular response in 3D microenvironment. For the detection of various metabolites in body, hydrogel-based biosensors were implemented by Li et al. [76]. Hydrogel-based biosensors and various other types are widely exploited in pharmaceutical industry, medical research and healthcare fields.

### **2.3 Biosensors**

Since the 3D microenvironment provided to the cells mimics the natural environment of the cells in which they can proliferate and remain viable. However, in order to detect their growth, their metabolic activities, some tools are required to get a complete insight through their continuous measurements. Several techniques and methods have been exploited to develop a remarkable system termed as biosensor, which can be used to detect the cellular physiological parameters such as metabolism, pharmaceutical effects, extracellular potentials, environmental toxicity effects and medical diagnostics etc. [77, 78]. The qualities which are supposed to found in an ideal biosensor includes fast detection time, its compact size, low power consumption, minimal amount of sample, low cost fabrication and potential for realizing multiplex analysis [79]. Researchers have always been interested in developing innovative analytical devices having enhanced sensitivity and specificity. In recent development of biosensing systems, this technique has already made its contribution. Various biosensing techniques ensured their success after the development of first optical biosensor [80]. The optical detection methods which have been applied in microfluidic biosensors include absorbance [81], fluorescence [82], chemiluminescence [83] and LS biosensors [84]. Some of the detection systems coupled with optical devices are shown in Table 4.



<b>Optical Detection</b>	<b>Coupling Technique</b>	<b>Assay Type</b>	<b>Reference</b>
Fluorescence	Inorganic photodiode	Competitive aptamer assay	[85]
Fluorescence	CMOS image sensor	Microscopy	[86]
Chemiluminescence	Inorganic photodiode	HRP luminol reactions	[87]
Chemiluminescence	Microplate reader	Capillary immunoassay	[83]
Absorbance	CMOS image sensor	Colorimetric enzyme assay	[88]
Absorbance	Visual without sensor	Colorimetric enzyme assay	[81]
Laser Induced Fluorescence	Microscope based PMT detector set up	Assay based on DNA analyte	[89]
Laser Induced Fluorescence	Optical fibres, lens, PMT detector set up	Assay based on fluorescein, rhodamine	[90]
Light Scattering	OPD, notch filter, impedance electric signal	T cells stimulation and cytotoxicity assay	[91]
Light Scattering	OPD, notch filter, impedance electric signal, electrode arrays	Cell based assay and cytotoxicity screening	[92]

Table 4: Applications of optical detection methods in microfluidic systems.

Optical detection techniques have made their mark in the field of biosensors in which optical devices like microscopes, charged coupled devices (CCD), photomultiplier tubes (PMTs) or lasers can be coupled to lab-on-a-chip (LoC) system but their miniaturization would not be cost effective and it is difficult to make them a portable detection devices. Grenville has fabricated a planar optical biosensors by making a comparison with the available biosensors incorporated with optical fibres and filter [93]. Optical detection systems can be categorised into off-chip and on-chip approaches [94]. In off-chip approach the macro scale detection devices are large enough and coupled to micro size detection areas by means of pinholes to focus the area. This approach leads to high optical losses and minimises the signal-to-noise ratio (SNR) [95]. Having a large detection system that may include CCDs or PMTs also limits the portability of the microfluidic system. However, the incorporation of LEDs and photodiodes in the detection system are a good choice in miniaturizing technique of LoC. Photodiodes utilized in optical biosensors are vulnerable at high temperatures, however apart from their minor complication they are surely advantageous in the long run [96]. Among photodiodes, OPD offers high sensitivity for detection systems and it minimizes the optical loss. Efficiency of OPD detection is based on the collection efficiency of photons which in turn depends on the efficiency of photosensors that offers low dark currents and high quantum efficiency. Integrating LEDs and OPDs, Bürgi et al., developed a sensor on a single substrate [97]. Hence, OPDs compared to other detection technologies have the best potential for biosensor miniaturization as they can be easily fabricated and are cost effective.

Based on optical sensing methods, recent trend of biological cell-based assays has provided new opportunities for label-free technologies to get information on the phenotypic changes of 3D cell culture systems [98]. The aim of establishing optical biosensors is to provide a non-invasive and label-free technology by exploiting microchip technology for generating bio-relevant data. LS detection has long been exploited in flow cytometry as the gold standard for the label-free analysis of cell suspensions. By using the concepts of forward and side scattering, characteristics of cells that are irradiated by a laser beam provide information for cell size and their structural complexity, such as the internal granularity of cells [99]. Since biological

tissues have higher refractive index compared to air and are optically inhomogeneous and due to the inhomogeneous behaviour of tissue, light interaction phenomenon like refraction, partial reflection and scattering at the air-tissue interface occurs [100]. Hence, propagation of light through a biological tissue largely depends on the scattering and absorption properties of its constituents and their structures. Therefore, tissue anisotropy like size, shape, material, density and refractive index plays a vital role in tissue-light interaction. One of the two tissue models are generally used to describe its behaviour in the presence of light [101]. In the first model it is considered as a medium having continuous random spatial distribution whereas, in the second case it is modelled as a discrete ensemble of scatterers. LS based model, optical coherence tomography (OCT) was utilized by Golnaz et al., on mouse cells to get insights of bladder carcinoma tumors [102]. By observing significant difference between speckle decorrelation times (DT) between tumorous and surrounding normal tissue, chemotherapy was exploited on the tumorous tissues. The same group also studied the variations in intracellular motion by inducing apoptosis in acute myeloid leukemia cells [103]. In order to judge the quality of human embryonic stem cell colonies, scattering signals were analysed and concluded that light scattering technique provides 87% better identification response compared to conventional methods [104]. Bacterial colony structures were also studied to find out the bacterial growth morphology by forward scattering patterns because forward scattering phenomenon provides a tool to determine the size [105]. Mammalian cells properties were also investigated by LS and the size and volume of organelles were analysed by Mourant et al. [106]. Hence, LS detection technique has a benefit that the optical components used in developing such systems seem ideal, with the benefit of non-contact, fast response, compactness, high sensitivity and multiplex operation possibility [107]. These are assembled into compact detectors to develop a portable instrumentation based on microfluidic devices [108]. However, any type of system that is being newly developed for cell viability and morphology measurement needs to be characterized first and particles or particles of various sizes and shapes provide a good choice for the characterization of such devices as they resemble cells [109-111]. Availability of various particle sizes and shapes enable the system to characterize the devices more precisely. For

measurement of particle sizes, there are basically three methods [112-114] to check the size of particles in a solution. Such methods include:

1. Ensemble methods e.g. ultrasonic attenuation spectroscopy and light scattering
2. Counter methods e.g. electrozone counting and microscopic counting
3. Separation methods e.g. capillary hydrodynamic fractionation or differential and sedimentation

All the above mentioned methods have their own specification however, ensemble methods are comparatively simple and data collection rate is faster than other methods. Its non-destructive testing makes it more suitable and applicable than others as the samples can be recovered after testing [115]. Among ensemble methods, photon correlation spectroscopy has an advantage of detecting mixture of different particles if they are embedded in a medium of known viscosity. This method needs a very small amount of sample and it can detect an extremely small size of a sample. Back scattering spectroscopy is another example of ensemble method with a benefit of its application in samples of higher concentrations. Hence, light based detection techniques are relatively reliable compared to other methods.

To characterize the LS system for determining scattering response from cell proliferation, physical concepts of light interaction with matter are also necessary to understand. The next section deals with the theory of light scattering and the factors on which it depends.

## **2.4 Theory of Light Scattering**

Prior to understand the LS, nature of light, its interaction with matter and various phenomenon associated with light needs to be clear. Basically, light is an electromagnetic wave as it propagates through a medium without showing any physical displacements. This propagation is due to the perpendicular oscillations of electric and magnetic fields and the wave travel orthogonal to both of these fields [116]. Light does not carry any charge and therefore, does not require any medium for its propagation. In case of propagating through a medium, its direction is effected by the refractive index of that material. Such type of waves show variation in the

wavelength which includes radio waves, microwaves, infrared radiation, visible, UV radiations and X-rays. The propagation of electromagnetic waves through time and space, carrying energy and momentum can be explained by Maxwell's equations [117]. The aim of these equations is to explain how electric field (E-field) and magnetic field (B-field) propagates, interacts, and how they are affected by objects. These equations basically describe the rules that govern the behaviour of E and B-fields. According to these equations, flow of electric current generates B-field and if the current varies with time the B-field will also produce an E-field. These equations also explains that the separated charge either positive or negative, generates an E-field and if it varies in time, it gives rise to a propagating E-field which further generates a propagating B-field. Maxwell's equations in case of vacuum can be easily derived from the set of equations in dielectric medium, as in vacuum the charge density  $\rho$  and current density  $J$  are set to zero. In general, Maxwell's equations in dielectric medium are given as

$$\begin{aligned}
 \nabla \cdot D' &= \rho \\
 \nabla \cdot B &= 0 \\
 \nabla \times E &= - \frac{\partial B}{\partial t} \\
 \nabla \times H &= J + \frac{\partial D'}{\partial t}
 \end{aligned}
 \tag{2.3}$$

where, symbol  $\nabla$  (pronounced 'del') interprets how a quantity varies in space,  $E$  and  $B$  are electric and magnetic fields whereas  $D'$  is the electric field and  $H$  is the magnetic field inside the dielectric, which can be written as

$$\begin{aligned}
 D' &= \epsilon_0 E + p \\
 B &= \mu_0 H + M
 \end{aligned}
 \tag{2.4}$$

where  $\epsilon_0$  is the permittivity  $\mu_0$  is the permeability of free space.  $p$  is the polarization and  $M$  is the magnetization of the medium, these are important parameters to describe the propagation of light through the medium. The Maxwell's equations are a set of coupled differential equation which shows that the electric field and magnetic field components vary from each other and are dependent on current and charge

density as well. In order to decouple Maxwell's equations for solving the involved variables independently and by assuming that the electromagnetic wave is travelling through a homogeneous medium, wave equations for electric field vector  $E$  and magnetic field vector  $H$  can be written as

$$\begin{aligned}\nabla^2 E - \epsilon\mu \frac{\partial^2 E}{\partial t^2} &= 0 \\ \nabla^2 H - \epsilon\mu \frac{\partial^2 H}{\partial t^2} &= 0\end{aligned}\tag{2.5}$$

where  $\epsilon$  is the permittivity and  $\mu$  the permeability of dielectric and  $c$  the speed of light in vacuum. The above mentioned equations describe the wave propagation with velocity

$$v = \frac{c}{n}\tag{2.6}$$

where  $n$  is the refractive index of the material equal to  $\sqrt{\epsilon\mu}$ .

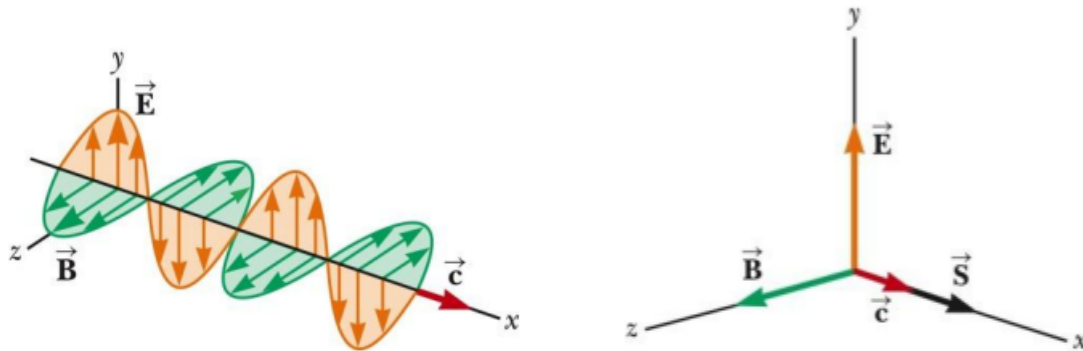


Figure 4: Direction of EM wave propagation perpendicular to electric and magnetic field [118].

Hence, when a beam of light propagates with a velocity  $c$ , it may reflect back or refract through a medium however, besides reflection and refraction, diffraction and scattering are the important phenomenon exhibited by light due to its interaction with matter. Diffraction is a wave phenomenon which can only be observed when the wavelength of light is comparable to the size of the obstacle. Diffraction is regarded

as a slight bending from the edges of an object which means bending depends on the relative size of the wavelength of light to the size of an opening. If the opening size is larger than the wavelength of light, the diffraction would be unnoticeable whereas considerable diffraction can be observed if the opening size is equal or smaller than the light's wavelength [119]. However, scattering can be observed if light behaves as a particle. In scattering there is an alteration in the scattered angle and the intensity of light after striking with the medium that might be due to the combined effect of refraction, reflection and diffraction but there would be an absence of absorption. The wavelength of the scattered wave changes but the wavelength of reflected wave does not change. When the particles get finer then scattering is used as a tool to determine their size characterization.

Static light scattering (SLS) technique determines particle size extracted from intensity characteristics depending upon various scattering angles. One or more detectors are implemented to measure the intensity at one or more angles. It can be used to determine the molecular weight, radius of gyration, form or structure factor. However, dynamic light scattering (DLS) also known as quasi-elastic light scattering is a non-invasive technique for determining the size and distribution of particles [120]. Particle size is determined by correlating random changes in the light intensity.

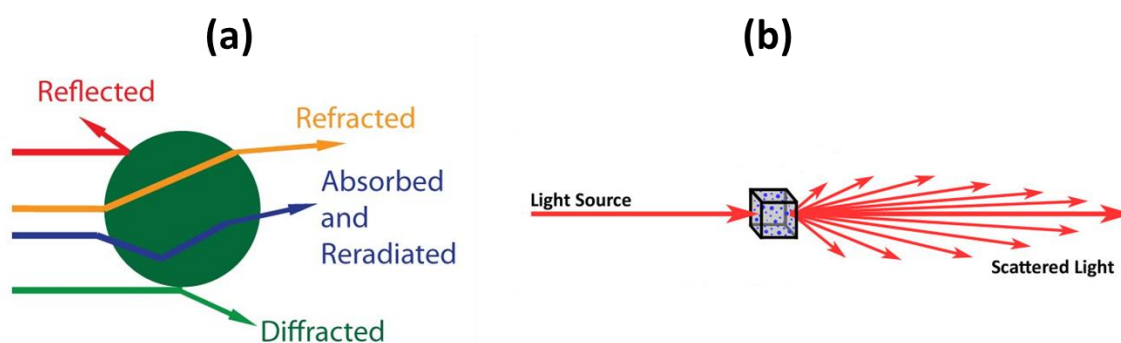


Figure 5: Difference between (a) reflection, refraction, diffraction and (b) scattering phenomenon [121].

Therefore, LS is one of the important technique to characterize molecules, cells, aerosols or colloids by either determining the molecular weight of molecules or by analysing the particles size and their distributions. By utilizing this technique we can also figure out the size and shape of aggregates and the properties of dilute polymer solutions. The scattered light intensity depends on the size, concentration, refractive index of the material of particles and their polarizability. Other factors include angle of scattering, solvent and solute interactions and the wavelength of incident light.

The scattered intensity determined as a function of scattering angle  $\Theta$  and the momentum transferred by the scattered light is given by a scattering vector  $\vec{q}$ . The magnitude of the scattering vector is defined as

$$q^2 = |k_i - k_s|^2 \quad 2.7$$

If the interactions are elastic then  $k_i = k_s$  i.e.

$$\vec{q} = \frac{4\pi n}{\lambda_s} \sin\left(\frac{\Theta}{2}\right) \quad 2.8$$

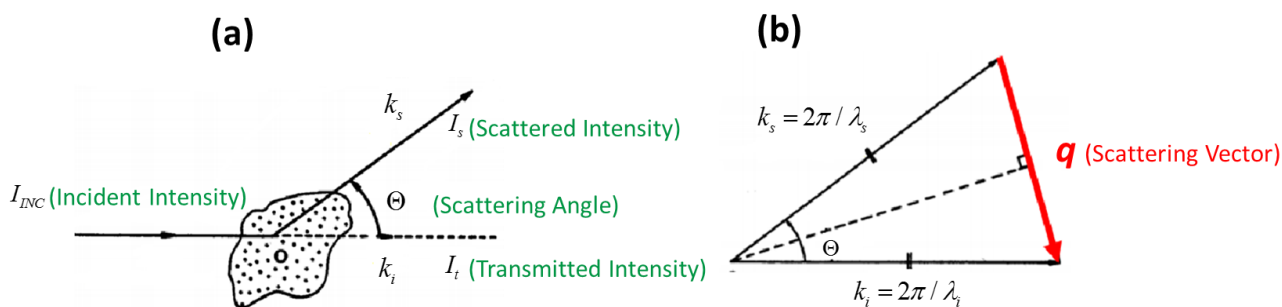


Figure 6: (a) Incident, scattered and transmitted intensities (b) scattering vector  $q$  representation [122].

Scattering can be categorized into three main domains [123],

- i) Rayleigh scattering where  $\pi D / \lambda \ll 1$  (particle size is  $1/10^{\text{th}}$  of wavelength),
- ii) Mie scattering where  $\pi D / \lambda \approx 1$  (valid only for spheres) and



iii) Geometric scattering where  $\pi D / \lambda \gg 1$

where  $D = 2r$  is the diameter of particle and  $\lambda$  is the wavelength of incident light. Dealing with Rayleigh scattering is preferred to avoid the complex formulations involved in Mie scattering. Mie theory depends on the relative refractive index = refractive index of a particle/refractive index of a medium. Therefore, one needs to determine the refractive index of material of the particle. In case of complex composition of particle, the effective refractive index needs to be determined. Mie theory provides the information about the scattered electromagnetic field at all points of the particle and at all points of the medium in which the particles are embedded. Hence, complex composition of the particle demands to encounter the complex part of refractive index as well. If  $n$  is the refractive index of the scattering particle then its representation in terms of its complex part is defined as

$$m = n - in^* \quad 2.9$$

where  $n$  is defined as the speed of light in vacuum divided by the speed of light in the material of the particle, whereas the complex part of above relation  $n^*$  is linked to the absorption. The relationship between absorption coefficient  $\alpha$  and the complex part of refractive index  $n^*$  of the material is

$$\alpha = \frac{4\pi n^*}{\lambda} \quad 2.10$$

The value of  $n^*$  can never be exactly zero for any material. As considered in Rayleigh scattering that the particle size is sufficiently small (i.e.  $1/10^{\text{th}}$  of the wavelength) as compared to incident wave so the particle encounters a uniform electric field at any moment, whereas the time for penetration and absorption of the electric field is much less than the period of oscillation of the electromagnetic wave. Hence, Rayleigh scattering is considered as scattering without absorption and the polarizability can only be expressed as a real refractive index. Scattering phase function [124] is a term used to define the energy scattered per unit solid angle in a given direction to the average energy in all directions. The phase function that describes the dependence of the scattered beam by explaining the angular distribution of light intensity is given as

$$\frac{1}{4\pi} \int_{\Omega} P(\cos \Theta) d\Omega = 1 \tag{2.11}$$

where  $\Omega$  is the solid angle and  $\cos \Theta = \theta \cdot \theta'$  describes the relation between angle of incidence  $\theta$  and the angle of observation  $\theta'$  with  $\Theta$  being a scattering angle. For the preferred direction of scattering either forward or backward scattering, a function named asymmetry factor  $g'$  is defined in terms of scattering phase function

$$g' = \frac{1}{2} \int_{-1}^1 P(\cos \Theta) \cos \Theta d(\cos \Theta) \tag{2.12}$$

The value of  $g'$  ranges for -1 to +1 for backward to forward scattering respectively and for isotropic scattering  $P(\cos \Theta) = 1$ , in which the scattering events are evenly distributed that makes  $g' = 0$ . If the scattering angle  $\Theta < \pi/2$  then this referred to as forward scattering and  $g' > 0$ , whereas for backward scattering  $\Theta > \pi/2$  which implies  $g' < 0$ .

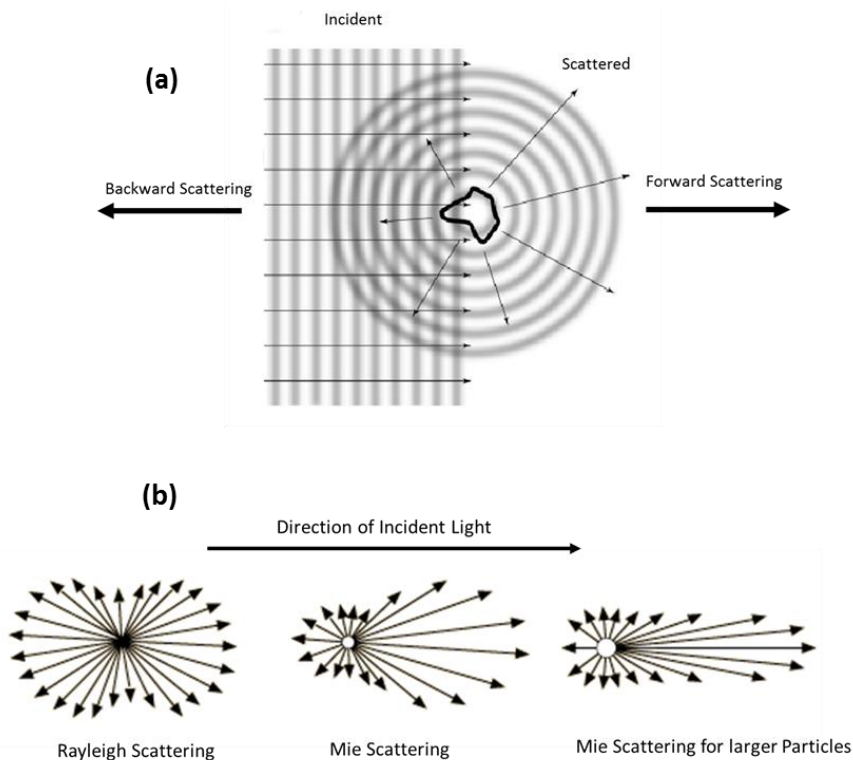


Figure 7: (a) A schematic of backward and forward scattering (b) Influence of backward and forward scattering in regime of Rayleigh and Mie scattering [125].

Since matter is composed of discrete electric charges like electrons and protons that oscillate when light is incident with matter. As discussed above, Maxwell's equations were employed to describe the electromagnetic wave propagation through a material. Particle size, geometry, material, refractive index of the surrounding medium and intensity of incident light are the major factors that affects the scattering of light while propagating through a medium. Mie scattering particularly explains the scattering affects due to structural and morphological features of the interacting constituents. Since its discovery in 1908, the Mie theory has become the main characterization tool for particle-induced scattering [126, 127]. Mie theory can also be incorporated to investigate the fundamental physical concepts of electromagnetic waves [128] and to calculate the radiation forces on particles which are considered to be important in optical manipulations [129]. Therefore, despite all its complex formulation, Mie scattering remains a trustworthy and reliable model that is applicable to a wide range of particle sizes.

## **2.5 Light Scattering Detection**

In order to build a real self-contained miniaturised LS detection system, it is ultimately required to have highly integrated components that give a benefit of reduction in detection volumes and decreasing the number of analytes available for detection. Components involved in developing LS detection systems seem ideal, with the benefits of non-contact, fast response, compactness, high sensitivity and multiplex operation possibility. For implementation of above concepts of Rayleigh and Mei scattering there must be a detection system that can determine the size, composition, number and the movement of particles in a given medium with high precision and sensitivity. Such system obviously depends on the efficiency of light source and the detectors used. Researchers have been developed the devices based on LS which can be widely used in chemical, biological diagnosis and biomedical analysis. There are two main factors on which the LS detection method for microfluidic devices depends which are sensitivity and scalability to smaller dimensions [92]. There is a developing interest to couple and integrate LS components into microfluidic devices. The optical components used in these detectors are mainly light emitting diodes (LEDs) or laser diodes as light sources,

optical fibres, gradient refractive index lenses, diffractive elements and OPDs. These are assembled into compact detectors to develop a portable instrumentation based on microfluidic devices [108].

Laser as a light source has remarkable contributions in medical and military fields as well. Since the invention of the laser in the early 1960s, it has been used as a powerful tool for medical, surgical, research, therapeutic and diagnostic purposes. To get maximum advantage of this valuable invention with the highest margin of safety it is necessary to understand how the light influences the characteristics of the living cells [130, 131]. However, for secure propagation of light there must be a channel that can transmit the laser beam with maximum efficiency. Optical fibres act like waveguides that are constructed from some kind of glass but are flexible. Due to the low propagation losses, the optical intensity can be achieved over long lengths of fibre. A focused beam of the laser travelling through optical fibre behaves as an extremely sharp scalpel in medical applications [132]. For long range transmission, they are utilized for secure data transfer [133]. Large amount of data can be transferred securely. Subsequently, after transmission, the main goal is the detection of light to get a final conclusion. For precise sensing OPDs provide a good choice for LS detection because of their low processing temperature and fabrication with glass or plastic that offers more flexibility and compatibility. Generally, OPDs convert the light into an electric signal and are the most advanced field of research. They often work at a negative bias and due to which an internal field becomes higher than the built-in field that boost up the response speed and photosensitivity as well. The signal becomes higher with increased negative bias and the dark current or leakage current also enhances however low leakage current is in favour of reducing noise and optimal OPD performance. By optimization of the morphology of the active layer and by using a suitable electron or hole blocking layer, the leakage current can be minimized [134]. The growing field of LoC demands smaller OPDs that make on-chip integration possible.

In modern LoC devices, LS based system was exploited by Charwat et al. [91] for label-free cell analysis that contained embedded interdigital electrode structures (IDES) and OPD array. The system was able for the continuous and non-invasive

monitoring of 3D co-cultured cell system. From the co-cultured assay they also showed the metastatic invasion of T-cells by integrating sensors. The same group utilized LS system to study a cell based assay for the identification of subgroupings of a cell suspension with single cell resolution [92]. Therefore, the novel application of LS includes the study of adherent 3D cell culture systems that provides information about cytotoxicity, cell linkage and numbers to cell adhesion by comparing cellular granularity. In conclusion, LS detection study is a novel technology for the continuous, non-invasive and label free monitoring of adherent and non-adherent cells to get a complete insight of cell dynamics, cell-to-cell and cell-to-matrix interactions.

### 3. Materials and Methods

This chapter describes the materials and techniques that were used in characterizing the LS system and to make it functional for measuring cell morphology and viability.

Component	Company	Cat. No.	Component	Company	Cat. No.
Sapphire 488-75	Coherent GmbH	LDP.1116054.091969	46nm	Kisker Biotech	GK809W
Fibre Coupler	Thorlabs	FC488-50B-FC	794nm	Kisker Biotech	GK893W
Beam Splitter	Thorlabs	BS010	5 $\mu$ m	Kisker Biotech	GK1810801-42
Kinematic Mirror Mount	Thorlabs	KM100	10 $\mu$ m	Kisker Biotech	GK2891301-08
Notch Filter	Melles Griot	Specifications of 03FIN-series	60nm Amidine	Invitrogen	1111730
OPD	Siemens	Siemens Design	60nm Sulfate	Invitrogen	545541
Collimator	Thorlabs	F240SMA-A	NIH-3T3 Cells	ATCC	CRL-1658
Optical Beam Shutter	Thorlabs	SH05	Jurkat Cells	ATCC	E6-1
Reflective Filter	Thorlabs	ND10A	Chondrocytes	Isolated from Horse	Isolated from Horse
Shutter Controller	Thorlab	SC10	HAM's F12	Lonza	LONBE12-615F
Power Supply	Coherent GmbH	1105375	FCS	Sigma Aldrich	F7524-500ML
Laser Head	Coherent GmbH	J4-T0	L-Glutamin	Biochrom	K 0302
Thermal Bath	Julabo	HL-4	Penstrep	Sigma Aldrich	P4333-100ML
Fibrin	Baxter	1503794	Amphotericin B	Biochrom	A 2612
Matrigel	Corning	354234	Trypan Blue	Sigma	93595
PEG-Dextran	Cellendes	G90-1	SYLGARD 184 Silicone Elastomer Kit	Sigma Aldrich	761028-5EA
PBS Dulbecco w/o Ca <sup>2+</sup> and Mg <sup>2+</sup>	Biochrom	L 1820	Plasma Treater	Corona	BD-20AC

Trypsin	Biochrom	L 2143	Biopsy Punch	Stiefel	2153 15E07
RPMI	Lonza	BE12-702F	HEPES	Gibco	15630
Hoechst 33342	Thermofisher	H1399	Neubauer Chamber	Marienfeld	0640710

Table 5: Components utilized for manufacturing the LS detection system and for the characterization experiments.

### 3.1 Light Scattering System

The laser used for light scattering was Sapphire laser with visible wavelength of 488nm and a power ranges from 7.5mW to 82.5mW (coherent). The laser beam from the source was split into two parts by a 50/50 beam splitter and each of the two beams was then further split into two parts by polarization beam splitter (PBS) with the use of optical fibres which transmit the laser beam to the detection station.

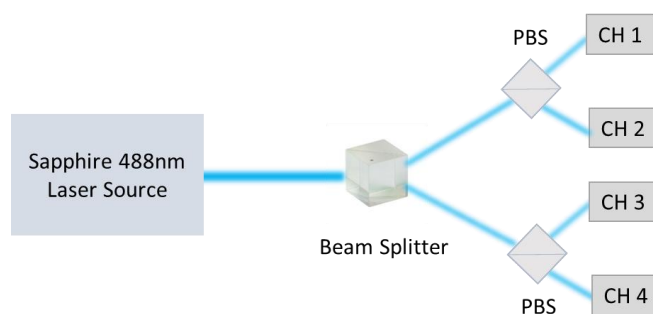


Figure 8: 488nm Laser system splitting into four channels

The detection station was equipped with an OPD having four sensors. A notch filter located above the OPD allowed the specific angled rays to pass through it, which registered a signal. The OPD and notch filter were adjusted with a metallic plate which was equipped with a thermal or heating bath (Julabo) that maintained the

temperature of the plate at  $37 \pm 0.5$  °C by setting the temperature of the thermal bath at 43°C. The microchips were placed inside a chamber of the metallic plate above the notch filter. The scattering signals from particles or cells were detected by the OPD. Generally, PDs convert the light into an electric signal. Stack of OPD layers include indium-tin-oxide (ITO) and semi-transparent Ca/Ag as a bottom and a top contact layer, respectively. Xylene solution of regioregular poly(3-hexylthiophene) (rr-P3HT) and [6,6]-phenyl C61 butyric acid methyl ester (P3HT:PCBM) was also applied on the bulk heterojunction (BHJ) layer by spraying and Poly(3,4-ethylenedioxythiophene) poly(styrenesulfonate) (PEDOT:PSS) was used as a hole conductor layer which also improved the reproducibility of the OPD characteristics [135].

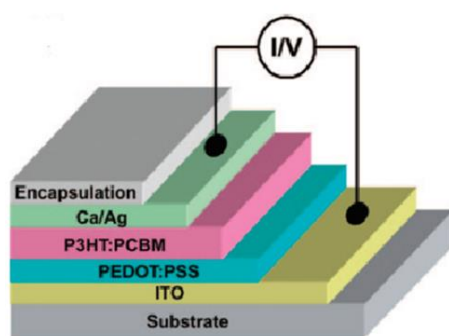


Figure 9: OPD layers with Indium-tin-oxide as bottom and Ca/Ag as top contact, PEDOT:PSS as hole conducting layer and rr-P3HT:PCBM as BHJ [192].

The Sapphire laser emitted a light beam at a wavelength of 488nm laser, iterating at 50msec and the illumination interval was controlled by a shutter controller. Detection of the scattering signals occurred through OPD sensors, which converted the light signal into an electric signal. The electrical signals produced in the form of potential difference and the whole LS system, including iteration time, were regulated by the LabView software. At the iteration of 50msec, the system stored the collected data in an Excel file which was then analysed by GraphPad Prism, version 5.01.



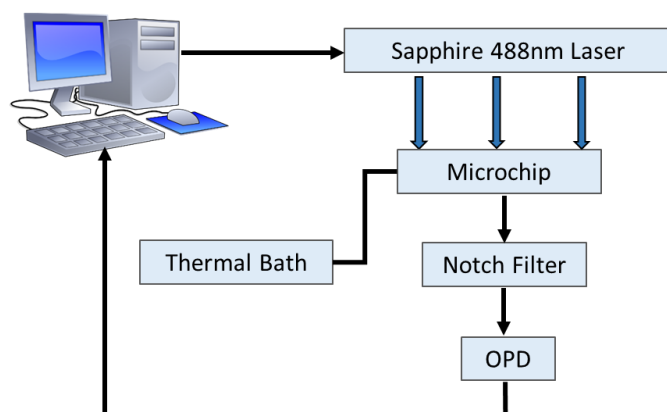


Figure 10: Workflow of laser scattering system

### 3.2 Microchip Fabrication

A 3D printed mold was utilized by designing on AutoCAD-7 with dimensions shown in Figure 11. In order to make a microchip, the silicone elastomer curing agent (PDMS) was diluted in silicone elastomer 1:10 (SLYGARD) and set it in the mold for 1-2 hrs in a mini incubator (VWR INCU-Line) at 70°C. After setting, PDMS was removed manually from the 3D printed mold to be used.

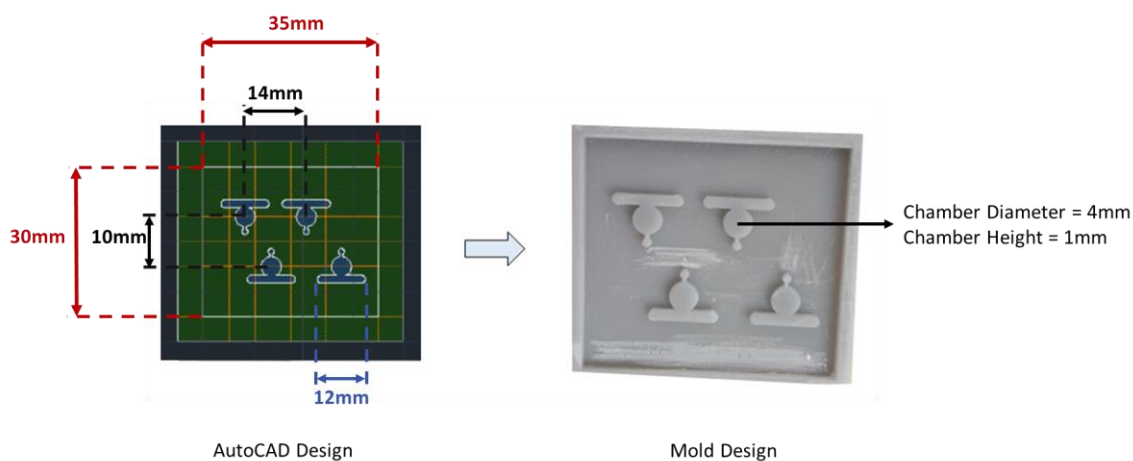


Figure 11: Chip preparation by mold.

**Chip Preparation by CO<sub>2</sub> Laser:** The chamber and the fluidic channel were made by applying a CO<sub>2</sub> laser (Speedy300-Trotec) having a wavelength of 10.6μm. A

cardboard sheet was irradiated with the laser to cut the particular designs, which were then glued onto a petri dish to make a mould for setting the PDMS layer.

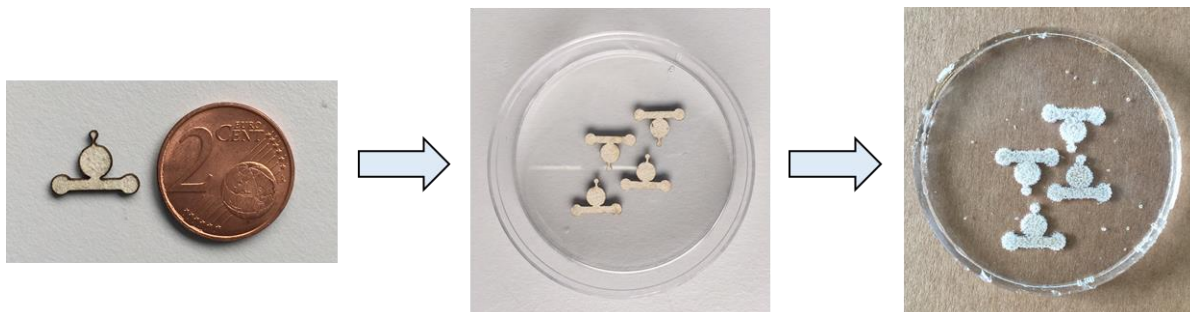


Figure 12: Mould fabrication by using CO<sub>2</sub>

**Chip Preparation by Hand Cut Design:** The PDMS layer was set in a 10cm petri dish till it hardened, after which the designs were cut out with a scalpel and biopsy punches having diameters of 4mm and 2mm were made. The PDMS layer was bonded between two plane glass slides, one of which had pre-drilled holes that were used as inlets for the cell/particles in hydrogel/PBS and cell culture medium.

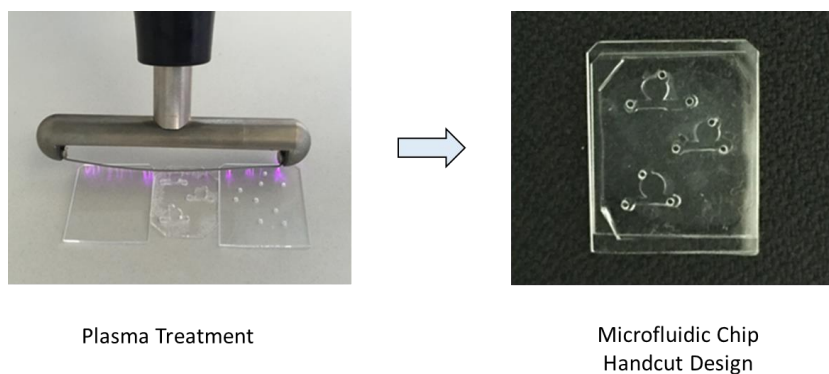


Figure 13: Microfluidic chip preparation by hand cut design

### 3.3 3D-Hydrogel Preparation

Three types of hydrogels including matrigel, fibrin and PEG-dextran were prepared according to the following protocols.

**Matrigel:** To prepare a clot of 18 $\mu$ L of matrigel (Corning, 354234), 12 $\mu$ L of matrigel was mixed with 6 $\mu$ L of medium.

**Fibrin:** The fibrin kit (Baxter, 1503794) contained thrombin of a concentration of 50U/mL, CaCl<sub>2</sub> of a concentration of 40mM and fibrinogen of a concentration of 100mg/mL. To prepare a clot of 18 $\mu$ L of fibrin gel, 0.9 $\mu$ L of thrombin was mixed in 8.1 $\mu$ L of CaCl<sub>2</sub>. 5.4 $\mu$ L of medium was added in fibrinogen and this solution was mixed with the thrombin and CaCl<sub>2</sub> solution.

**PEG-Dextran:** The PEG-dextran kit (Cellendes, G90-1) contained maleimide-dextran of a concentration of 30mmol/L, PEG-link of a concentration of 20mmol/L, thioglycerol of a concentration of 20mmol/L, 10x conjugate buffer (pH 7.2 and 5.5) and water. To prepare a clot of 18 $\mu$ L of PEG-dextran, 1.5 $\mu$ L of conjugate buffer, 0.9 $\mu$ L of water, 3 $\mu$ L of maleimide, 6 $\mu$ L of thioglycerol were mixed with 3 $\mu$ L of medium in an eppi. 3.6 $\mu$ L of PEG-link was introduced at the end that immediately polymerised the PEG gel.

### 3.4 Preparation of Particles and Cells for Calibration

Particles or cell suspensions shown in Table 6 and Table 7 were prepared according to the following protocols and then applied to the microchips for measurement.

**Particles Suspension Preparation:** The volume of particle solutions shown in Table 6 with concentrations of 125 $\mu$ g/mL, 250 $\mu$ g/mL, 500 $\mu$ g/mL and 1000 $\mu$ g/mL were re-suspended in PBS for the characterization of LS system by concentration of particles. As varying particle sizes were tested, it meant that at a constant concentration, the number of particles in a fixed volume of PBS would vary according to the size of the particles. Knowing the stock concentration, volume and diameter of each particle, the particle number was calculated with the following formula,

$$\text{Number of Particles} = \frac{\text{Total Volume of Particles}}{\text{Volume of One Particle}} \quad 3.1$$

The volumes having suspension of 1 $\times 10^6$ , 5 $\times 10^5$ , 2.5 $\times 10^5$  and 1.25 $\times 10^5$  particles in PBS shown in Table 7 were introduced into the microchips and then into the LS

system for the characterization of particles by number and material as well as to find out the limit of detection of the LS system with particle size.

**Particles Suspended in Hydrogels:** The volume of particles were mixed in three hydrogels according to the volumes shown in the Table 7, and introduced into the microchips and then into the LS system for the characterization experiments.

**Cells Suspension Preparation:** Subsequently, to characterize the LS system with cells, dead mouse embryonic fibroblast cells, NIH-3T3 (ATCC) of volume shown in Table 7, were re-suspended in PBS Dulbecco w/o  $\text{Ca}^{+2}$  and  $\text{Mg}^{+2}$  (Biochrom) with low endotoxin at a cell concentrations of  $27 \times 10^6$  cells/mL whereas a cell concentrations of  $27 \times 10^6$  cells/mL,  $13.8 \times 10^6$  cells/mL and  $6.9 \times 10^6$  cells/mL of dead Jurkat cells were mixed in PBS according to the volumes shown in Table 7. These suspensions were pipetted into microchips through the drilled holes and then introduced into the LS system for the characterization of the system and to find out the scattering signal.

**Cells Suspended in Hydrogels:** Dead NIH-3T3, mouse embryonic fibroblasts were re-suspended in matrigel or PEG-dextran according to the volume mentioned in Table 7 at a cell concentration of  $27 \times 10^6$  cells/mL, whereas a cell concentrations of  $27 \times 10^6$  cells/mL,  $13.8 \times 10^6$  cells/mL and  $6.9 \times 10^6$  cells/mL of dead Jurkat cells were mixed in  $18 \mu\text{L}$  of both hydrogels.

Living chondrocytes were also re-suspended in matrigel. For the cultivation of the chondrocytes, a cell concentration of  $6.25 \times 10^4$  cells/mL were seeded in a T25 flask in HAM's F12 (Lonza) medium supplemented with 10% FCS (Sigma Aldrich), 1% L-Glutamine (Biochrom), 1% Penstrep (Sigma Aldrich) and 1% Amphotericin B (Biochrom). The medium was changed on every second day until they reached a confluency of approximately 90%. Adherent cells were trypsinized for 3min at  $37^\circ\text{C}$  and then medium was added to inactivate the trypsinization. The harvested cells were washed and re-suspended in PBS and then centrifuged for 5min at 1500 rpm. After removing the supernatant,  $10 \mu\text{L}$  of cells suspension was mixed with  $10 \mu\text{L}$  of Trypan blue (Sigma) and counted using a digital counter (nexcelom). Following the cell count, the chondrocytes were re-suspended in matrigel in following concentrations

750cells/ $\mu\text{L}$ , 1500cells/ $\mu\text{L}$  and 3000cells/ $\mu\text{L}$ , prior to being pipetted into the microchips through the drilled holes and introduced into the LS system for the characterization of the system.

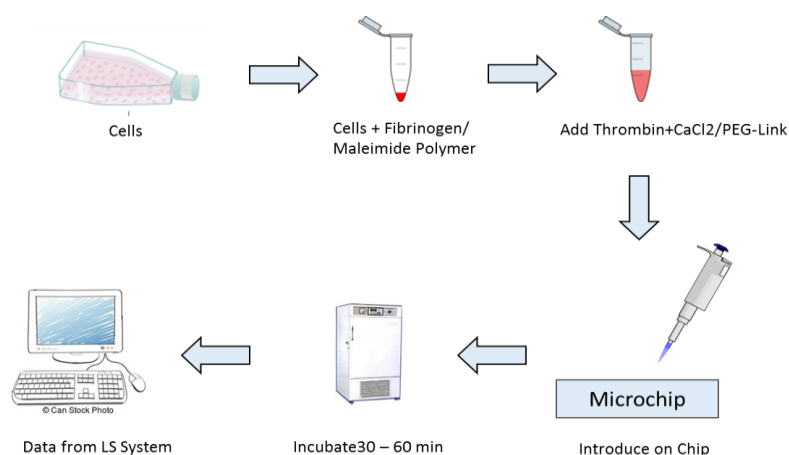


Figure 14: Schematic of the steps involved in embedding cells in 3D-hydrogels.

### 3.5 Cell Migration Assay

For preparation of starvation medium, RPMI-1640 medium (Lonza) is supplemented with 1% Penstrep (Sigma Aldrich) and 1% Hepes buffer (Gibco), whereas for preparing full medium, 10% of FCS (Sigma Aldrich), is added in the starvation medium. To prepare a clot of 12 $\mu\text{L}$  of 3% PEG-dextran (Cellendes), 0.6 $\mu\text{L}$  of water was mixed with 1 $\mu\text{L}$  of conjugate buffer, 2 $\mu\text{L}$  of melaimide, 4 $\mu\text{L}$  of thiolglycerol and 2 $\mu\text{L}$  of starvation medium and then 2.4 $\mu\text{L}$  of PEG link was introduced in it. However, to prepare a clot of 12 $\mu\text{L}$  of 20% PEG-dextran, 0.6 $\mu\text{L}$  of water was mixed with 1 $\mu\text{L}$  of conjugate buffer, 3.09 $\mu\text{L}$  of melaimide, 4 $\mu\text{L}$  of thiolglycerol and 3.09 $\mu\text{L}$  of starvation medium and then 0.216 $\mu\text{L}$  of PEG link was introduced in it.

12 $\mu\text{L}$  of hydrogel was introduced in the middle chamber, 15 $\mu\text{L}$  of cell suspension with concentration of 1000cells/ $\mu\text{L}$  stained with Hoechst-33342 (Thermofisher) by a ratio 1 $\mu\text{L}$  in 1mL of cell suspension is introduced in the left chamber and 15 $\mu\text{L}$  of only medium is introduced in the right chamber as shown in Figure 15. Two controls were used for migration experiment. In one control cells were re-suspended in full medium

and the medium towards which cells were supposed to migrate also was full medium. In the other control cells were re-suspended in starvation medium and the medium towards which cells were supposed to migrate also was starvation medium.

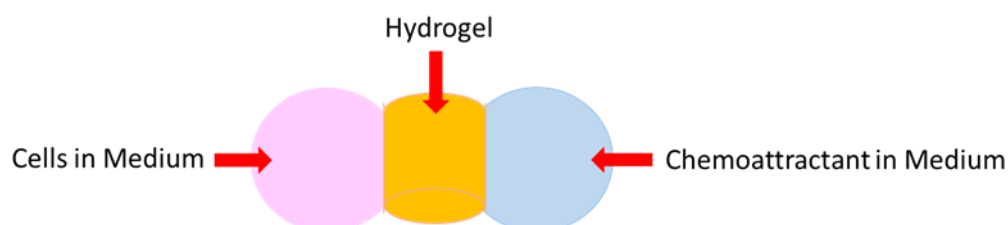


Figure 15: Chip design for cell migration assay in hydrogel.

Particles	Stock Conc. (mg/mL)	Working Conc. ( $\mu\text{g/mL}$ )	Vol. of Stock Conc. ( $\mu\text{L}$ )	Vol. of PBS ( $\mu\text{L}$ )	Total Vol. ( $\mu\text{L}$ )
46nm	25	1000	1.8	16.2	18
		500	0.9	17.1	18
		250	0.45	17.55	18
		125	0.225	17.77	18
794nm	25	1000	1.8	16.2	18
		500	0.9	17.1	18
		250	0.45	17.55	18
		125	0.225	17.77	18
5 $\mu\text{m}$	25	1000	1.8	16.2	18
		500	0.9	17.1	18
		250	0.45	17.55	18
		125	0.225	17.77	18
10 $\mu\text{m}$	12.5	1000	1.44	16.56	18
		500	0.72	17.28	18
		250	0.36	17.62	18
		125	0.18	17.82	18

Table 6: Specifications of particles utilized for characterization by concentration experiments.

Particles/Cells	Given Stock Conc. (mg/mL)	Calculated Stock Conc. (Particles/mL)	Working Conc. (Particles/mL)	No. of Particles/ Cells	Vol. of Working Conc. ( $\mu$ L)	Vol. of PBS/Hydroge I ( $\mu$ L)	Total Vol. ( $\mu$ L)
46nm	25	$4.9 \times 10^{14}$	$9.8 \times 10^7$	$5 \times 10^5$	5.095	12.905	18
				$2.5 \times 10^5$	2.54	15.46	18
				$1.25 \times 10^5$	1.27	16.73	18
				$5 \times 10^4$	0.5	17.5	18
				$5 \times 10^3$	0.05	17.95	18
				$5 \times 10^2$	0.005	17.995	18
794nm	25	$9.5 \times 10^{10}$	$5.9 \times 10^7$	$5 \times 10^5$	8.3	9.7	18
				$2.5 \times 10^5$	4.18	13.8	18
				$1.25 \times 10^5$	2.93	15.07	18
				$5 \times 10^4$	0.8	17.2	18
				$5 \times 10^3$	0.08	17.92	18
				$5 \times 10^2$	0.008	17.992	18
5 $\mu$ m	25	$3.8 \times 10^7$	$3.8 \times 10^7$	$5 \times 10^5$	1.3	16.7	18
				$2.5 \times 10^5$	0.65	17.35	18
				$1.25 \times 10^5$	0.325	17.67	18
				$5 \times 10^4$	0.13	17.87	18
				$5 \times 10^3$	0.013	17.987	18
				$5 \times 10^2$	0.0013	17.998	18
10 $\mu$ m	12.5	$2.3 \times 10^7$	$2.3 \times 10^7$	$5 \times 10^5$	18	0	18
				$2.5 \times 10^5$	10.4	7.6	18
				$1.25 \times 10^5$	5.2	12.8	18
				$5 \times 10^4$	2	16	18
				$5 \times 10^3$	0.2	17.8	18
				$5 \times 10^2$	0.02	17.98	18
60nm Amidine	41	$2.4 \times 10^{14}$	$1.4 \times 10^9$	$1 \times 10^6$	0.69	17.31	18
				$5 \times 10^5$	0.34	17.6	18

60nm Sulfate	38	$3.2 \times 10^{14}$	$1.9 \times 10^9$	$1 \times 10^6$	0.48	17.52	18
				$5 \times 10^5$	0.24	17.76	18
NIH-3T3 Cells	---	$1 \times 10^8$	$1 \times 10^8$	$5 \times 10^5$	4.34	13.65	18
Jurkat Cells	---	$15 \times 10^6$	$15 \times 10^6$	$5 \times 10^5$	33.3 <sup>a</sup>	18 <sup>b</sup>	18
				$2.5 \times 10^5$	16.6	1.4	18
				$1.25 \times 10^5$	8.33	9.7	18
				$5 \times 10^4$	3.3	14.7	18
				$5 \times 10^3$	0.3	17.7	18
				$5 \times 10^2$	0.03	17.97	18
Chondrocytes	---	$3.19 \times 10^5$	$3.19 \times 10^5$	$3 \times 10^6$	126.9 <sup>a</sup>	18 <sup>b</sup>	18
				$1.5 \times 10^6$	84.6 <sup>a</sup>	18 <sup>b</sup>	18
				$7.5 \times 10^5$	42.3 <sup>a</sup>	18 <sup>b</sup>	18

Table 7: Specification of particles and cells used in experiments. <sup>a</sup> represents volume of cell suspension before centrifugation and then re-suspended in a volume shown with <sup>b</sup>.

### 3.6 LS System Measurement and Data Generation

Particles or cell suspension in the microchip were radiated from a source emitting 488nm laser beams. The illumination of particles/cells was iterated at 50msec and the illumination interval was controlled by a shutter controller. Detection of the scattering signals occurred through OPD sensors, which converted the light signal into an electric signal. The electrical signals were produced in the form of potential difference and the whole LS system including iteration time was regulated by the LabView software. At the iteration of 50msec, the data was collected for 2min at various powers of laser and the system stored the collected data in an Excel file which was then analysed by GraphPad Prism, version 5.01.



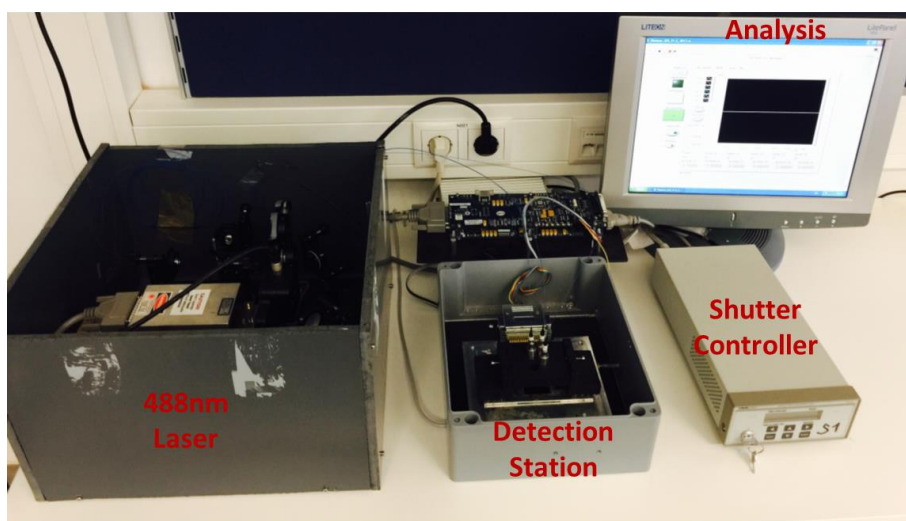


Figure 16: LS system equipped with 488nm laser source, detection station, shutter controller to operate laser and data collection equipment.

### 3.7 Statistical Analysis of LS System

For statistical analysis 2-way ANOVA test with the Bonferroni post-test were applied to characterize the LS system by utilizing different concentrations. A P-value less than 0.05 was considered statistically significant. The statistical test was applied by using a software GraphPad Prism, version 5.01. The formulas involved in analysing the results are as under:

$$\begin{aligned}
 CM &= \frac{(\text{Sum of All Observations})^2}{rab} \\
 SS_{Total} &= \sum (\text{Each Observation})^2 - CM \\
 SS(A) &= \frac{\sum_{i=1}^a A_i^2}{rb} - CM \\
 SS(B) &= \frac{\sum_{i=1}^b B_i^2}{ra} - CM \\
 SS(AB) &= \frac{\sum_{i=1}^a \sum_{j=1}^b (AB)_{ij}^2}{r} - CM - SS(A) - SS(B) \\
 SSE &= SS_{Total} - SS(A) - SS(B) - SS(AB)
 \end{aligned}
 \tag{3.2}$$

where  $A_i$  are the row sums and  $B_j$  are the column sums.  $(AB)_{ij}$  be the sum of all observations of level  $i$  of A and level  $j$  of B.  $r$  be the number of replicates in the experiment. Then the total number of observations for each level of factor A is  $rb$  and the total number of observations for each level of factor B is  $ra$  and the total number of observations for each interaction is  $r$ . Finally, the total number of observations  $n$  in the experiment is  $rab$ .

## 4. Results and Discussion

### 4.1 Physical Characterization of Lab-on-a-Chip System

#### 4.1.1 Calibration of Laser Power of LS System

To ensure similar laser output between four channels of the detection station, the changes in scattering signals of the detection station were investigated. The first step was to characterize the laser beam path, the input laser power and the output beam at every splitting branch, by measuring the signal detected by the sensors and recording them. As shown in Figure 17(a), the 488nm laser was split using a beam splitter and each path was coupled into a fibre beam splitter using input fibre coupler and collimator.

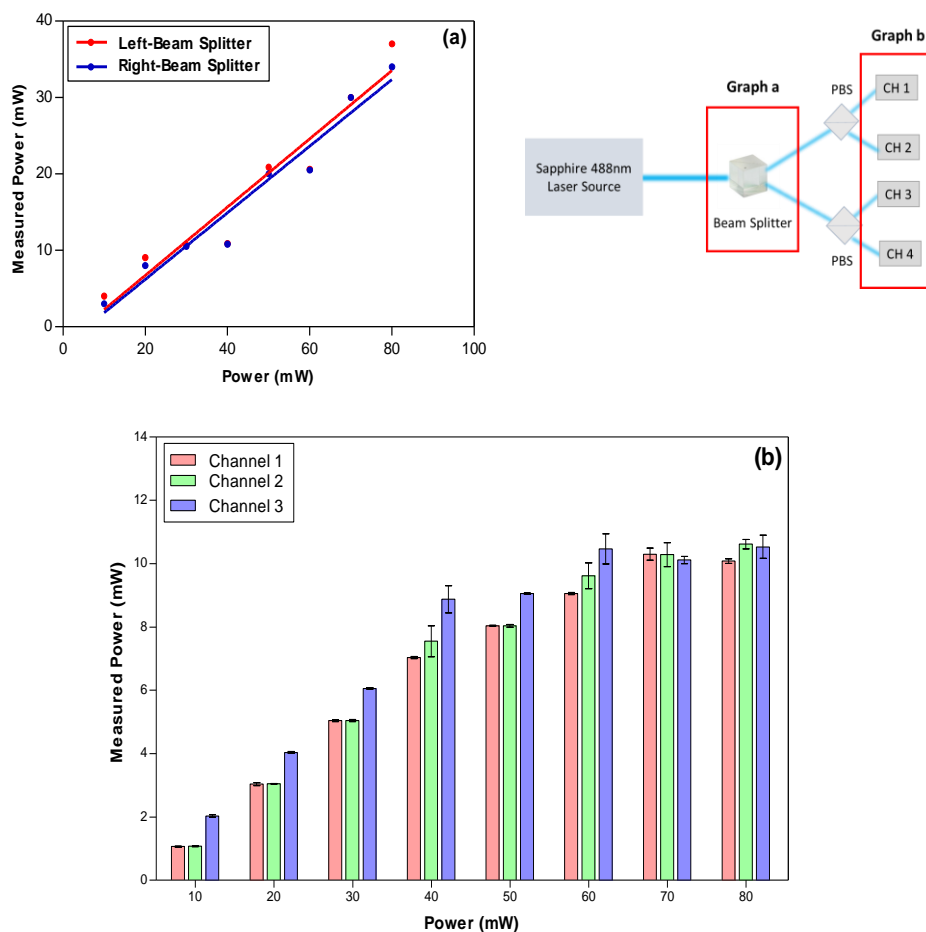


Figure 17: Characterization of (a) beam splitter and output power of laser, (b) laser power for the optical fibre light path.

The laser beams from output fibre coupler and collimator were directed into the detection station by optical fibre. Irregularities in core diameter or change in fibre axis may affect the power of the laser while transmitting from the beam splitter to the detection station, however the optical fibre made the transmission more secure and less distorted [133]. Each optical fibre that was used for transmission of laser beams had two outputs but one output of one optical fibre was damaged so the laser beams were transmitted to the detection station through three channels and the laser powers were again measured with a powermeter by placing it in front of each of the three channels. Out of the four channels of lasers, three of them were functional and could transmit the laser beam to the detector station and same was the case with OPD, as three out of four sensor of OPD were functional. The three sensors of OPD were detecting the beams falling upon them which means there were three replicates for each data. Figure 17(a) demonstrates the output powers of laser after passing through the beam splitter after which it divides into two beams and each beam measurement was approximately the same, showing the ability of the beam splitter to work efficiently. The two output beams from the beam splitter were further divided into four beams by two polarization beam splitters which were then propagated through the optical fibres to the detection station. The power range that can be measured at the detection station is about -0.14V to 10.08V. The laser powers at the output ends of optical fibres displayed in Figure 17(b) showed an increase in power as the intensity of laser source increased. The channel whose other part was damaged showed a slight increased power output at the powermeter. Considering the laser beam as a photon stream, it is known that it always needs a path to flow, therefore the higher power measurement at one channel was probably because the photons could not flow through the other channel and therefore diverted to flow from the functional channel. From these results it can be concluded that the left-beam splitter and right-beam splitter give a similar linear response (Figure 17). Furthermore, it can be seen that after the two laser beams are further split into four beams, the power measured at channel 1 and 2 of the optical fibre are comparable, whereas channel 3 gives a higher signal, due to non-functioning channel 4, however this difference vanishes at a power of 70mW and 80mW (Figure 17(b)).

### 4.1.2 Calibration of Temperature of LS System

In order to find out the suitable temperature for cell's survival and their proliferation in the microchip, the LS system must be set at a temperature suitable for cellular proliferation and viability. Temperature has a great impact on cell survival, as it interferes with the metabolism, enzymatic activity and general function. Although cells are able to cope with temperature fluctuation between 25°C and 37°C, constant change in the temperature may affect their viability and proliferation, leading to cell death, which will affect the scattering signals.

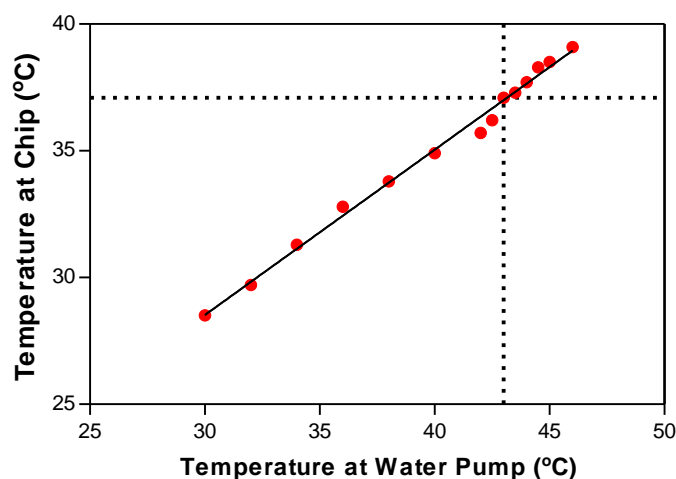


Figure 18: Temperature offset between water heating and chip heating system.

The detection station was connected with a water pump or thermal bath that maintained the temperature of the microchip placed in the detection station. Different temperatures were selected on the thermal bath to maintain the temperature at the microchip. Figure 18 displays the linear increase in temperature at the chip as the temperature of the thermal bath was increased. As cellular metabolic activity ideally functions at 37°C, the temperature of the water bath was raised until it reached the optimum temperature in the chip. The results from this experiment showed that 43°C set at the thermal bath was the most suitable temperature that maintained the temperature of  $37 \pm 0.6^\circ\text{C}$  in the microchip. Multiple measurements showed slight fluctuation as the standard deviation shows, however they were within the durable range.

### 4.1.3 Calibration of OPD Sensors of LS System

The next experiment was conducted to check the maximum detection capacity of OPD sensors and the signal detected by them from the four different channels. This experiment was important to ensure that the sensors were fully functional and that the sensor would only detect the signal coming from the laser beam passing through the sample and not from any possible surrounding light sources while measuring the sample later on. The four sensors of OPD were characterized by full light illumination and also without any light to access the dark current. The sensors were characterized without light by covering the detection station with a lid and thereby preventing light from any source from entering the sensors, whereas during the characterization with maximum light, the lid was removed and light was entering from the laser source and the external source as well.

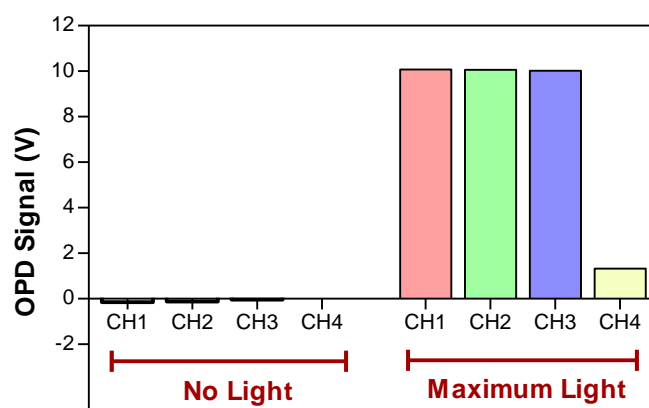


Figure 19: Characterization response of OPD's sensors without any illumination of light and with maximum illumination.

In Figure 19 it can be seen that while checking the dark current a signal in the minus range of -0.14V could be detected with the three functional sensors of channel 1-3, whereas the sensor of channel 4 did not detect any signal. On the other hand, when the sensors were exposed to maximum light, three of them detected the signal compared to the fourth sensor which seemed to be less functional. Sensors of channel 1-3 detected a maximum OPD signal of 10.08V, showing the maximum

detection capacity. From this it can be concluded that the functional range of the sensors is from -0.14V to 10.08V.

After the characterisation of the laser, OPD's sensors and calibration for temperature, the system was ready to start characterisation experiments with nanoparticles.

## 4.2 Preparation of Microchip

In the presented work, the main goal was to enable the LS system and to make it operational for determining the cell morphology, viability, proliferation and migration in 3D microenvironment. However, the basic requirement for analysing the particles or cells was to fabricate a microchip on which the samples could be introduced and examined with the LS system. To provide the cells with a 3D microenvironment, microchips were prepared and particles/cells were mixed in PBS or in 3D-hydrogels, pipetted into the microchip to measure the scattering signals. The following three techniques were tried to determine the most feasible and reproducible method for preparing microchips: (1) 3D printed mold design, (2) mold fabricated by CO<sub>2</sub> laser and (3) the hand cut design.



Figure 20: Microchip fabrication design.

The very first technique, 3D printed design was not suitable for the future experiments due to the roughness of its surface that prevented the plasma bonding of PDMS with the glass slide. The 3D printed design needed to be modified by making it as plane and shiny as possible. Consequently, to fabricate the same chip design, CO<sub>2</sub> laser with a wavelength of 10.6 $\mu$ m was exploited. The design was prepared by irradiating CO<sub>2</sub> laser on a cardboard sheet to form the shape of the inlets for the hydrogel and medium, however this method was not feasible either due to the absorbance property of cardboard. When the PDMS layer was set into the



mold, bubbles appeared around the design that made it opaque making it impossible to detect the scattering signals. Hence, after the failure of these two techniques, PDMS hand cut designs were tried with a successful outcome. The PDMS layer was bonded between two plane glass slides, one of which had pre-drilled holes that were used as inlets for the cell/particles in hydrogel/PBS and cell culture medium. The characterization experiments were conducted using the hand cut design. This design would make it possible to study the cells in a 3D environment as found *in vivo*.

In *in vivo* environment, cells are surrounded by other cells and different types of ECM which provide them a 3D environment, however 2D cell culture does not take into account the natural 3D environment of cells and it may give misleading and non-predictive data. Hence, fabrication of microchip was basically aimed to give cells a suitable microenvironment that mimics the natural environment of the cells where they reside in tissues.

### 4.3 Performance Analysis of LS System

The aim of these experiments was to enable the LS system to measure the morphology and number of the cells present in the 3D volume. Any type of system that is being newly developed for determining cell viability and morphology measurement needs to be characterized and for the characterization of such devices particles of various sizes and shapes are utilised as they resembles cells [110, 111].

#### 4.3.1 Ability to Determine Particle Size in LS

Since different cells have different sizes and shapes, these attributes can influence the scattering signals. Therefore prior to observing the scattering of cells, it is important to characterise scattering signals using different size particles. Hence, the aim of this experiment was to determine the potential of LS system to detect the scattering signals of various particles of different sizes, which could later be used as a standard calibration when analysing the scattering signals of different types of cells.

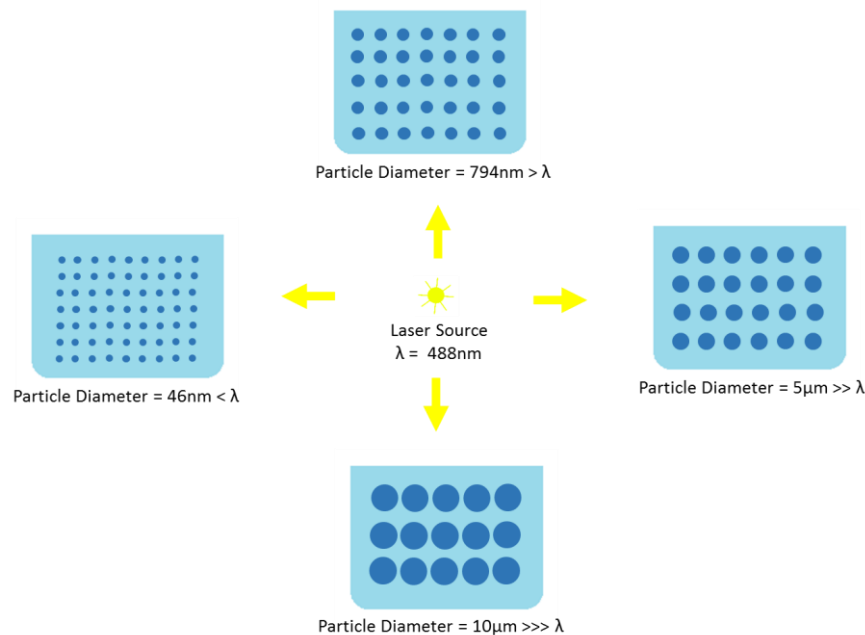


Figure 21: Schematic displaying characterisation of different particle sizes.

In order to enable the LS system to observe the scattering effects from various sizes of cells, different polystyrene particles of diameters 46nm, 794nm, 5 $\mu$ m and 10 $\mu$ m were utilized. To be able to determine the linearity of the signals at different powers, four different powers of laser from a minimum power 7.5mW to a maximum power of 82.5mW to observe the scattering response from different particle sizes.

A graph of size characterization shown in Figure 22(a) illustrates that laser wavelength of 488nm is approximately ten times higher in case of 46nm particle, whereas it is smaller in rest of the cases. From this it can be said that the scattering occurring due to particle of 46nm is a case of Rayleigh scattering and the light scattering taking place with the rest of the particle sizes can be described as a case of Mie scattering.

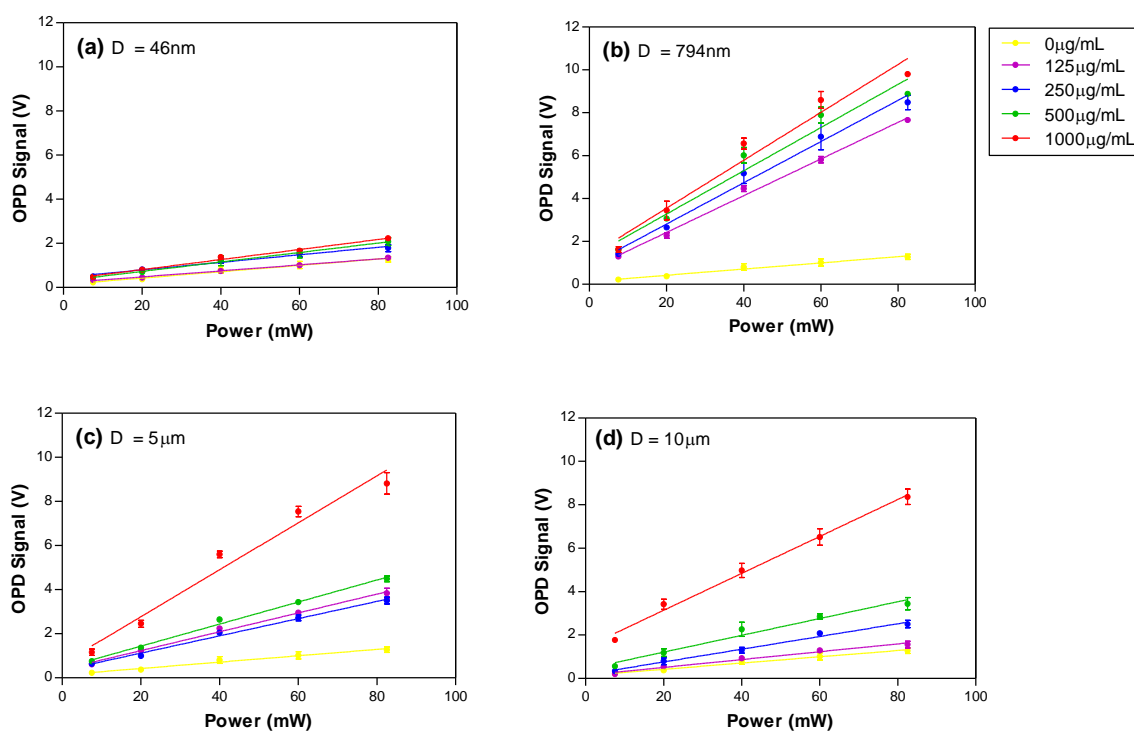


Figure 22: Characterization curves of particles of (a) 46nm, (b) 794nm, (c) 5 $\mu$ m and (d) 10 $\mu$ m at different concentrations. The scattering effects were seen by varying the laser power from 7.5mW to 82.5mW.

Comparison of the data in Figure 22 shows that the scattering effects increased linearly by increasing laser powers in all sizes of particles [136]. However, at low power of 7.5mW the OPD signal for 46nm particle was relatively low compared to the signal of 794nm, 5 $\mu$ m and 10 $\mu$ m, where the signals could be distinguished. As the power increases, the scattering effects became more prominent when particles larger than the wavelength (488nm) [137] were used, which could not be said for the 46nm particles even at a maximum power of 82.5mW. This pointed to a phenomenon known as Rayleigh scattering, where particles size was much smaller compared to the incident wavelength 488nm and the particle scattered symmetrically [138]. This implies that the backward and the forward scattering was same in case of 46nm particles. This experiment showed that the LS system is able to detect light scattering signals from different sized particles, even if the particle (46nm) is smaller than the wavelength. However, to determine the quantity of particles that can be distinguished and observed significantly, limit of detection experiments will be performed later.

The cellular structure having larger diameter have higher scattering efficiency compared to the smaller once. Size analysis from various particles sizes also made it possible to select a suitable laser power range for different sizes. High laser powers can even detect smaller cells, however, at low intensities, the difference could hardly be observed [139]. Hence, size analysis of particles by utilizing LS system is a remarkable technique for determination of cell sizes.

### 4.3.2 Influence of Particle Concentration in LS

The concentration of cells is an important figure to note in biomedical research, as the quantification of any analysis is normalized to cell concentration. Therefore, to be able to properly quantify the obtained data, knowing the cell concentration at the start and end of the experiment is very critical. Hence, in order to measure the influence of concentration in scattering, data was collected for 46nm, 794nm, 5 $\mu$ m and 10 $\mu$ m polystyrene particles at following concentrations: 125 $\mu$ g/mL, 250 $\mu$ g/mL, 500 $\mu$ g/mL and 1000 $\mu$ g/mL and using power intensities from 7.5mW to 82.5mW. The significances were determined with respect to 0 $\mu$ g/mL for all particle sizes.

To calculate the significances, the 2-way ANOVA test was applied to all concentrations with the Bonferroni post-test, as all the groups were compared with each other. The four graphs in Figure 23 are divided according to particle size; the same particle sizes of varying concentrations measured at three different powers are depicted next to one another in one graph. By varying laser power and from the level of significance it can be determined up to what concentration, the LS system is able to give response and with what level of confidence. The trend of OPD signal detected for each concentration at varying powers was the same. In all the controls, the signal was low compared to the other concentration as there were no particles in it. In Figure 23(a), despite varying the concentration of the 46nm particles and measuring them with three different power intensities, there seemed to be a limit of detected signal at each power from the concentration of 250 $\mu$ g/mL onwards. This can be explained by the Rayleigh scattering phenomenon, as when the particle size is smaller than the wavelength of the laser (488nm), there is not much scattering, despite increasing the concentration [140]. Due to this, the results obtained were not significant compared to control. In Figure 23(b), already at a power of 7.5mW, the signal of different concentration of beads was significantly higher than the control and this trend continued as the power was increased, showing that the Rayleigh scattering is not applicable here. However, it is interesting to note that in Figure 23(b), no doubling of signal could be seen as the concentration of beads was doubled. This however changed when particles of 5 $\mu$ m Figure 23(c) were exposed to the laser. The OPD signal increased almost 2-fold irrelevant of power between

500 $\mu\text{g}/\text{mL}$  and 1000 $\mu\text{g}/\text{mL}$ ; this could not be seen between 125 $\mu\text{g}/\text{mL}$  and 250 $\mu\text{g}/\text{mL}$  or 250 $\mu\text{g}/\text{mL}$  and 500 $\mu\text{g}/\text{mL}$ . In the case of 10 $\mu\text{m}$  particles Figure 23(d), the 2-fold increase could already be observed between the particle concentrations of 250 $\mu\text{g}/\text{mL}$  and 500 $\mu\text{g}/\text{mL}$ , which continued between 500 $\mu\text{g}/\text{mL}$  and 1000 $\mu\text{g}/\text{mL}$  irrelevant of power intensity.

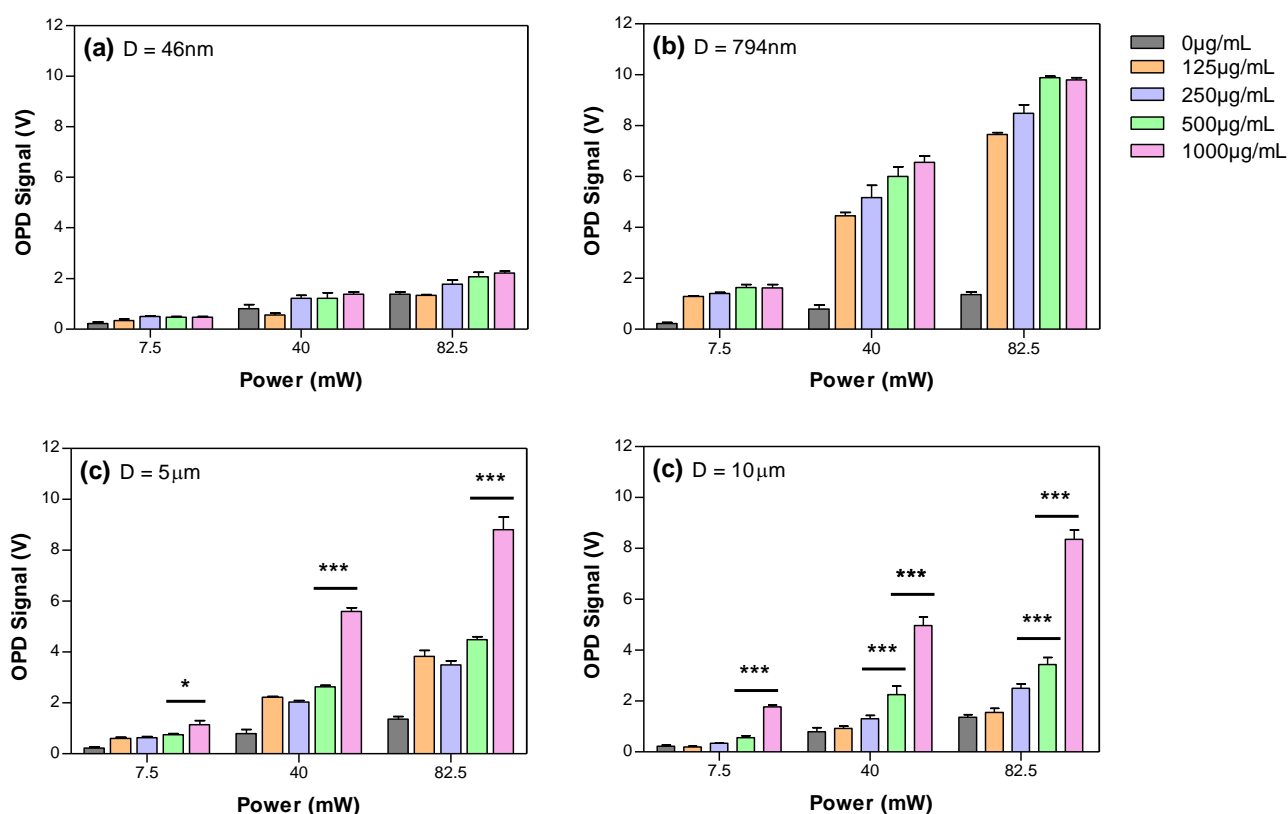


Figure 23: Characterization by utilizing concentrations of 125 $\mu\text{g}/\text{mL}$ , 250 $\mu\text{g}/\text{mL}$ , 500 $\mu\text{g}/\text{mL}$  and 1000 $\mu\text{g}/\text{mL}$ ; particles of (a) 46nm, (b) 794nm, (c) 5 $\mu\text{m}$  and (d) 10 $\mu\text{m}$  were analysed at 7.5mW, 40mW and 82.5mW. The significance of the data was determined by using 2-way ANOVA test. \* indicates significant difference of  $P < 0.05$ , \*\* indicates significant difference of  $P < 0.01$  and \*\*\* indicates significant difference of  $P < 0.001$ .

Furthermore, it is noteworthy that while comparing the signals at the highest concentration of 794nm, 5 $\mu\text{m}$  and 10 $\mu\text{m}$ , the signal for the 794nm particles is higher compared to the bigger particles almost reaching the maximum signal of 10.08V. This shows that not only does the surface of bigger but fewer particles scatter more

light, but smaller particles which are higher in number and therefore also offer more scattering surface give a higher OPD signal. When particles larger than the laser wavelength were used, as is known in Mie scattering, then scattering effects were higher in case of the 794nm particles, However, as the particles size increased the scattering signal started reducing for the same concentrations and for the same powers, For example, at 82.5mW and a concentration of 1000 $\mu$ g/mL, 10 $\mu$ m particles showed less scattering than 794nm particles [141]. When particles having diameter 5 $\mu$ m were used, the scattering started decreasing although the same power of laser and same concentrations were used as shown in Figure 23(c). Although the scattering effects were not as high as that of 794nm particles, it still showed Mie scattering. However, as mentioned earlier, the conclusion that increasing concentration and power leads to the increase in signal is still valid, only for individual particles size.

The reason why there is an increased signal for 794nm lies in the fact that concentration is interpreted as mass per unit volume, which means that for the same concentrations of particle solutions, the larger particles such as 10 $\mu$ m would be less in number compared to smaller once [142]. Hence, smaller particles being higher in number would make the solution turbid [143] and can be explained nicely through Figure 21. A decrease in signal at the same concentration of different particle sizes is due to the reduced number of larger particles versus more particle number in the solution of smaller particles. On the basis of observations of the experiment, 794nm particles showed good scattering effects compared to other sizes of particles.

It could also be observed that linearity of signal with increasing particle concentration was only observed in 794nm particles illuminated with laser at a power of 40mW. Same sized particles exposed to a higher power of 82.5mW showed no linearity, which could be due to the limit of the system to detect OPD signals higher than 10V, leading to an overflow. As the detected signal at 82.5mW for the lowest concentration of 125 $\mu$ g/mL already starts at approximately 8V, the higher concentrations reach a maximum already at a concentration of 500  $\mu$ g/mL. In the case of 5 $\mu$ m and 10 $\mu$ m particles, the non-linear signal compared to concentration

could be due to the difference in the number of particles present in the given concentrations, as mentioned earlier.

From this experiment it can be concluded that while working with particular particle sizes (794nm at defined power of 40mW) can give a linear signal response with increasing concentration. However, this method is limited as at higher power the limit of the detection system is reached and with particles of bigger size linearity is not reached. This data is relevant so as to know if cell of varying sizes should be embedded in hydrogel by considering concentration or cell number. The next experiment will clarify which parameter is more sound.



### 4.3.3 Ability to Determine Particle Number in LS

The main goal of performing this experiment was to determine the influence of cell numbers in scattering. The concentration of the cells means that how much mass of cells is present in the given volume however, cell number gives an exact digit about the cell count in a given volume. The number of cells provide important information about if cells divide, proliferate, which helps to find out if they are growing abnormally or if they are hypertrophic, meaning that the cells are growing larger in size without growing in number [144]. A future aim of characterizing the LS system was to enable it to detect cells and their proliferation over a longer period of time. For verification of the scattering response based on the number of particles, experiments were performed by considering the same number of polystyrene particles of different sizes. To check the influence, following quantity of particles,  $1.25 \times 10^5$ ,  $2.5 \times 10^5$  and  $5 \times 10^5$  particles of all available sizes were introduced in PBS solution and the signal was measured with the LS system

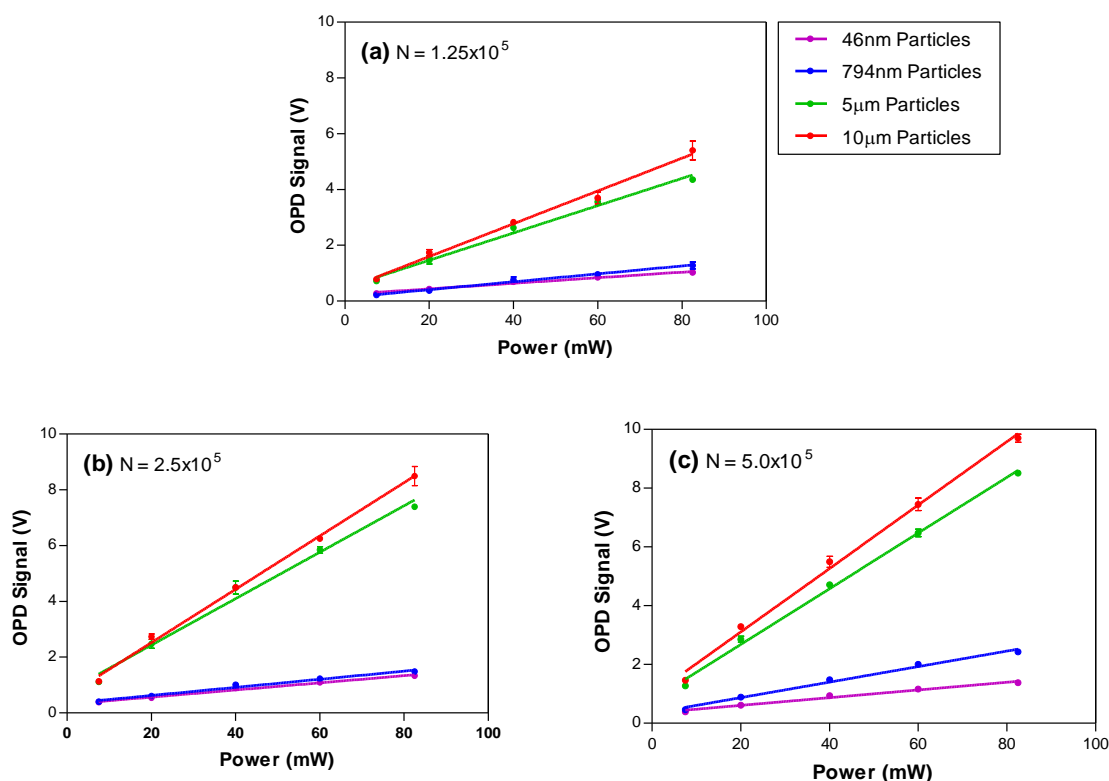


Figure 24: OPD response by introducing (a)  $1.25 \times 10^5$ , (b)  $2.5 \times 10^5$  and (c)  $5 \times 10^5$  particles of 46nm, 794nm, 5μm and 10μm diameter in PBS ( $n = 3$ ).

The results showed that the larger particles with the same number of particles showed more scattering effects compared to small particles. This is due to the fact that particles larger than the laser wavelength exhibit forward scattering explained in Mie scattering in contrast to Rayleigh scattering [145]. As an example the laser scattering seen in all the three cases shown in Figure 24, 10 $\mu$ m particles have higher signal than 5 $\mu$ m although the same number of particles were introduced and similarly scattering by 5 $\mu$ m particles was much greater than 794nm particles.

From the previously performed experiments it is now obvious that the laser intensity enhances the scattering response which can be observed in Figure 25 where when 5 $\times 10^5$  particles of 10 $\mu$ m diameter were used, the scattering signal was below 2V at a power of 7.5mW, however at 82.5mW the signal almost reached the maximum detectable signal of 10.08V.

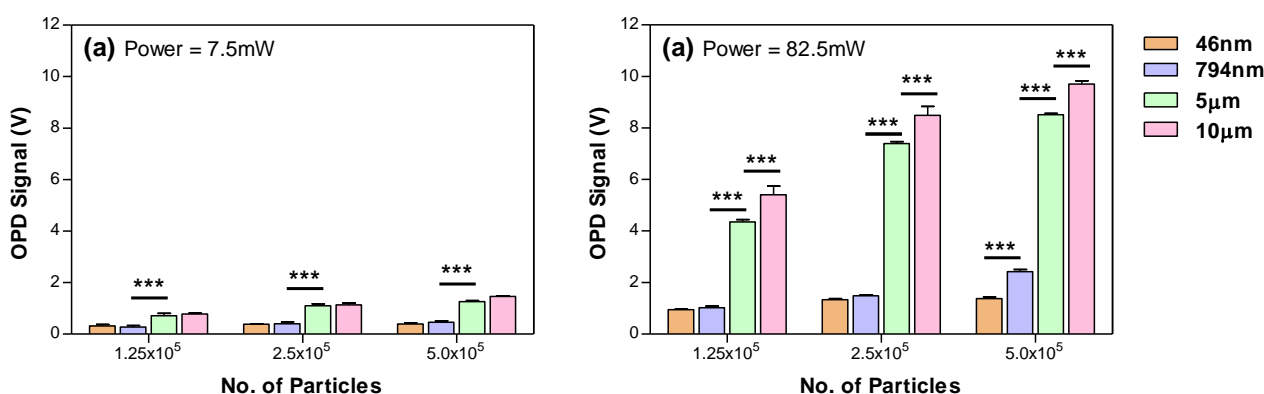


Figure 25: Scattering behaviour of 1.25 $\times 10^5$ , 2.5 $\times 10^5$  and 5 $\times 10^5$  particles at (a) 7.5mW and (b) 82.5mW (n = 3).

The 2-way ANOVA test was applied to all number of particles with Benferroni post-test, at a power of 7.5mW and 82.5mW, as all the groups were compared with each other. In Figure 25(a) and (b), the trend was similar with a same level of significance, when the OPD signals of 794nm and 5 $\mu$ m were observed. The signal from 5 $\mu$ m became 3 times higher than the signal from 794nm particles. It is interesting to note that, no significant difference was observed between 5 $\mu$ m and 10 $\mu$ m at 7.5mW, however, at a power of 82.5mW the significance level reached to its maximum value

with  $P < 0.001$ . Another important difference to note at maximum power was the significance difference between OPD signal of 46nm and 794nm particles which was not observed unless and until  $5 \times 10^5$  particles were observed at 82.5mW, showing again the increased significance by increasing the number of particles at high power values.

From the obtained results it can be said that the cells larger in diameter contribute more in scattering compared to those having smaller diameter provided their numbers are kept constant. Furthermore, it could be seen that using the number of particles instead of concentration of particles gives a linear result, concluding that the former is a more reliable parameter to consider when measuring cell size with a LS system.

#### 4.3.4 Limit of Detection

To gain a better understanding about the least number of cells that could be detected by the LS system, the following experiments provide a basis to develop a comparison between LS and other biosensors. The ultimate aim of finding the limit of detection using particles was to determine the sensitivity of the system by which later on it could measure the morphology, viability and proliferation using a minimum number of cells. According to IUPAC, limit of detection defines the minimum amount of concentration or absolute amount of analyte that generates a signal significantly higher than the signal arising from a blank [146]. Mathematical relation for finding detection limit is given as

$$\text{Limit of Detection} = \text{Signal from Blank} + 3 \times \sigma \quad 4.1$$

where  $\sigma$  represents the standard deviation of the signal from blank. Hence the objective of performing these experiments with innate particles was to check the reproducibility of the results and to find out the significant range of particles due to which the scattering signal can be achieved. Polystyrene particles of a diameter of 46nm, 794nm, 5 $\mu$ m and 10 $\mu$ m were analysed in PBS by varying the number of particles from 5x10<sup>2</sup> to 5x10<sup>5</sup> and comparing them with the signal received with zero particles i.e. signal from blank. The limit of detection was calculated by applying the formula on the signals of the blank received at different laser powers. According to the calculation, the limit of detection for the power of 7.5mW is at 0.41V, for 40mW it is at 0.79V and for 82.5mW it is at 3.86mW.

The weakness of the formula shown in Eq. 4.1 is that there is no evidence to ensure that a low concentration of the analyte will produce a signal distinguishable from a blank. Therefore, a linear calibration curve, with the equation  $y=ax+b$ , is used as it is assumed that the OPD signal  $y$  is linearly related to the laser power  $x$  for a limited range of number of particles. So the formula used for limit of detection considering the slope of curve is shown in Eq. 4.2

$$\text{Limit of Detection} = \frac{3 \times \sigma}{\text{Slope}} \quad 4.2$$

where  $\sigma$  represents the standard deviation of the intercept. The limit of detection calculated by applying the formula on the signals received at different laser powers of 7.5mW, 40mW and 82.5mW are shown in Table 8.

Power (mW)	46nm	794nm	5 $\mu$ m	10 $\mu$ m
7.5	6.9x10 <sup>5</sup>	9.7x10 <sup>5</sup>	2.1x10 <sup>5</sup>	7.0x10 <sup>4</sup>
40	1.3x10 <sup>5</sup>	3.9x10 <sup>4</sup>	1.4x10 <sup>4</sup>	8.0x10 <sup>4</sup>
82.5	1.0x10 <sup>5</sup>	2.4x10 <sup>3</sup>	2.6x10 <sup>3</sup>	1.9x10 <sup>3</sup>

Table 8: Number of particles of 46nm, 794nm, 5 $\mu$ m and 10 $\mu$ m that can be differentiated from a blank signal at 7.5mW, 40mW and 82.5mW.

The Eq. 4.2 used to calculate the limit of detection is more reliable compared to Eq. 4.1 because Eq. 4.1 describes the minimum signal above which the signals should be detectable, however, Eq. 4.2 gives the minimum number of particles that would generate a signal different from the blank.

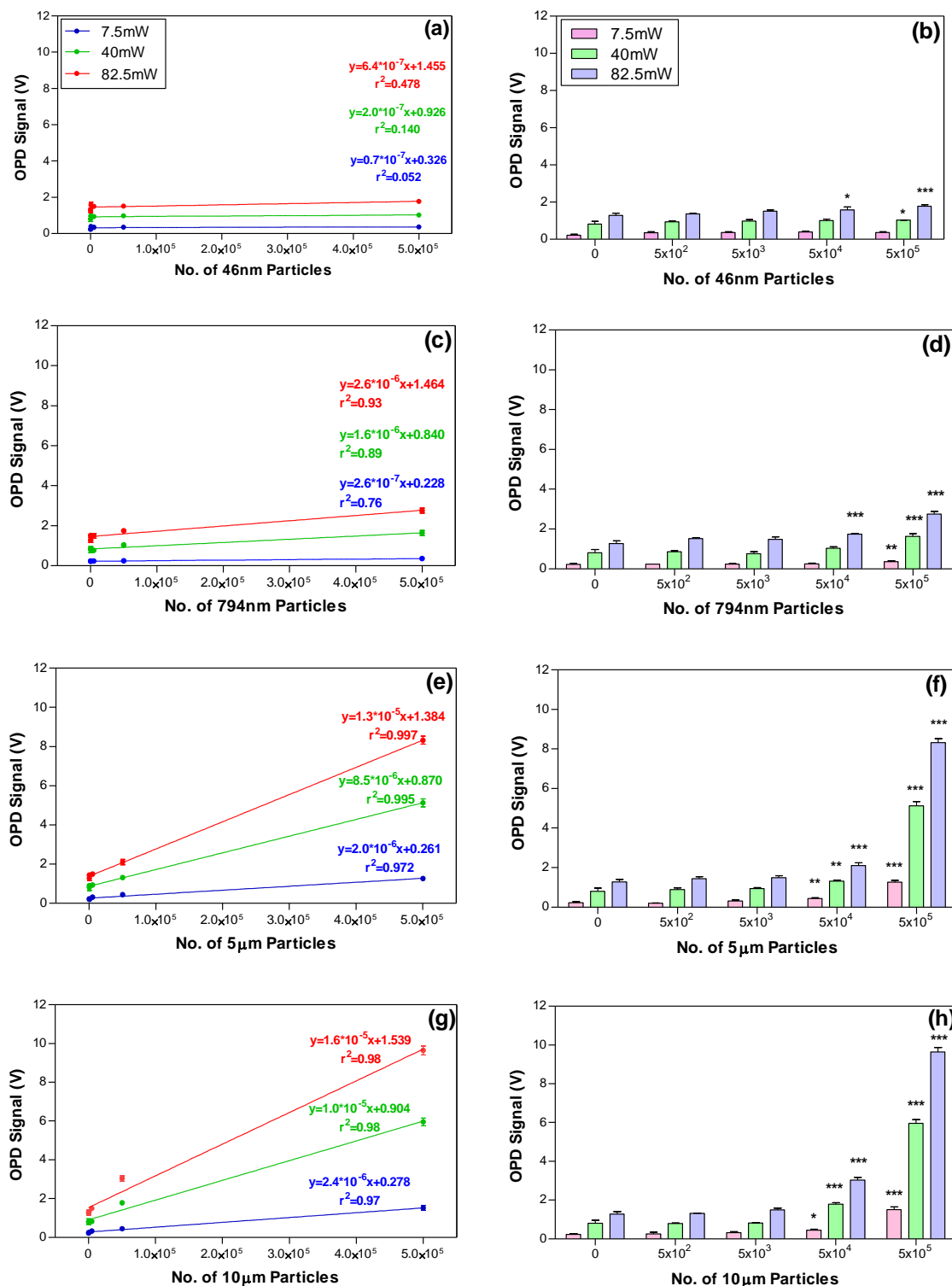


Figure 26: Scattering signal from 46nm, 794nm, 5µm and 10µm particles at 7.5mW, 40mW and 82.5mW. (a), (c), (e) and (g) represent curves with slopes and intercepts whereas (b), (d), (f) and (h) represent significance of number of particles with respect to zero number of particles. \* indicates significant difference of  $P < 0.05$ , \*\* indicates significant difference of  $P < 0.01$  and \*\*\* indicates significant difference of  $P < 0.001$  ( $n = 3$ ).

It can be seen in Figure 26(a) that at a low laser power of 7.5mW intercept-value was below 0.32V however, at 82.5mW the intercept increased to a level of approximately 1.45V which has already proven that as the power increases, scattering effects also increase. The same result can also be observed in case of larger particles. There is a small variation in slopes (sensitivity) at all power ranges which shows a consistent but very small increase in scattering signal that shows the system is not sensitive to detect the particles of 46nm particles at minimum power. At 82.5mW, only  $5 \times 10^4$  particles of diameter 46nm were giving a significant scattering signal with  $P < 0.05$  as shown in Figure 26(b) whereas, particles are not significantly distinguishable at power of 7.5mW.  $5 \times 10^5$  particles can be significantly determined with  $P < 0.001$  at a power of 82.5mW and with  $P < 0.05$  at a power of 40mW with respect to the control group. At 7.5mW, 46nm particles were not distinguishable compared to zero particles. When 794nm particles were placed in the LS system to find out the limit of detection, it was observed that the slopes of the curve increased gradually when higher power was applied, as can be seen in Figure 26(c). Moreover, the data becomes more significant for  $5 \times 10^4$  particles compared to the same number of 46nm particles.  $5 \times 10^5$  particles of 794nm diameter were detectable even at 7.5mW with  $P < 0.01$  which was not observed in case of 46nm particles as shown in Figure 26(d) and the data became more significant at 40mW and 82.5mW.

When 5 $\mu$ m particles were analysed, the increased scattering effects compared to smaller particles were clearly noticeable from their slopes as shown in Figure 26(e). It can also be observed that the significance of the data was increased for  $5 \times 10^4$  particles even at low laser power i.e. 7.5mW and became more significant when the particle range reached to a level of  $5 \times 10^5$  particles as the Figure 26(f) represents. When 10 $\mu$ m particles were immersed in PBS to find the limit of detection, trend of the slope was similar to the 5 $\mu$ m particles.  $5 \times 10^4$  and  $5 \times 10^5$  particles can be significantly determined at all power ranges.

In all particle sizes, goodness-of-fit i.e.  $r^2$ -value were calculated shown in Figure 26(a), (c), (e) and (g). An increase in the  $r^2$ -value towards 1, the higher the laser power used was, indicated that the obtained data points fitted better to the

regression line. This means that the data points are not scattered and they produced a reliable curves as they were close to the regression line [147]. It was observed that for the 46nm and 794nm particles the goodness-of-fit was not as good as the  $r^2$ -value for the larger particles that were analysed. The  $r^2$ -value for 5 $\mu\text{m}$  and 10 $\mu\text{m}$  was closer to 1 and became almost similar for all power ranges, meaning that the scattering data for larger particles was closer to the regression line. Intercept values were also increased for all particle sizes that were exposed to the higher ranges of laser power. High slope values in comparison with low slope values indicate that the variation along y-axis is more abrupt for similar amount of change along x-axis, thus

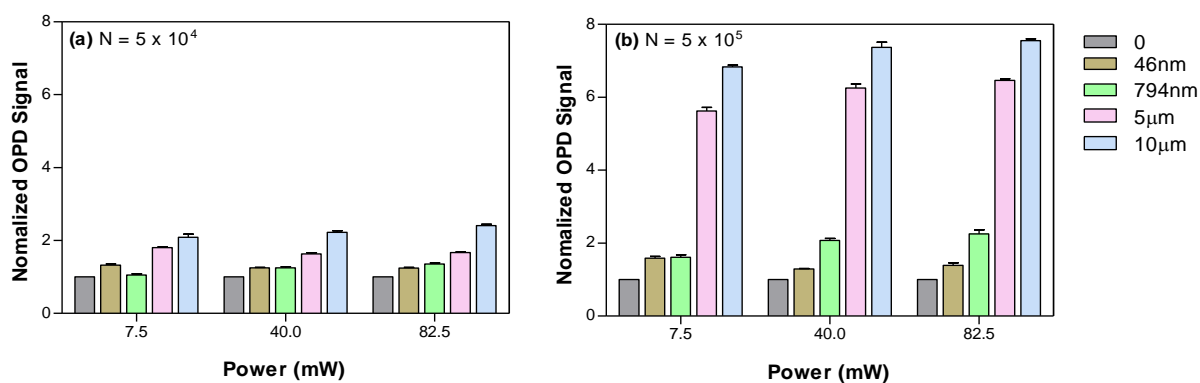


Figure 27: Normalized OPD signal of (a)  $5 \times 10^4$  and (b)  $5 \times 10^5$  particles at powers 7.5mW, 40mW and 82.5mW. The signals were normalized according to the control group ( $n = 3$ ).

The data was also analysed by using 2-way ANOVA test as shown in Figure 26(b), (d), (f) and (h) and it was observed that as the size of the particles was increased, the more significant results were produced even if the laser power was kept lower. This can be seen clearly in Figure 26(b) and (d) that  $5 \times 10^5$  particles of 46nm were not significant at 7.5mW, however in case of 794nm particles, significance scattering was observed at  $P < 0.01$ . In case of 5 $\mu\text{m}$  and 10 $\mu\text{m}$  particles, the significance level reached its maximum with  $5 \times 10^5$  particles at  $P < 0.001$ . Hence by analysing the level of significance, it can be determined up to what particle range and for what particle size, the scattering signal is measurable and with what level of confidence interval [150]. In order to observe scattering response by utilizing large particles, normalized OPD signals from  $5 \times 10^4$  and  $5 \times 10^5$  particles were observed as shown in Figure 27. It can be seen that at high power levels system is more sensitive to detect even



smaller particles because 46nm particles cannot be differentiated from the blank signal at 7.5mW but as the power increases to 40mW,  $5 \times 10^5$  particles can be detected and at highest power of 82.5, less number of particles i.e.  $5 \times 10^4$  are detectable.

When a newly developed device is introduced, the initial step is to finding out the detection of limit as it reveals the sensitivity of the system This is, obviously, a very critical point, because high sensitive systems are preferred in the medical and diagnostic fields. These experiment provided a basis on which the sensitivity of the LS system could be evaluated. These experiments were important to determine how many cells could produce the least detectable response which is different from the blank. In cell analysis, evaluation of detection limit of cells can be helpful in monitoring the cell proliferation, invasion and migration. In 3D cell culture system it becomes even more important to determine the limit of detection so that the cell behaviour and fate can be analysed with precision.

### 4.3.5 Influence of Material Properties in LS

The purpose of this experiment was to determine the influence of material in scattering since the optical signal varies depending upon the material properties of a tissue and its environment. In order to determine the influence of material in scattering, sulfate polystyrene latex and amidine polystyrene latex were re-suspended in PBS and measured in the LS system with a wavelength of 488nm. When amidine polystyrene latex particles of diameter 60nm were introduced into the system, the signals for  $1 \times 10^6$  particle was obviously higher compared to the signal of  $0.5 \times 10^6$  number of particles. However, using the same number of sulfate polystyrene latex of diameter 60nm showed higher scattering effects compared to amidine polystyrene latex nanoparticles. As an example it can be observed in Figure 28 that at a power of 82.5mW, the signal from amidine particles was below 2V however, for sulfate particles it was close to 2.5V.

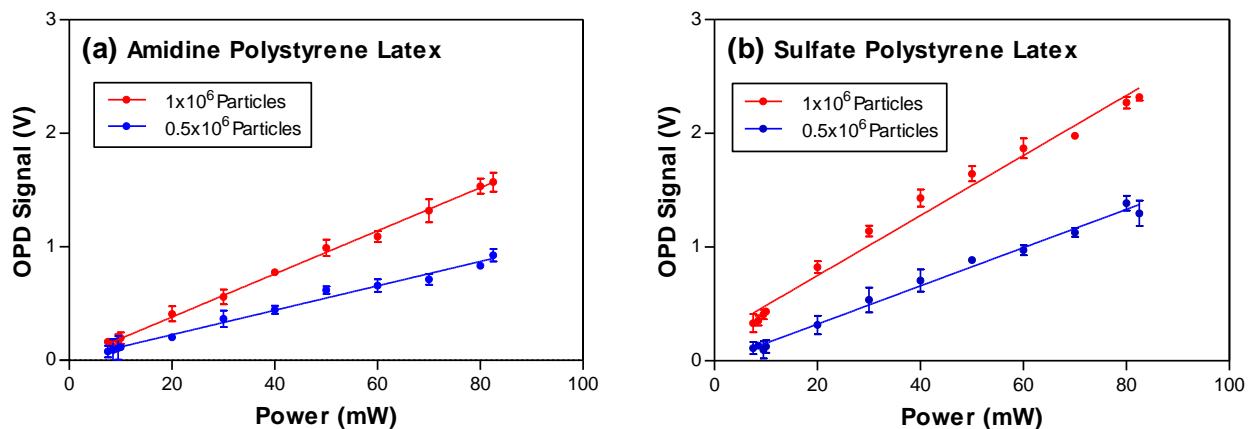


Figure 28: Scattering behaviour of (a) amidine polystyrene latex and (b) sulfate polystyrene latex ( $n = 3$ ).

The experiment was performed at different laser powers from minimum power of 7.5mW to maximum power of 82.5mW. At higher power values, the difference between the materials can be observed more clearly compared to the lower power as shown in Figure 29.

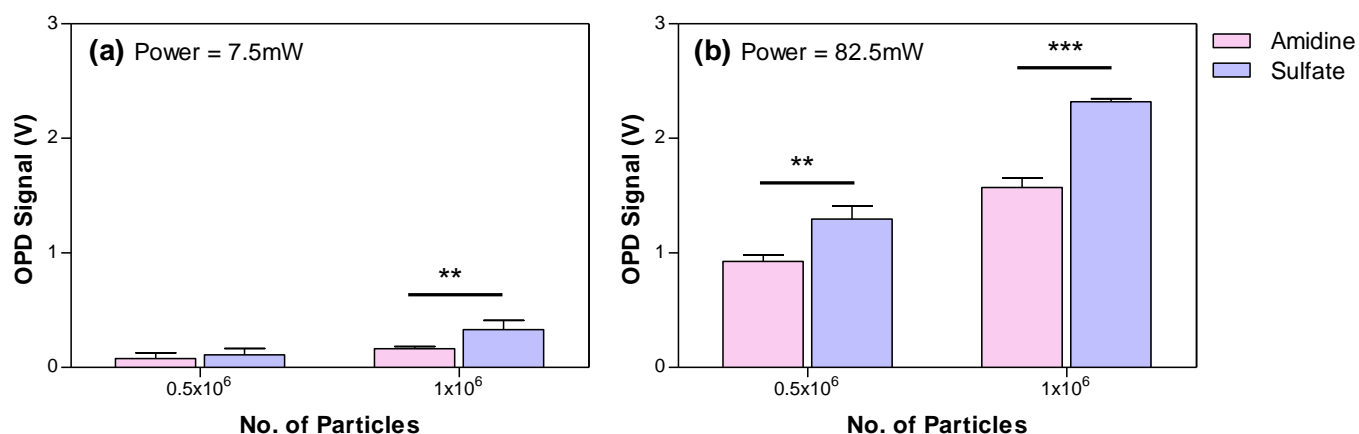


Figure 29: Comparison of 60nm amidine polystyrene latex and sulfate polystyrene latex at power (a) 7.5mW and (b) 82.5mW ( $n = 3$ ).

To calculate the significances, 2-way ANOVA test was applied to all particle numbers with Benferroni post-test, as all the groups were compared with each other at a minimum power of 7.5mW and at a maximum power of 82.5mW. It can be seen in Figure 29(a), that the signals of  $5 \times 10^5$  particles from amidine and sulfate groups were not significantly different. However, it is interesting to note the doubling of the signal and making it significant as the number of particles was doubled. In Figure 29(b), the significant increase in signal from  $5 \times 10^5$  particles at power of 82.5mW could be observed, which was not the case at a power of 7.5mW showing the significance level increases with the increase in power. The OPD signal also increased significantly with  $P < 0.001$  at a power of 82.4mW when  $1 \times 10^6$  particles were observed which was low compared to the particles observed at 7.5mW.

On the basis of above performed experiments it can be extracted that depending upon the cell type, scattering signals would also be different. If the different cell types have same diameter then their membrane composition may influence the scattering signals. The outcome of these experiment was that not only the size, shape, concentration and number of cells are important for light scattering, but the particle material is another important factor that widely contributes in scattering.

#### 4.4 3D-Biosensing of 3D-Hydrogels using LS

Up to this point characterization of the LS system with particles was carried out by embedding them in PBS, however, cells proliferation requires a medium containing nutrients, which could potentially also influence the scattering signals. To determine the effects of 3D-hydrogels as a medium for cells, three different hydrogels were chose, matrigel, fibrin or PEG-dextran. 18 $\mu$ L of each hydrogel was injected into the microchip. After polymerization of the hydrogels, the microchip was inserted into the LS system and scattering effects were observed by determining how the polymer chains of hydrogels influence the scattering signal.

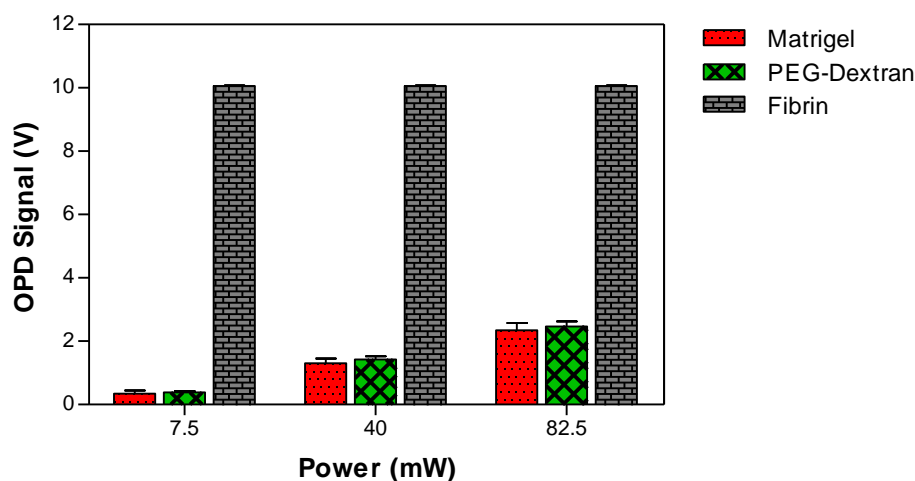


Figure 30: Characterization of the scattering behaviour of 3D-hydrogels, matrigel, PEG-dextran and fibrin (n = 3).

In Figure 30, it can be seen that due to the translucent nature of matrigel and PEG-dextran, their scattering had limited influence on the LS. With increasing power the OPD signal also increased and was comparatively the same for both hydrogels. The 20% fibrin gel already appeared very turbid when it was injected into the microchip and it gave a maximum signal of 10.08V at all power intensities. Afterwards, the fibrin was diluted to 10% and 5% and measured again, however, the scattering signals were still found to be in the overflow range because of its turbidity (data not shown).

The above performed experiment describes the fact that not only the cells show scattering but the other factors such as materials of the particle (as shown in the last experiment) and the nature of the medium in which they are immersed also influence the signals. The refractive index and the constituents of a medium also play a vital role in scattering which was observed by exploiting 3D-hydrogels in the above experiment. Since hydrogels mimic the natural 3D environment for the cells so their utilization is advantageous for 3D cell culture as they are permeable for cell culture media, cell nutrients and their waste products which cells generate during metabolic activities. Hence, while measuring scattering from cells embedded in hydrogel, scattering behaviour of hydrogels needs to be taken into account because the polymer chains of hydrogels also impart in scattering.

As a further step to confirm the above statement and to observe the effects of hydrogels,  $5 \times 10^5$  particles of 794nm diameter were introduced into the three different hydrogels; these were pipetted into separate microchips and measured with the LS system.  $5 \mu\text{m}$  and  $10 \mu\text{m}$  particles were not measured in combination with the gels, as the particles of these sizes were already giving a signal near to the maximum and they would surely give an overflow value, if they were embedded in hydrogels. Scattering effects were measured by utilizing 794nm particles, which were measured at three power levels.

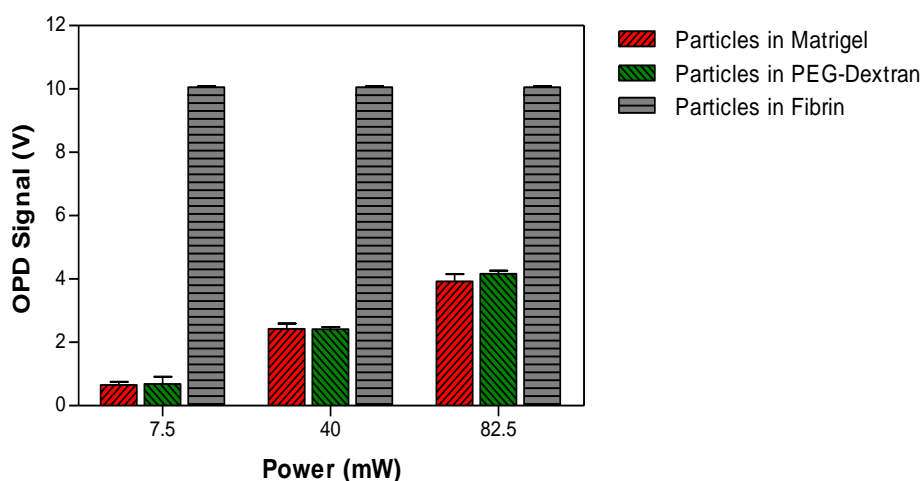


Figure 31: Scattering effects with  $5 \times 10^5$  particles of 794nm diameter in matrigel, PEG-dextran and fibrin.

The comparison of Figure 30 and Figure 31 revealed that particles in hydrogels showed an increased signal compared to hydrogel or particles alone. However, these signals were not only due to the scattering effects of particles but also due to the hydrogel polymer chains that participate in the scattering phenomenon. At a power of 82.5mW, the scattering signal from particles embedded in matrigel and PEG-dextran was close to 4V whereas, at 7.5mW the signals were below 1V and fibrin being turbid enough always showed the same maximum signal of 10.08V. When comparing the signal given by particles only or hydrogel only, a difference can be seen for all three hydrogels vs. particles only in Figure 32. It can be seen very clearly that the signal noted for the particles embedded in the hydrogel is a sum of the individual signals of hydrogels and particles, with the exception of fibrin. This can be seen in Figure 32 that the particles were giving a signal of 1.15V and the scattering response of matrigel was about 2.34V. The sum of the values would be 3.49V, however when particles in matrigel were observed, scattering signal of approximately 3.89V was measured, the difference being negligible. Fibrin was behaving differently because of its turbid appearance. Even without using particles it was showing the maximum signal so with particles it was obvious result but necessary for comparing the variety of gels. Higher number of particles suspended in a medium makes it more turbid which will influence the scattering effects of the light passing through the medium [151]. PEG-dextran and matrigel appeared translucent compared to PBS so the scattering was observed because they were not as transparent as PBS. As the trend of the medium goes towards transparency, the scattering reduces and become even lower for transparent mediums [152]. Hence, from the series of these experiments, it is now clearly understood that transparent and translucent medium or hydrogel provide a good choice to observe scattering phenomenon whereas, opacity restricts the scattering behaviour of light.

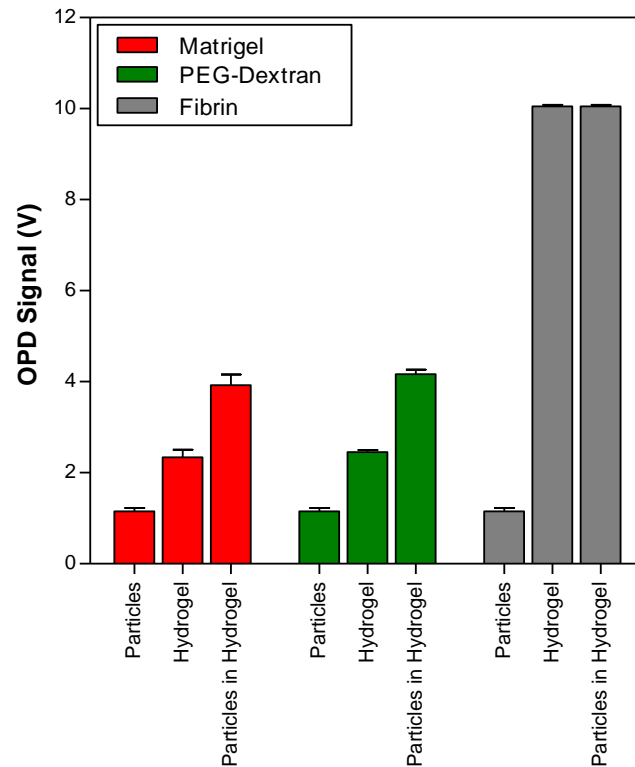


Figure 32: Comparison between the scattering signal of  $5 \times 10^5$  particles of diameter 794nm, hydrogels and similar particle in hydrogels at 82.5mW laser power

From the scattering results obtained for hydrogels, it was concluded that the medium has a great impact on scattering [153]. Hence on the basis of these data, it shows that while observing scattering of cells when they proliferate in hydrogels, its response should also be taken into account.



Figure 33: Difference between transparent, translucent and opaque materials.

#### 4.5 3D-Biosensing of Dead Mouse Embryonic Fibroblasts with LS

Prior to measuring the light scatter of live cells, whose morphology is more spread out, dead cells were measured, which differ from live cells, as they are more round and compact in nature, similar to the innate particles. After utilizing hydrogels and polystyrene particles, dead mouse embryonic fibroblast cells (NIH-3T3) were immersed firstly, in PBS and subsequently in three different hydrogels. These were then pipetted into the microchip which was laid into the LS system. The ultimate goal of characterizing the LS system was to make it reliable for measuring the cell scattering response in 3D microenvironment. Therefore, in this experiment with dead NIH-3T3 the aim was to see the comparability between the size of the particles and the size of the mouse fibroblast and to see if it was feasible to determine the cell size by relating the cell scattering signals to the particle scattering signals.

The data was collected for  $5 \times 10^5$  NIH-3T3 cells in PBS and in each hydrogel, at a minimum power of 7.5mW and the maximum laser power of 82.5mW. The signal from the cells in fibrin was again over the range whereas, in the case of PEG-dextran and matrigel, the signal was about 1V at 7.5mV and approximately 8V at 82.5mW as shown in Figure 34.

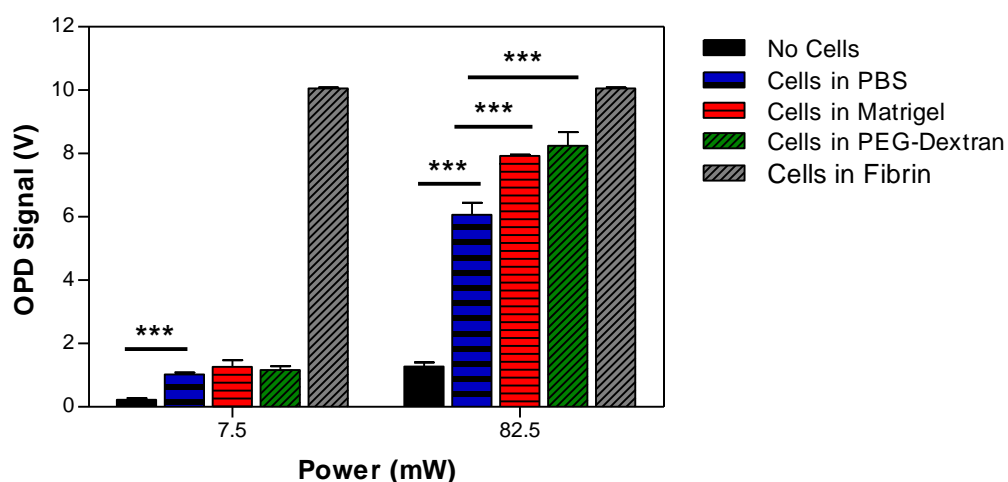


Figure 34: Comparison of NIH-3T3 in PBS and hydrogels at three power levels



2-way ANOVA test was applied to calculate the significance among all groups. At highest power of laser, the signal from cells in PBS became 5-folds compared to the signal at lowest power. Another interesting feature observed in Figure 34 was the significant signal of cells in matrigel and PEG-dextran with respect to the cells in PBS, but only at highest power. This probably be due to the polymer chains which also contribute to the scattering at high laser powers.

From the signal that was obtained from the LS system, another conclusion that can be drawn from this experiment, is about the expected size of the dead cells due to the signal received. By comparing the obtained results from the dead cells with the particles analysis, it can be concluded that the size of the dead NIH-3T3 was less than 5 $\mu$ m particles but higher than 794nm particles as the signals were in-between these two particle sizes at 7.5mW and 82.5mW. This deduction can be made as the number of particles used in the previous experiment and the number of cells used in this experiment are constant, same as the signal of the hydrogels. Using the signal received from the particles at different powers as a calibration curve the size of the cells can be determined. To get a more precise signal comparison, particle larger than 794nm, but smaller than 5 $\mu$ m can be tested.

#### 4.6 3D-Biosensing of Dead Jurkat Cells with LS

After characterization of the system and comparing the signal of dead NIH-3T3 with the signal of innate beads, the aim of the next experiment was to measure the scattering response of dead Jurkat cells by embedding them in 3D-hydrogels. Since Jurkat cells are comparatively smaller compared to NIH-3T3 as their diameter is about 10-13 $\mu\text{m}$  [154], these cells were used to compare their scattering with that of the innate particles in the previous experiments. To determine the scattering signals of Jurkat cells in hydrogels,  $1.25 \times 10^5$ ,  $2.5 \times 10^5$  and  $5 \times 10^5$  cells were mixed with PEG-dextran or matrigel. These were pipetted into the microchip and placed under the LS system for scattering measurement.

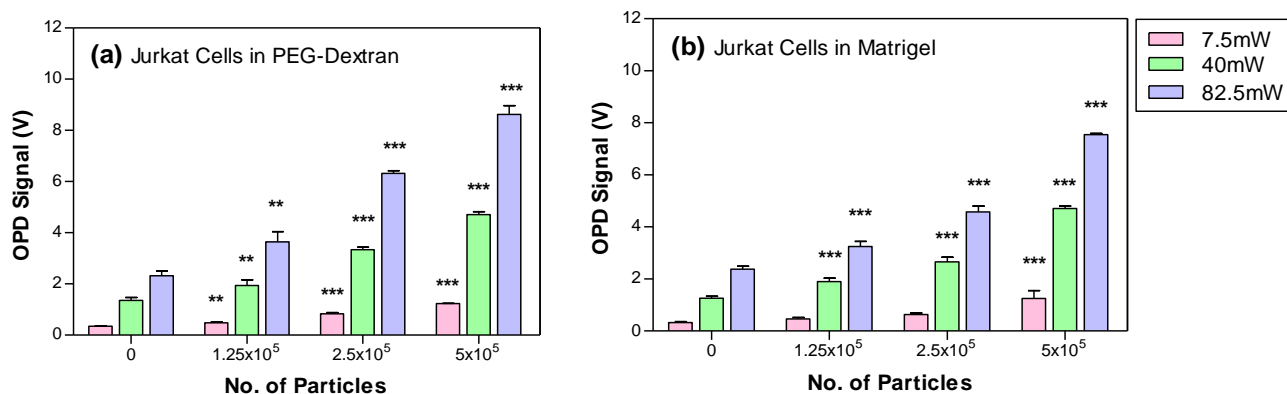


Figure 35: Scattering signals by embedding  $1.25 \times 10^5$ ,  $2.5 \times 10^5$  and  $5 \times 10^5$  Jurkat cells in (a) PEG-dextran and (b) matrigel. \*\* indicates significant difference of  $P < 0.01$  and \*\*\* indicates significant difference of  $P < 0.001$ . Indicated significance is in comparison to zero number of cells.

The results were analysed by 2-way ANOVA test, which showed that all the cell ranges in both hydrogels gave significant signals at 40mW and 82.5mW as shown in Figure 35(a) & (b). The signals were also significant at all power ranges for the cell numbers embedded in PEG-dextran. However, when  $1.25 \times 10^5$  and  $2.5 \times 10^5$  of Jurat cells were mixed in matrigel, they showed no significant scattering signal, however the signal from  $5 \times 10^5$  cells was significantly noticeable.

The diameter of living Jurkat cells is about 10-13 $\mu\text{m}$  [154] but as the cells were dead, the signals were expected to be low as cells shrink when they die [155]. The careful

examination of the data revealed that the scattering can be due to the reduced size of the cells due to shrinkage as the signals were less than the 5 $\mu\text{m}$  particles but higher than 794nm particles. This again can be explained by the fact that particle and cell number was the same in both experiments, as well as the hydrogels used. Comparing the signals received at the same power intensities and using the particle signals as a calibration curve, it can be determined what size the Jurkat cells may have.

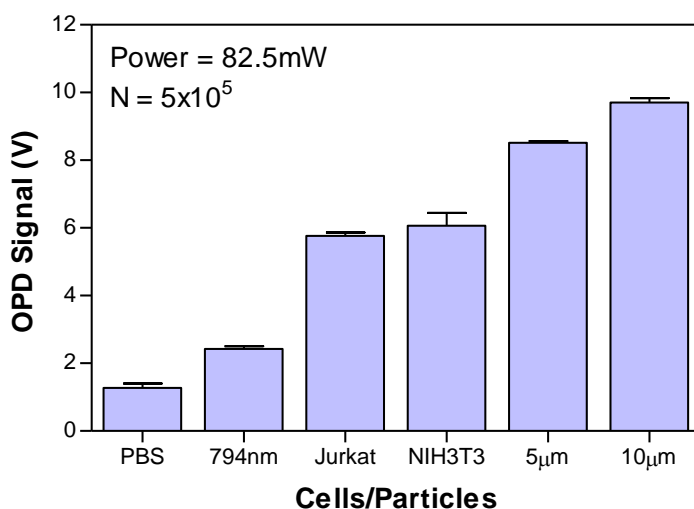


Figure 36: Comparison of scattering signal of NIH-3T3, Jurkat cells with particles of 794nm, 5 $\mu\text{m}$  and 10 $\mu\text{m}$ .

To get a clear view of scattering from dead cells and how they can be compared to the scattering from particles, a comparison of scattering effects by NIH-3T3, Jurkat cells and particles of 794nm, 5 $\mu\text{m}$  and 10 $\mu\text{m}$  suspended in PBS can be seen in Figure 36. The aim of making this comparison of the data obtained from the LS system was to be able to measure different sizes of cells by comparing them with the particle's data and thereby determine and comparing/contrasting their dimensions. . In Figure 36, it can be seen that the signal emitted by PBS only is lower compared to the particles. As the particle and cell number and power remained constant in this experiment, the figure shows nicely an increase in the signal as the size of the particles or cells increase. As mentioned earlier the mouse embryonic fibroblasts and human lymphocytes have a size between 794nm and 5 $\mu\text{m}$ . It is known from literature

that living NIH3T3 cells are approximately 18 $\mu$ m in diameter, whereas Jurkat cells are between 10-13 $\mu$ m. However after cell death, cells are known to shrink, which part of the apoptosis process. Therefore it can be explained why the signal received for dead fibroblasts and lymphocytes is similar, as both were not living during the experiment. In conclusion it can be said that by making a calibration with innate particles with known number in known hydrogels and at fixed power, it is possible to estimate the size of cells by comparison the signals of the two.

#### 4.7 Practical Application: Monitoring Cell Proliferation in Hydrogel

Since the LS system had provided successful results to determine the cell size by keeping the number constant, the next experiment was to look at the signal emitted by living cells during proliferation for a longer extend of time. In order to monitor the proliferation of cells, live chondrocytes were used as they have a similar morphology to the dead cells used in the previous experiments. As this cells were alive, they were able to proliferation in 3D and thereby possibly give a higher signal compared to control. To achieve this aim, the experiment was performed using cartilage-on-a-chip for which equine chondrocytes in the 2<sup>nd</sup> passage were embedded in matrigel. The cell concentrations used in matrigel were 3000cells/ $\mu$ L, 1500cell/ $\mu$ L and 750cells/ $\mu$ L. As a control, a chip was prepared without any cells i.e. only matrigel. The very first measurement was taken half an hour after injecting the chondrocytes into the microchip chambers and leaving the chips into the incubator for polymerization. Afterwards, the data was collected after every second day. The chip having 1500cells/ $\mu$ L showed cell proliferation as can be seen by the increase in signal over 7 days compared to the controlled group and the other two cell concentrations as shown in Figure 37. Interestingly, the signal of cells with a concentration of 750cells/ $\mu$ L remains equal to the control over the 7 days of the experiment. This could be explained by the fact that cells need cell-to-cell contact to receive signals to grow, if they do not receive that, it hinders their proliferation and may result in cell death [156]. Whereas, a cell concentration of 750cells/ $\mu$ L was insufficient for proliferation to occur, a cell concentration of 3000cells/ $\mu$ L seemed too much for the amount of space in the hydrogel, as can be seen by the reduced signal compared to the 1500cells/ $\mu$ L signal.

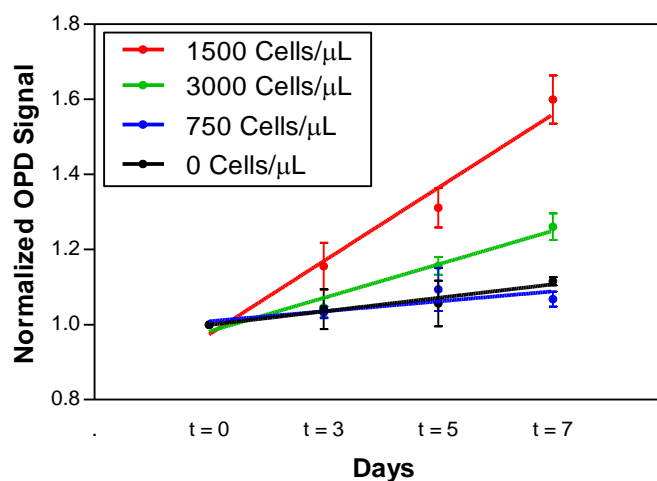


Figure 37: Normalised scattering response of 3000, 1500, 750 and 0 chondrocytes per  $\mu\text{L}$ . The measurements were taken after injecting them into the microchips and then on 3<sup>rd</sup>, 5<sup>th</sup> and 7<sup>th</sup> day ( $n = 3$ ).

In Figure 38, the proliferation of chondrocytes, which have a diameter around  $20\mu\text{m}$  [157], can be seen clearly. From the graph it can be concluded that 1500 chondrocytes/ $\mu\text{L}$  showed better proliferation on every data collection measurement compared to the other two concentrations.

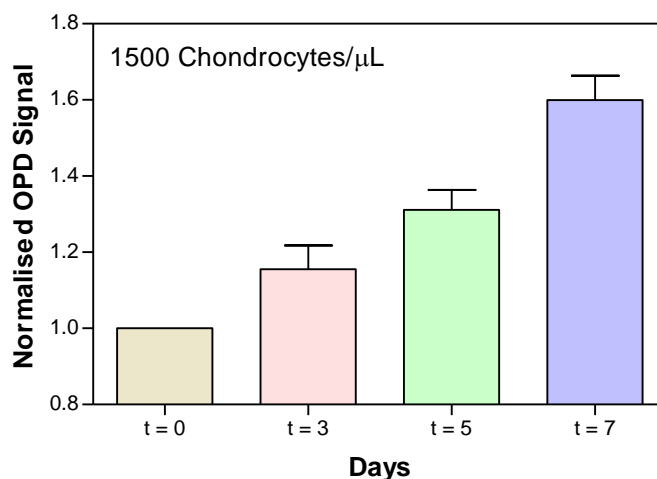


Figure 38: Cell proliferation of 1500chondrocytes/ $\mu\text{L}$  in matrigel ( $n = 3$ ).

It can be interpreted from the obtained results that LS is a powerful tool to detect the proliferation of cells in 3D environment. However, cell number in the given volume of medium or gel is also an important factor in proliferation and for proliferation, cells need to communicate. Cells communicate with each other using chemical signals and cell-to-cell communication [156], which is absolutely essential for multicellular organisms, as they die and do not proliferate if they do not communicate.

#### 4.8 Practical Application: Monitoring Cell Migration in Hydrogel

After successfully measuring the signal of proliferating cells over multiple days, it was interesting to see if migration and invasion could also be measured by the LS system. By studying cell migration and cell invasion through ECM it gives a deep insight into the way leukocytes, for example, migrate through the blood vessel wall into the ECM due to the emission of chemoattractants released by damaged or inflamed cells in need of assistance. Another example of migration is of starved cells, which also move in the direction of nutrients if they are deprived of it. Therefore, the aim of this experiment was to detect the invasion and migration of Jurkat cells by LS system through the polymers of PEG hydrogel by depriving cells of nutrients and attracting the cells with a full-nutrient medium, which was situated on the opposite side of the hydrogel. The microfluidic chip provided three connected chambers; the left chamber was filled with 1000 cells/ $\mu\text{L}$  in starvation medium without FBS, the middle chamber was filled with 3% or 20% PEG hydrogel gel and the right chamber was filled with a medium containing FBS, which acted as a chemoattractant. Cell invasion and migration was observed every hour up to 5 hours.

Figure 39 are images taken of Jurkat cells stained with Hoechst stain to observe how many cells migrate into the hydrogel depending on the medium the cells were in, the PEG concentration and the presence of a chemoattractant in the right chamber. In Figure 39(a) it can be clearly seen that more cells which were suspended in starvation medium were able to move towards the chemoattractant through a 3% PEG hydrogel compared to few cells in a 20% PEG hydrogel (Figure 39(b)). Figure 39(c), (d), (e) and (f) are negative controls; here some cells can be seen in the hydrogel but less in quantity compared to the image Figure 39(a). This also shows the natural inclination of cells to migrate into a 3D structure compared to adhering to a flat surface.



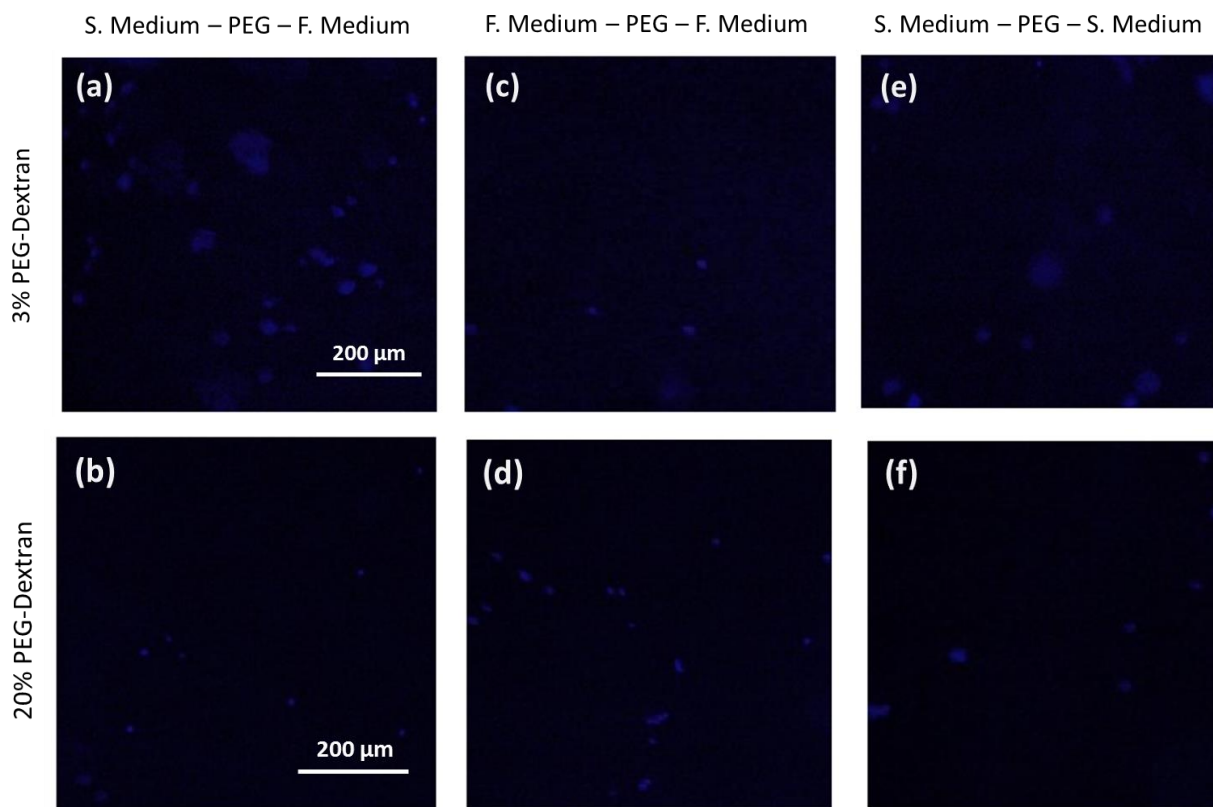


Figure 39: Microscopic images of Jurkat cells migration through 3% and 20% PEG-dextran.

The results in Figure 40(a) show that 3% PEG-dextran gel allows more cells to invade and migrate through its polymer chains compared to the 20% PEG. Due to the high strength of PEG-link in the hydrogel, it hardens more compared to a 3% PEG and therefore, does not allow the cells to pass through its pores. Another parameter that can influence the cell migration through hydrogel is the chemical concentration. As can be seen in microscopic images, the Jurkat cells in starvation medium started migrating towards the full medium whereas, the cells embedded in full medium did not show invasion in hydrogels as no gradient of chemoattractant existed. Figure 40(b) shows that the Jurkat cells already in full medium did not show promising feature of migration as they have enough nutrients in full medium. Only

few of the cells that might be close to the hydrogel tried to invade through the hydrogel which can also be observed in Figure 39(d).

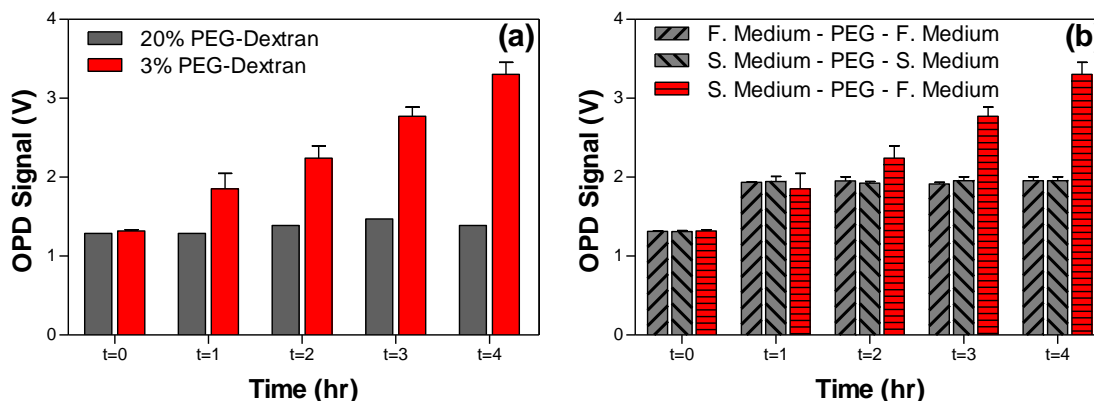


Figure 40: (a) Jurkat cell migration through 3% and 20% PEG-dextran hydrogel from cells in starvation medium (S. Medium) towards the full medium (F. Medium) whereas (b) represents the comparison of migration of cells in starvation/full medium towards the full/starvation medium.

Since cell movement is critical to a variety of developmental processes and the effects of various agents to determine cell movement can be measured using different in vitro chemotactic assays. Invasive cells move through the ECM into neighbouring tissues in a process that involves ECM degradation and proteolysis. On the basis of above performed experiment, it can be said that the LS system offers a remarkable contribution to study migration of cells.

## 5. Summary and Conclusion

The LS system is an ideal system due to its non-contact, rapid response and high sensitivity. Microfluidic devices would become more efficient if they were coupled with LS detection systems, due to their reactivity and down scaling of samples. Therefore, the goal of the presented work was to characterize the LS system and make it operational for determining the cellular morphology, viability, proliferation and migration in 3D microenvironment. Firstly the functionality of the laser beam splitting into four channels was verified. Secondly, the maximum detection capacity of the OPD sensors was tested. In a final step, before beginning the experiment, three different microchip designs were assessed for usability. Thirdly, the temperature in the water bath ideal for the cells, inserted in the microchip, was adjusted. Prior to applying the system on cells, multiple experiments were carried out to understand the system and create a calibration with known particles. Particles of various diameters were mixed in PBS or embedded in hydrogel first to see how size, concentration, number and material influenced scattering signal. As hydrogels and cell culture medium also show scattering, those were investigated on their own as well. Data from this and previous experiment could potentially be used as a calibration, to compare cell signals to particle data and thereby get derive different information. As dead cells conventionally have a round structure before bursting, the scattering signal of dead NIH-3T3 and dead Jurkat cells was registered and related to the particle signals. Once the particle data was successfully translated onto dead cells, cell proliferation was investigated by utilizing live chondrocytes, in addition to observing migration through a 3D-hydrogel by live Jurkat cells suspended in medium.

LS system was complemented with OPD sensors, as they possess beneficial attributes such as low processing temperature and more flexibility and compatibility due to fabrication with glass or plastic compared to their inorganic variant detectors [158]. Besides yielding high sensor activity, the spray coating of OPD also provides a high extent of fabrication freedom to vary the sensor height, area and overall geometry as observed by Charwat et al. in [92]. Not only are the sensitive sensors

able to monitor the cellular activity but also external factors like temperature and pH changes, which are critical for cell survival. Keeping the temperature regulated is essential as its fluctuation influences the form of the cells [159] as well as the cross-linking density of the hydrogel which impacts the scattering pattern [160]. Virtually every important structure and function in the cell, such as molecular motor activity and polymerisation velocity of actin filament, are temperature sensitive [161, 162]. Experiments carried out by the group of Kessling et al. showed that an increase in temperature led to a reduced viscosity and increase elasticity of the cytosol and protein structures in the cell membrane causing a deformation of the cell. This change can vary the scattering signals obtained at different time points and give misleading results. The same can be said for hydrogels, as their strength is dependent on the swelling of the polymer chains and their crosslinking. Earlier studies have shown that a rise in temperature of 3°C leads to variation in the cross-links of hydrogels, although there may be local swelling equilibrium [163, 164]. Dogu et al. (2002) argues that this variation could be based on the assumption that there is some inhomogeneity in the cross-linking density of the gel. So when temperature rises, the osmotic pressure decreases, while chain elasticity remains constant. Consequently, dense cross-linked regions de-swell, whereas less densely cross-linked regions don't, which causes a change in the scattering pattern of the whole gel. Therefore, it is crucial to keep the temperature steady as huge variations cause a change in cellular structure and hydrogel strength skewing data.

Once the laser, OPD sensors and temperature of the LS system was calibrated, the scattering of polystyrene particles with different diameter of 46nm, 794nm, 5µm and 10µm was collected. Hence, the basic aim of determining scattering response of different sizes of particles was to observe what size of particle corresponds to what type of cell or its organelles as cell size has always been an important issue. From the performed experiments it can be deduced that corresponding to particle sizes, various cell types according to their sizes would generate different scattering signals as was observed in case of particles where 46nm particles showed Rayleigh scattering and 794nm, 5µm and 10µm particles belong to Mei scattering regime. Hence the LS system can be exploited to study the cellular morphology as

suggested in the literature where average cell sizes and shapes were compared by light scattering with electron and light microscopy [165]. The assessment of cell morphology (size, shape and surface) is the first indicator for the evaluation of the health status of a cell culture [166]. According to Rayleigh theory, if the particles are smaller than the wavelength of incident beam then dipole separation would be much smaller than the wavelength, because of which the phase differences would become smaller and scattering would be roughly the same in all directions [127]. Rayleigh theory is considered as a special case of Mie theory provided that the size of the particles is small enough. In general, particles having a size  $1/10^{\text{th}}$  of the wavelength show symmetric scattering in all direction and lie in Rayleigh regime [167] however, if the size is  $1/4^{\text{th}}$  of the wavelength then forward scattering would be higher and it goes on increasing as this ratio becomes lower and ultimately enters into the Mie scattering regime. From this it can be concluded that the scattering of the 46nm cannot be seen as reliable data as there is scattering in all directions and not in the forward direction which could not be properly detected by the OPD sensor.

Afterwards different concentration of particles were measured at different powers and the results were compared to the scattering of the number of particles. The signals measured at different concentrations gave significant results, however the signal was not linear to the doubling of the concentration. This was in contrast to the outcome of the experiments performed with particle numbers where the signal increased proportionally to the increase in particle number. Nurse et al. studied that the basic processes of cell physiology, for example, flux across membranes, is dependent on cell size and their number [168]. Different kinds of injuries may cause cells to die either via necrosis or by apoptosis [169] and ultimately, the cell size, number and consistency is affected. In the case of measuring cellular metabolism after some stimuli or a couple of days in culture, if the cell number is not known, it is difficult to deduce if metabolism of the cells has increased or if cells have proliferated and therefore a higher metabolism is being detected [170]. On the basis of these facts, cell number is another important factor that can influence the signal. From the data produced by LS system, it can be derived that the number of scattered particles

is directly proportional to the area of cross section of the target particles [149] by a relation of

$$N_{scatter} = N_{incident} \frac{(\sigma_{target})_{Total}}{A} \quad 5.1$$

where  $(\sigma_{target})_{Total}$  is the total cross sectional area and  $A$  is the area of the assembly of the target particles,  $N_{scatter}$  and  $N_{incident}$  are the number of scattered and incident particles respectively. This means that the increase in signal by increasing particle size and keeping their number constant has been mathematically proven. The bigger the particles the more they scatter in the forward direction relative to the backward direction. For larger particles, firstly the fine-scale measurement of scattering from the microstructure surface needs to be considered and then integrate over the larger scale structure. Based on the results collected from these experiments, it can be said that if the number of cells is known than LS offers a suitable choice by which cellular size and their activities can be judged. It provides an efficient tool for studying cell morphology as during adherence the morphology of the cells of same type changes significantly and LS systems has a benefit that it can produce a specific signal with a specific cells count in a precise way and describes the structural information. Therefore, using the number of particles instead of concentration of particles is a more reliable parameter to consider when measuring cell size with a LS system, as it gave a linear response.

Verifying the limit of detection illustrated the sensitivity of the LS system. Scattering responses could be registered using low number of particles, however the signal was very low. To be able to quantify the limit of detection, two different calculation methods were tested. The first was based on multiplying the standard deviation of the blank three times and adding to the mean of blank. Although this is a simple calculation, it is a weak method as it does not take into consideration the signal of the least number of particles, which may be well over the blank [146]. For this reason, a second calculation method was applied which took into account the linear regression of the particles measured by multiplying the standard deviation of the y-intercept by three and divided it by the slope. Another advantage of this formula was

that it gave the number of particles at which limit of detection would be in comparison to the first method where the least signal measured with blank was given. Number of particles used in each replicating experiment is a more reliable and constant parameter compared to signal, as this may deviate from analysis to analysis. By knowing the particle number it can be concluded that while measuring low amount of particles or cells a higher power should be used, whereas a low power can be used to detect high number of particles or cells.

Other factors that influence the scattering signal are the surface of cells, the nature and strength of the medium, in which they are immersed. The performed experiments showed that depending on the surface of the material scattering changes. To evaluate this, scattering from sulfate polystyrene latex particles was compared to the amidine polystyrene latex particles and found that scattering in case of sulfate is higher due its acidic nature compared to amidine particles. In a study done by Marina et al. [171] they showed that by applying acetic acid to tumorigenic cells, it reduced the pH-value due to which the light scattering also enhanced, proving that acidity increases the scattering effect. On the basis of this literature, it can be said that being a strong acid, the sulfate group may have reduced the pH of PBS whereas, amidine is a weak base which may have increased the pH of PBS and made it basic. In case of sulfate group, the acid dissociation constant,  $pK_a < 2$  and smaller  $pK_a$  value leads to a stronger acid [172]. On the other hand, amidine functional groups are basic in nature and have a base dissociation constant value of,  $pK_b \approx 10-11$ , which shows that it is a weak base [173]. When mixed with PBS, it also becomes basic by increasing the pH-value of PBS. The acidic solutions lower pH-values and thus increasing the turbidity of the solution and giving a higher scattering signal as suggested in literature where RNA solution with pH-value of 5.5 increases the turbidity of solution [174, 175]. From this it can be concluded that not the cell membrane itself influences forward scattering (Meyer, 1979), however the acidic or basic components protruding from the membrane can influence scattering.

The constituents of a medium also play a vital role in scattering which was observed by exploiting 3D-hydrogels. Not only do the particles but also the medium, in which

particles are embedded, take part in scattering [176] which was studied by utilizing different 3D-hydrogels. It is important to analyse the scattering of hydrogels, as in life sciences, cell culture techniques are generally used for removing cells or tissues from an organs and subsequently placing them into an artificial environment, suitable for their survival and proliferation. For the optimal growth of cells, basic environmental requirements include appropriate growth medium [177]. A culture medium or growth medium supports the growth of cells and it can either be a liquid or hydrogel which are usually designed to support the cells over longer period of time. To see the influence of hydrogels in scattering, the performed experiments concluded that fibrin gel was not a suitable candidate to observe scattering effects due to its opacity whereas, matrigel and PEG-dextran showed promising features to see scattering behaviour of cells embedded in hydrogels. Hence, while measuring scattering from cells embedded in hydrogel, scattering behaviour of hydrogels needs to be taken into account because their polymer chains also take part in scattering as Wang et al. in [178] suggested that due to swelling behaviour of polymers, the diffusion process through polymers becomes faster which affects the scattering dynamics. This indicates how the 3D cell culture medium can influence the scattering measurements.

As a further step after characterizing the LS system with various particles, dead NIH-3T3 and dead Jurkat cells were used to notice the morphology of these cells. Literature suggested that living NIH-3T3 cells have a diameter of  $18\mu\text{m}$  [179] and living Jurkat cells are about  $10\text{-}13\mu\text{m}$  [154] however, the generated results do not even correspond to the scattering of  $10\mu\text{m}$  particles. The living fibroblasts have elongated structure with spindles but when they die they start shrinking and become round. It may be possible that either the size determined through light scattering is of the shrunken dead cells or that they burst due to apoptosis [155] and the organelles like mitochondria, lysosomes, nuclei and vacuoles inside the cell membrane were released. Marina et al. studied side scattering from fibroblasts and cervical carcinoma cells and concluded that among other organelles, lysosomes and nuclei are the main contributors in light scattering respectively, when studied with a source wavelength of  $785\text{nm}$  [180]. Another important study by Mourant et al. utilized



polystyrene particles to validate backscattering effects and reached to the conclusion that scattering of visible light from cells is governed by the size and composition of intracellular organelles structures smaller than nuclei are the major contributors in light scattering [181]. Since the diameter of mitochondria in mammalian cells is round about 0.75-3 $\mu$ m which is smaller than the diameter of nuclei [182], so the signals could probably be emerging from the mitochondria of the dead mouse fibroblasts [183] and dead Jurkat cells. However, until further experiments are not done to confirm if organelles were present in the suspension, this assumptions stays open to debate.

As a next step after utilizing dead cells, proliferation of line chondrocytes was examined for a whole week by embedding them in matrigel. It was concluded that 1500cells/ $\mu$ L showed good proliferation results compared to other concentrations. The other concentrations exhibited less proliferation either due to less or too many cells. Biological cells communicate with each other using chemical signals and cell-to-cell communication [156], which is absolutely essential for multicellular organisms, as they die if they do not communicate. The performed experiment indicates another promising feature of monitoring cell proliferation through LS system. In literature, forward light scattering was implemented to note the activation and proliferation for screening cytokine and drug effects on human T-cells by Böhmer et al. [184]. Another study used chondrocytes of rabbit to determine their adhesion and vascularization capabilities by mixing CECM powder in matrigel and injected it into mice [185]. Hence, from the evidences available in literature, the given LS system was exploited to see the proliferation response of chondrocytes in matrigel and it showed the expected results.

As a final experiment, migration of live Jurkat cells were examined in synthetic hydrogel by varying the gel strength. It was concluded that the link between polymer chains effects the migration of cells as less cells were present in the 20% PEG compared to the 3% PEG. Regulated cell movement is critical to those processes associated with an effective immune response. Unregulated cell movement can cause abnormalities and neoplasia, and can trigger autoimmune disease. Cell migration occurs by directed interaction of cells with extracellular matrix,

neighbouring cells or chemoattractants in response to gradients. In the microchip model used the chemoattractant was placed on one side of the hydrogel, which then diffused into it towards the cells on the other side forming a linear gradient. The cells were prompted to move toward the increasing concentrations into and through the hydrogel. In literature, endothelial cells migration through HA-Collagen hydrogel was studied by varying growth factor gradients and strength of hydrogel by Jeong et al. [186] in a microfluidic system. In another example chemoattractants CXCL11 and CXCL12 influence the invasion of T-cells when they were placed on the top of hydrogel in a well plate [187]. Thus using a suitable chemoattractant can influence the cells to migrate across the hydrogel if the suitable concentration of chemoattractant is supplied for the cells. This experiment governs the novelty of LS system as it can also be utilized to determine the cell migration through hydrogels. Signals recorded each hour over 5 hours, showed how the scattering signal, due to increasing cell number inside the hydrogel, intensified. In the future when enough particle number calibrations data will be collected, a comparison of the signals, could facilitate the estimation of the number of cells which migrated into the hydrogel over time. This could be confirmed by staining the cells and counting them under the microscope and thereby the calculation of their migration velocity would also be possible.

To enable prospective measurements, characterization by utilizing different shaped particles will have to be adapted. By analysing the signals from different shapes, the data obtained from the system could be evaluated more realistically as the cells are not always round. Also, using larger particles will allow to further extend the system capabilities however, before using particles larger than 10 $\mu$ m either the range of the detecting signal needs to be increased or the laser power should be set lower. In order to make the system more sensitive, scattering signals from the sides of the microchip can also be determined by employing the scattering sensors on the sides of the microchip, as in three-dimensional environment, particles scatter the light in all direction.

All in all the LS detection system for the evaluation of cellular morphology and proliferation is a promising technique, which will open up many possibilities and it is a step further in complementing the lab-on-a-chip technology.

---

## 6. Bibliography

1. Schwarz, M.A. and P.C. Hauser, *Recent developments in detection methods for microfabricated analytical devices*. Lab on a Chip, 2001. **1**(1): p. 1-6.
2. Vandelli, N., et al., *Development of a MEMS microvalve array for fluid flow control*. Journal of Microelectromechanical Systems, 1998. **7**(4): p. 395-403.
3. Kovarik, M.L., et al., *Micro total analysis systems: fundamental advances and applications in the laboratory, clinic, and field*. Analytical chemistry, 2013. **85**(2): p. 451-472.
4. Lisowski, P. and P.K. Zarzycki, *Microfluidic paper-based analytical devices ( $\mu$ PADs) and micro total analysis systems ( $\mu$ TAS): development, applications and future trends*. Chromatographia, 2013. **76**(19): p. 1201-1214.
5. Lee, S.J. and S.Y. Lee, *Micro total analysis system ( $\mu$ -TAS) in biotechnology*. Applied Microbiology and Biotechnology, 2004. **64**(3): p. 289-299.
6. Kovarik, M.L., et al., *Micro total analysis systems for cell biology and biochemical assays*. Analytical Chemistry, 2012. **84**(2): p. 516-540.
7. Vilknier, T., D. Janasek, and A. Manz, *Micro total analysis systems. recent developments*. Analytical Chemistry, 2004. **76**(12): p. 3373-3386.
8. Yang, D.K., S. Leong, and L.L. Sohn, *High-throughput microfluidic device for circulating tumor cell isolation from whole blood*. Micro total analysis systems, 2015. **2015**: p. 413-415.
9. Bhatia, S.N. and D.E. Ingber, *Microfluidic organs-on-chips*. Nat Biotech, 2014. **32**(8): p. 760-772.
10. van der Helm, M.W., et al., *Microfluidic organ-on-chip technology for blood-brain barrier research*. Tissue Barriers, 2016. **4**(1): p. e1142493.
11. Moraes, C., et al., *Organs-on-a-chip: a focus on compartmentalized microdevices*. Ann Biomed Eng, 2012. **40**(6): p. 1211-27.
12. Kastrup, C.J., et al., *Using chemistry and microfluidics to understand the spatial dynamics of complex biological networks*. Acc Chem Res, 2008. **41**(4): p. 549-58.
13. Kim, D., et al., *Microfluidics-based in vivo mimetic systems for the study of cellular biology*. Acc Chem Res, 2014. **47**(4): p. 1165-73.
14. Khademhosseini, A., et al., *Microscale technologies for tissue engineering and biology*. Proc Natl Acad Sci U S A, 2006. **103**(8): p. 2480-7.
15. Shander, A., et al., *A new perspective on best transfusion practices*. Blood Transfusion, 2013. **11**(2): p. 193-202.
16. Basu, D. and R. Kulkarni, *Overview of blood components and their preparation*. Indian Journal of Anaesthesia, 2014. **58**(5): p. 529-537.
17. Kempton, C.L. and G.C. White, *How we treat a hemophilia A patient with a factor VIII inhibitor*. Blood, 2009. **113**(1): p. 11-17.
18. Cartotto, R. and J. Callum, *A review of the use of human albumin in burn patients*. J Burn Care Res, 2012. **33**(6): p. 702-17.
19. Blumberg, N., et al., *Platelet transfusion and survival in adults with acute leukemia*. Leukemia, 2007. **22**(3): p. 631-635.
20. Levy, Y.S., et al., *Embryonic and adult stem cells as a source for cell therapy in Parkinson's disease*. J Mol Neurosci, 2004. **24**(3): p. 353-86.
21. Griesenbach, U. and E.W. Alton, *Progress in gene and cell therapy for cystic fibrosis lung disease*. Curr Pharm Des, 2012. **18**(5): p. 642-62.
22. Van Dyke, D.C., et al., *Cell therapy in children with Down syndrome: a retrospective study*. Pediatrics, 1990. **85**(1): p. 79-84.

23. Pirnay, J.-P., et al., *Access to human tissues for research and product development: From EU regulation to alarming legal developments in Belgium*. EMBO Reports, 2015. **16**(5): p. 557-562.
24. Coleman, R.A., *Human tissue in the evaluation of safety and efficacy of new medicines: a viable alternative to animal models?* ISRN Pharmaceuticals, 2011. **2011**: p. 806789.
25. Ikada, Y., *Challenges in tissue engineering*. Journal of the Royal Society Interface, 2006. **3**(10): p. 589-601.
26. Frantz, C., K.M. Stewart, and V.M. Weaver, *The extracellular matrix at a glance*. Journal of Cell Science, 2010. **123**(24): p. 4195-4200.
27. Meredith, J.E., B. Fazeli, and M.A. Schwartz, *The extracellular matrix as a cell survival factor*. Molecular Biology of the Cell, 1993. **4**(9): p. 953-961.
28. Caliarì, S.R. and J.A. Burdick, *A practical guide to hydrogels for cell culture*. Nat Meth, 2016. **13**(5): p. 405-414.
29. Edmondson, R., et al., *Three-dimensional cell culture systems and their applications in drug discovery and cell-based biosensors*. Assay Drug Dev Technol, 2014. **12**(4): p. 207-18.
30. Birgersdotter, A., R. Sandberg, and I. Ernberg, *Gene expression perturbation in vitro--a growing case for three-dimensional (3D) culture systems*. Semin Cancer Biol, 2005. **15**(5): p. 405-12.
31. Bhadriraju, K. and C.S. Chen, *Engineering cellular microenvironments to improve cell-based drug testing*. Drug Discov Today, 2002. **7**(11): p. 612-20.
32. Baharvand, H., et al., *Differentiation of human embryonic stem cells into hepatocytes in 2D and 3D culture systems in vitro*. Int J Dev Biol, 2006. **50**(7): p. 645-52.
33. Yang, L., et al., *Cell-based sensing: From 2D to 3D cell culture*. Meeting Abstracts, 2014. **MA2014-02**(10): p. 660.
34. Sánchez-Romero, N., et al., *In vitro systems to study nephrotoxicity: 2D versus 3D models*. European Journal of Pharmacology, 2016. **790**: p. 36-45.
35. DesRochers, T.M., et al., *Bioengineered 3D human kidney tissue, a platform for the determination of nephrotoxicity*. PLoS ONE, 2013. **8**(3): p. e59219.
36. Ravi, M., et al., *3D cell culture systems: advantages and applications*. J Cell Physiol, 2015. **230**(1): p. 16-26.
37. Kopeček, J., *Hydrogel biomaterials: a smart future?* Biomaterials, 2007. **28**(34): p. 5185-5192.
38. Oyen, M.L., *Mechanical characterisation of hydrogel materials*. International Materials Reviews, 2014. **59**(1): p. 44-59.
39. *Hydrogel Swelling: [www.slideshare.net](http://www.slideshare.net)*.
40. Ahmed, E.M., *Hydrogel: preparation, characterization, and applications: a review*. Journal of Advanced Research, 2015. **6**(2): p. 105-121.
41. Martin, B.D., R.J. Linhardt, and J.S. Dordick, *Highly swelling hydrogels from ordered galactose-based polyacrylates*. Biomaterials, 1998. **19**(1): p. 69-76.
42. Mohd Amin, M.C.I., et al., *Synthesis and characterization of thermo- and pH-responsive bacterial cellulose/acrylic acid hydrogels for drug delivery*. Carbohydrate Polymers, 2012. **88**(2): p. 465-473.
43. Förster, S. and M. Antonietti, *Amphiphilic Block Copolymers in Structure-Controlled Nanomaterial Hybrids*. Advanced Materials, 1998. **10**(3): p. 195-217.
44. Ray, D., et al., *Comparative delivery of diltiazem hydrochloride through synthesized polymer: hydrogel and hydrogel microspheres*. Journal of Applied Polymer Science, 2010. **116**(2): p. 959-968.
45. Gacesa, P., *Alginates*. Carbohydrate Polymers, 1988. **8**(3): p. 161-182.

46. Yokoyama, F., et al., *Morphology and structure of highly elastic poly(vinyl alcohol) hydrogel prepared by repeated freezing-and-melting*. Colloid and Polymer Science, 1986. **264**(7): p. 595-601.
47. Sperinde, J.J. and L.G. Griffith, *Synthesis and characterization of enzymatically-cross-linked poly(ethylene glycol) hydrogels*. Macromolecules, 1997. **30**(18): p. 5255-5264.
48. McGrath, K.P., et al., *Genetically directed syntheses of new polymeric materials. Expression of artificial genes encoding proteins with repeating -(AlaGly)<sub>3</sub>ProGluGly- elements*. Journal of the American Chemical Society, 1992. **114**(2): p. 727-733.
49. Zu, Y., et al., *Preparation and characterization of chitosan-polyvinyl alcohol blend hydrogels for the controlled release of nano-insulin*. International Journal of Biological Macromolecules, 2012. **50**(1): p. 82-87.
50. Zhao, W., et al., *Degradable natural polymer hydrogels for articular cartilage tissue engineering*. Journal of Chemical Technology & Biotechnology, 2013. **88**(3): p. 327-339.
51. McKinnon, D.D., A.M. Kloxin, and K.S. Anseth, *Synthetic hydrogel platform for three-dimensional culture of embryonic stem cell-derived motor neurons*. Biomaterials Science, 2013. **1**(5): p. 460-469.
52. Waldeck, H. and W.J. Kao, *Effect of the addition of a labile gelatin component on the degradation and solute release kinetics of a stable PEG hydrogel*. Journal of biomaterials science. Polymer edition, 2012. **23**(12): p. 1595-1611.
53. Akhtar, M.F., M. Hanif, and N.M. Ranjha, *Methods of synthesis of hydrogels ... A review*. Saudi Pharmaceutical Journal.
54. Miyata, T., N. Asami, and T. Uragami, *Preparation of an Antigen-Sensitive Hydrogel Using Antigen-Antibody Bindings*. Macromolecules, 1999. **32**(6): p. 2082-2084.
55. Kleinman, H.K., et al., *Isolation and characterization of type IV procollagen, laminin, and heparan sulfate proteoglycan from the EHS sarcoma*. Biochemistry, 1982. **21**(24): p. 6188-93.
56. Orkin, R.W., et al., *A murine tumor producing a matrix of basement membrane*. J Exp Med, 1977. **145**(1): p. 204-20.
57. Hadley, M.A., et al., *Extracellular matrix regulates Sertoli cell differentiation, testicular cord formation, and germ cell development in vitro*. J Cell Biol, 1985. **101**(4): p. 1511-22.
58. Kubota, Y., et al., *Role of laminin and basement membrane in the morphological differentiation of human endothelial cells into capillary-like structures*. J Cell Biol, 1988. **107**(4): p. 1589-98.
59. Ehrbar, M., et al., *Endothelial cell proliferation and progenitor maturation by fibrin-bound VEGF variants with differential susceptibilities to local cellular activity*. Journal of Controlled Release, 2005. **101**(1-3): p. 93-109.
60. Weisel, J.W., *Fibrinogen and fibrin*. Adv Protein Chem, 2005. **70**: p. 247-99.
61. Eyrich, D., et al., *Long-term stable fibrin gels for cartilage engineering*. Biomaterials, 2007. **28**(1): p. 55-65.
62. Mol, A., et al., *Fibrin as a cell carrier in cardiovascular tissue engineering applications*. Biomaterials, 2005. **26**(16): p. 3113-21.
63. Cakmak, O., et al., *Injectable tissue-engineered cartilage using commercially available fibrin glue*. Laryngoscope, 2013. **123**(12): p. 2986-92.
64. Albrecht, D.R., et al., *Multiphase electropatterning of cells and biomaterials*. Lab on a Chip, 2007. **7**(6): p. 702-709.
65. Burkert, S., et al., *Cross-linking of poly(N-vinyl pyrrolidone) films by electron beam irradiation*. Radiation Physics and Chemistry, 2007. **76**(8-9): p. 1324-1328.

- 
66. Chao, G., et al., *Preparation and characterization of pH sensitive semi-interpenetrating network hydrogel based on methacrylic acid, bovine serum albumin (BSA), and PEG*. Journal of Polymer Research, 2006. **13**(5): p. 349-355.
  67. Novin, M.G., et al., *In vitro application of Matrigel enhances human blastocyst formation and hatching* Iranian Journal of Reproductive Medicine, 2007. **5**(3): p. 103-107.
  68. Ratnalingam, V., et al., *Fibrin adhesive is better than sutures in pterygium surgery*. Cornea, 2010. **29**(5): p. 485-489.
  69. Bezemer, J.M., et al., *Zero-order release of lysozyme from poly(ethylene glycol)/poly(butylene terephthalate) matrices*. Journal of Controlled Release, 2000. **64**(1-3): p. 179-192.
  70. Mullen, P., *The use of matrigel to facilitate the establishment of human cancer cell lines as xenografts*, in *Cancer Cell Culture: Methods and Protocols*, S.P. Langdon, Editor. 2004, Humana Press: Totowa, NJ. p. 287-292.
  71. Ryu, J.H., et al., *Implantation of bone marrow mononuclear cells using injectable fibrin matrix enhances neovascularization in infarcted myocardium*. Biomaterials, 2005. **26**(3): p. 319-326.
  72. Hovgaard, L. and H. Brøndsted, *Dextran hydrogels for colon-specific drug delivery*. Journal of Controlled Release, 1995. **36**(1): p. 159-166.
  73. Fridman, R., et al., *Enhanced tumor growth of both primary and established human and murine tumor cells in athymic mice after coinjection with Matrigel*. J Natl Cancer Inst, 1991. **83**(11): p. 769-74.
  74. Chen, W., et al., *Umbilical cord stem cells released from alginate-fibrin microbeads inside macroporous and biofunctionalized calcium phosphate cement for bone regeneration*. Acta Biomaterialia, 2012. **8**(6): p. 2297-2306.
  75. Sun, G., et al., *Dextran hydrogel scaffolds enhance angiogenic responses and promote complete skin regeneration during burn wound healing*. Proceedings of the National Academy of Sciences, 2011. **108**(52): p. 20976-20981.
  76. Li, L., et al., *A nanostructured conductive hydrogels-based biosensor platform for human metabolite detection*. Nano Letters, 2015. **15**(2): p. 1146-1151.
  77. Thomas, C.A., Jr., et al., *A miniature microelectrode array to monitor the bioelectric activity of cultured cells*. Exp Cell Res, 1972. **74**(1): p. 61-6.
  78. Keefer, E.W., et al., *Characterization of acute neurotoxic effects of trimethylolpropane phosphate via neuronal network biosensors*. Biosens Bioelectron, 2001. **16**(7-8): p. 513-25.
  79. Gubala, V., et al., *Point of care diagnostics: status and future*. Anal Chem, 2012. **84**(2): p. 487-515.
  80. Giaever, I., *The antibody-antigen reaction: a visual observation*. J Immunol, 1973. **110**(5): p. 1424-6.
  81. Jokerst, J.C., et al., *Development of a paper-based analytical device for colorimetric detection of select foodborne pathogens*. Analytical Chemistry, 2012. **84**(6): p. 2900-2907.
  82. Ishimatsu, R., et al., *An organic thin film photodiode as a portable photodetector for the detection of alkylphenol polyethoxylates by a flow fluorescence-immunoassay on magnetic microbeads in a microchannel*. Talanta, 2013. **117**: p. 139-145.
  83. Xiang, A., et al., *A simple and rapid capillary chemiluminescence immunoassay for quantitatively detecting human serum HBsAg*. Eur J Clin Microbiol Infect Dis, 2013. **32**(12): p. 1557-64.
  84. Clarence, H., *Biosensors, light scattering and enzymes as analytical tools*. Analytical Chemistry, 1993. **65**(22): p. 1001A-1004A.
  85. Yildirim, N., et al., *Aptamer-based optical biosensor for rapid and sensitive detection of 17beta-estradiol in water samples*. Environ Sci Technol, 2012. **46**(6): p. 3288-94.

- 
86. Lee, L.M., X. Cui, and C. Yang, *The application of on-chip optofluidic microscopy for imaging Giardia lamblia trophozoites and cysts*. Biomedical microdevices, 2009. **11**(5): p. 951-958.
  87. de Cesare, G., A. Nascetti, and D. Caputo, *Amorphous silicon p-i-n structure acting as light and temperature sensor*. Sensors, 2015. **15**(6): p. 12260.
  88. Vykoukal, D.M., et al., *Quantitative detection of bioassays with a low-cost image-sensor array for integrated microsystems*. Angew Chem Int Ed Engl, 2009. **48**(41): p. 7649-54.
  89. Liu, B.-F., H. Hisamoto, and S. Terabe, *Subsecond separation of cellular flavin coenzymes by microchip capillary electrophoresis with laser-induced fluorescence detection*. Journal of chromatography. A, 2003. **1021**(1-2): p. 201-207.
  90. Miyaki, K., et al., *Fabrication of an integrated PDMS microchip incorporating an LED-induced fluorescence device*. Anal Bioanal Chem, 2005. **382**(3): p. 810-6.
  91. Charwat, V., et al., *Monitoring dynamic interactions of tumor cells with tissue and immune cells in a lab-on-a-chip*. Analytical Chemistry, 2013. **85**(23): p. 11471-11478.
  92. Charwat, V., et al., *Standardization of microfluidic cell cultures using integrated organic photodiodes and electrode arrays*. Lab Chip, 2013. **13**(5): p. 785-97.
  93. Robinson, G., *The commercial development of planar optical biosensors*. Sensors and Actuators B: Chemical, 1995. **29**(1): p. 31-36.
  94. Schmidt, H., *On-chip micro-optical detection*, in *Encyclopedia of Microfluidics and Nanofluidics*, D. Li, Editor. 2013, Springer US: Boston, MA. p. 1-8.
  95. Gai, H., Y. Li, and E.S. Yeung, *Optical detection systems on microfluidic chips*. Top Curr Chem, 2011. **304**: p. 171-201.
  96. Dey, D. and T. Goswami, *Optical biosensors: a revolution towards quantum nanoscale electronics device fabrication*. Journal of Biomedicine and Biotechnology, 2011. **2011**: p. 7.
  97. Burgi, L., et al., *In building european OLED infrastructure*. 1st ed.; SPIE: Cambridge, U.K. . Vol. 5961. 2005. 596104-34.
  98. Fang, Y., *Label-free drug discovery*. Frontiers in Pharmacology, 2014. **5**: p. 52.
  99. Wilson, J.D., et al., *Light scattering from intact cells reports oxidative-stress-induced mitochondrial swelling*. Biophysical Journal, 2005. **88**(4): p. 2929-2938.
  100. Sandell, J.L. and T.C. Zhu, *A review of in-vivo optical properties of human tissues and its impact on PDT*. Journal of Biophotonics, 2011. **4**(11-12): p. 773-787.
  101. Tuchin, V., *Tissue optics: light scattering methods and instruments for medical diagnosis*. Society of Photo-Optical Instrumentation Engineers, 2007.
  102. Farhata, G., et al., *Measuring intracellular motion using dynamic light scattering with optical coherence tomography in a mouse tumor model* Proceedings of SPIE - The International Society for Optical Engineering, 2012.
  103. Farhat, G., et al., *Detecting apoptosis using dynamic light scattering with optical coherence tomography*. J Biomed Opt, 2011. **16**(7): p. 070505.
  104. Chen, C.-S., et al., *Determine the quality of human embryonic stem colonies with laser light scattering patterns*. Biological Procedures Online, 2013. **15**(1): p. 2.
  105. Bae, E., et al., *Modeling light propagation through bacterial colonies and its correlation with forward scattering patterns*. J Biomed Opt, 2010. **15**(4): p. 045001.
  106. Mourant, J.R., et al., *Mechanisms of light scattering from biological cells relevant to noninvasive optical-tissue diagnostics*. Applied Optics, 1998. **37**(16): p. 3586-3593.
  107. Myers, F.B. and L.P. Lee, *Innovations in optical microfluidic technologies for point-of-care diagnostics*. Lab Chip, 2008. **8**(12): p. 2015-31.
  108. Kuswandi, B., et al., *Optical sensing systems for microfluidic devices: a review*. Anal Chim Acta, 2007. **601**(2): p. 141-55.



- 
109. Eddaoudi, M., *Characterization of Porous Solids and Powders: Surface Area, Pore Size and Density*. Journal of the American Chemical Society, 2005. **127**(40): p. 14117-14117.
  110. Emond, M.R. and J.D. Jontes, *Bead aggregation assays for the characterization of putative cell adhesion molecules*. J Vis Exp, 2014(92): p. e51762.
  111. Mercade-Prieto, R. and Z. Zhang, *Mechanical characterization of microspheres - capsules, cells and beads: a review*. J Microencapsul, 2012. **29**(3): p. 277-85.
  112. Calbeck, J.H. and H.R. Harner, *Particle size and distribution by sedimentation method*. Industrial & Engineering Chemistry, 1927. **19**(1): p. 58-61.
  113. Dunn, E.J., *Microscopic measurements for the determination of particle size of pigments and powders*. Industrial & Engineering Chemistry Analytical Edition, 1930. **2**(1): p. 59-62.
  114. Dilts, R.V., *Methods of separation: The sophomore analytical course*. Journal of Chemical Education, 1967. **44**(6): p. 313.
  115. Pratte, P., S. Cosandey, and C. Goujon-Ginglinger, *A scattering methodology for droplet sizing of e-cigarette aerosols*. Inhal Toxicol, 2016. **28**(12): p. 537-545.
  116. Ambrose, B.S., et al., *Student understanding of light as an electromagnetic wave: Relating the formalism to physical phenomena*. American Journal of Physics, 1999. **67**(10): p. 891-898.
  117. Youngquist, R.C., S. Carr, and D.E. Davies, *Optical coherence-domain reflectometry: a new optical evaluation technique*. Opt Lett, 1987. **12**(3): p. 158-60.
  118. *Propagation of Electromagnetic Waves: www.saroselectronics.com*.
  119. Dalrymple, R.A., J.T. Kirby, and P.A. Hwang, *Wave diffraction due to areas of energy dissipation*. Journal of Waterway, Port, Coastal, and Ocean Engineering, 1984. **110**(1): p. 67-79.
  120. Nickel, C., et al., *Dynamic light-scattering measurement comparability of nanomaterial suspensions*. Journal of Nanoparticle Research, 2014. **16**(2): p. 2260.
  121. *Light phenomenon: www.horiba.com*.
  122. *Scattering Vector: www.scienceinschool.org*.
  123. Gardiner, C., et al., *Measurement of refractive index by nanoparticle tracking analysis reveals heterogeneity in extracellular vesicles*. J Extracell Vesicles, 2014. **3**: p. 25361.
  124. Bohren, C.F. and D.R. Huffman, *Particles small compared with the wavelength*, in *Absorption and Scattering of Light by Small Particles*. 2007, Wiley-VCH Verlag GmbH. p. 130-157.
  125. *Direction of scattered light: www.hyperphysics.phy-astr.gsu.edu*.
  126. Born, M. and E. Wolf, *Principles of Optics*. 7th edn. (London: Pergamon) 2005.
  127. Hulst, H.C.v.d., *Light scattering by small particles*. Quarterly Journal of the Royal Meteorological Society, 1958. **84**(360): p. 198-199.
  128. Brevik, I., *Experiments in phenomenological electrodynamics and the electromagnetic energy-momentum tensor*. Phys. Rep., 1979. **52**: p. 133-201.
  129. Dienerowitz, M., M. Mazilu, and K. Dholakia, *Optical manipulation of nanoparticles: a review*. J. Nanophotonics, 2008. **2**(021875).
  130. Venugopalan, V., N.S. Nishioka, and B.B. Mikic, *The effect of CO2 laser pulse repetition rate on tissue ablation rate and thermal damage*. IEEE Trans Biomed Eng, 1991. **38**(10): p. 1049-52.
  131. Walsh, J.T., et al., *Pulsed CO2 laser tissue ablation: Effect of tissue type and pulse duration on thermal damage*. Lasers in Surgery and Medicine, 1988. **8**(2): p. 108-118.
  132. Chin, L.C.L., W.M. Whelan, and I.A. Vitkin, *Optical Fiber Sensors for Biomedical Applications*, in *Optical-Thermal Response of Laser-Irradiated Tissue*, J.A. Welch and J.C.M. van Gemert, Editors. 2011, Springer Netherlands: Dordrecht. p. 661-712.
  133. Brunet, C. and L.A. Rusch, *Invited Paper: Optical fibers for the transmission of orbital angular momentum modes*. Optical Fiber Technology, 2016. **31**: p. 172-177.

- 
134. Manna, E., et al., *Organic Photodetectors in Analytical Applications*. Electronics, 2015. **4**(3): p. 688.
  135. Tedde, S.F., et al., *Fully spray coated organic photodiodes*. Nano Letters, 2009. **9**(3): p. 980-983.
  136. Li, A., et al., *Influence of the intensity gradient upon HHG from free electrons scattered by an intense laser beam*. Applied Physics B, 2014. **117**(1): p. 95-101.
  137. Grigoropoulos, C.P., *Laser interactions with nanoparticles*, in *Transport in Laser Microfabrication: Fundamentals and Applications*. 2009, Cambridge University Press: Cambridge. p. 330-349.
  138. Bohren, C.F. and D.R. Huffman, *Absorption and scattering by a sphere*, in *Absorption and Scattering of Light by Small Particles*. 2007, Wiley-VCH Verlag GmbH. p. 82-129.
  139. Ng, B.L. and N.P. Carter, *Laser excitation power and the flow cytometric resolution of complex karyotypes*. Cytometry. Part A : The Journal of the International Society for Analytical Cytology, 2010. **77**(6): p. 585-588.
  140. Ponyavina, A.N. and V.G. Vereshchagin, *Concentration effects during coherent scattering by big size particles with density packing*. Journal of Applied Spectroscopy, 1984. **40**: p. 302-308.
  141. Wiederseiner, S., et al., *Refractive-index and density matching in concentrated particle suspensions: a review*. Experiments in Fluids, 2011. **50**(5): p. 1183-1206.
  142. Merek, E.L., *Estimating the size and concentration of unicellular microorganisms by light scattering*. Applied Microbiology, 1969. **17**(2): p. 219-221.
  143. Yao, G. and L.V. Wang, *Propagation of polarized light in turbid media: simulated animation sequences*. Optics Express, 2000. **7**(5): p. 198-203.
  144. Preisig, P., *What makes cells grow larger and how do they do it? Renal hypertrophy revisited*. Exp Nephrol, 1999. **7**(4): p. 273-83.
  145. Heinze, B.C. and J.Y. Yoon, *Nanoparticle immunoagglutination Rayleigh scatter assay to complement microparticle immunoagglutination Mie scatter assay in a microfluidic device*. Colloids Surf B Biointerfaces, 2011. **85**(2): p. 168-73.
  146. Long, G.L. and J.D. Winefordner, *Limit of detection a closer look at the IUPAC definition*. Analytical Chemistry, 1983. **55**(7): p. 712A-724A.
  147. Maydeu-Olivares, A. and C. García-Forero, *Goodness-of-fit testing*. International Encyclopedia of Education (Third Edition), ed. E. Baker and B. McGaw. 2010, Oxford: Elsevier. 190-196.
  148. Bewick, V., L. Cheek, and J. Ball, *Statistics review 7: Correlation and regression*. Critical Care, 2003. **7**(6): p. 451-459.
  149. *Scattering*: [www.quantummechanics.ucsd.edu/ph130a/130\\_notes/node441.html](http://www.quantummechanics.ucsd.edu/ph130a/130_notes/node441.html).
  150. du Prel, J.-B., et al., *Confidence Interval or P-Value?: Part 4 of a Series on Evaluation of Scientific Publications*. Deutsches Ärzteblatt International, 2009. **106**(19): p. 335-339.
  151. Omar, A.F. and M.Z. Matjafri, *Turbidimeter design and analysis: a review on optical fiber sensors for the measurement of water turbidity*. Sensors (Basel), 2009. **9**(10): p. 8311-35.
  152. Bolie, V.W., *Theory of scattering from a nearly transparent anomaly*. Applied Scientific Research, Section A, 1957. **6**(1): p. 422-428.
  153. Davis, M.A., S.M. Kazmi, and A.K. Dunn, *Imaging depth and multiple scattering in laser speckle contrast imaging*. J Biomed Opt, 2014. **19**(8): p. 086001.
  154. *Jurkat Cell Diameter*: [www.bionumbers.hms.harvard.edu/](http://www.bionumbers.hms.harvard.edu/).
  155. Formigli, L., et al., *Aponecrosis: morphological and biochemical exploration of a syncretic process of cell death sharing apoptosis and necrosis*. J Cell Physiol, 2000. **182**(1): p. 41-9.

- 
156. Ratajczak, J., et al., *Membrane-derived microvesicles: important and underappreciated mediators of cell-to-cell communication*. *Leukemia*, 2006. **20**(9): p. 1487-1495.
  157. Freitas, J.R.A., *Nanomedicine: Basic Capabilities*. 1999. **1**.
  158. Han, M.G., et al., *Narrow-Band Organic Photodiodes for High-Resolution Imaging*. *ACS Applied Materials & Interfaces*, 2016. **8**(39): p. 26143-26151.
  159. Tobias, R.K., et al., *Thermorheology of living cells—impact of temperature variations on cell mechanics*. *New Journal of Physics*, 2013. **15**(4): p. 045026.
  160. Dogu, S. and W. Oppermann, *Influence of observation temperature on light scattering of poly-N-isopropylacrylamide hydrogels*. *Soft Matter*, 2012. **8**(9): p. 2705-2713.
  161. Anson, M., *Temperature dependence and arrhenius activation energy of F-actin velocity generated in vitro by skeletal myosin*. *Journal of Molecular Biology*, 1992. **224**(4): p. 1029-1038.
  162. Kawaguchi, K. and S. Ishiwata, *Temperature dependence of force, velocity, and processivity of single kinesin molecules*. *Biochem Biophys Res Commun*, 2000. **272**(3): p. 895-9.
  163. Matsuo, E.S., et al., *Origin of structural inhomogeneities in polymer gels*. *Macromolecules*, 1994. **27**(23): p. 6791-6796.
  164. Shibayama, M., S.-i. Takata, and T. Norisuye, *Static inhomogeneities and dynamic fluctuations of temperature sensitive polymer gels*. *Physica A: Statistical Mechanics and its Applications*, 1998. **249**(1–4): p. 245-252.
  165. Latimer, P., *Light scattering vs. microscopy for measuring average cell size and shape*. *Biophysical Journal*, 1979. **27**(1): p. 117-126.
  166. Bettahalli, N.M., et al., *Development of multilayer constructs for tissue engineering*. *J Tissue Eng Regen Med*, 2014. **8**(2): p. 106-19.
  167. Moosmuller, H. and W.P. Arnott, *Particle optics in the Rayleigh regime*. *J Air Waste Manag Assoc*, 2009. **59**(9): p. 1028-31.
  168. Nurse, P., *Genetic control of cell size at cell division in yeast*. *Nature*, 1975. **256**(5518): p. 547-51.
  169. Gorczyca, W., M.R. Melamed, and Z. Darzynkiewicz, *Programmed death of cells (apoptosis)*. *Patol Pol*, 1993. **44**(3): p. 113-9.
  170. Agathocleous, M. and W.A. Harris, *Metabolism in physiological cell proliferation and differentiation*. *Trends in Cell Biology*. **23**(10): p. 484-492.
  171. Marina, O.C., C.K. Sanders, and J.R. Mourant, *Effects of acetic acid on light scattering from cells*. *Journal of Biomedical Optics*, 2012. **17**(8): p. 085002.
  172. Hand, C.W. and H.L. Blewitt, *Acid-base chemistry*. 1986, New York; London: Macmillan ; Collier Macmillan.
  173. *Base Dissociation Constant: [www.chemguide.co.uk](http://www.chemguide.co.uk)*.
  174. Deck, J.C., *Strong and weak acids and bases*. *Journal of Chemical Education*, 1979. **56**(12): p. 814.
  175. Preiss, J.W., *The influence of irradiated basic proteins on the light-scattering properties of ribonucleic acid: a radiation protection study*. *Radiat Res*, 1964. **22**: p. 564-76.
  176. Wriedt, T., *Mie theory: A review*, in *The Mie Theory: Basics and Applications*, W. Hergert and T. Wriedt, Editors. 2012, Springer Berlin Heidelberg: Berlin, Heidelberg. p. 53-71.
  177. Griffiths, J.B., *Serum and growth factors in cell culture media—an introductory review*. *Dev Biol Stand*, 1987. **66**: p. 155-60.
  178. Wang, W. and S.A. Sande, *A dynamic light scattering study of hydrogels with the addition of surfactant: a discussion of mesh size and correlation length*. *Polym J*, 2015. **47**(4): p. 302-310.
  179. *NIH-3T3 Diameter: [www.bionumbers.hms.harvard.edu/](http://www.bionumbers.hms.harvard.edu/)*.

180. Marina, O.C., C.K. Sanders, and J.R. Mourant, *Correlating light scattering with internal cellular structures*. Biomed Opt Express, 2012. **3**(2): p. 296-312.
181. Mourant, J.R., T.M. Johnson, and J.P. Freyer, *Characterizing mammalian cells and cell phantoms by polarized backscattering fiber-optic measurements*. Appl Opt, 2001. **40**(28): p. 5114-23.
182. Wiemerslage, L. and D. Lee, *Quantification of mitochondrial morphology in neurites of dopaminergic neurons using multiple parameters*. J Neurosci Methods, 2016. **262**: p. 56-65.
183. Beauvoit, B., T. Kitai, and B. Chance, *Contribution of the mitochondrial compartment to the optical properties of the rat liver: a theoretical and practical approach*. Biophys J, 1994. **67**(6): p. 2501-10.
184. Bohmer, R.M., E. Bandala-Sanchez, and L.C. Harrison, *Forward light scatter is a simple measure of T-cell activation and proliferation but is not universally suited for doublet discrimination*. Cytometry A, 2011. **79**(8): p. 646-52.
185. Choi, B.H., et al., *Inhibition of blood vessel formation by a chondrocyte-derived extracellular matrix*. Biomaterials, 2014. **35**(22): p. 5711-20.
186. Jeong, G.S., et al., *Microfluidic assay of endothelial cell migration in 3D interpenetrating polymer semi-network HA-Collagen hydrogel*. Biomed Microdevices, 2011. **13**(4): p. 717-23.
187. Clair, L.O., et al., *Quantification of cell migration and invasion using the incucyte™ chemotaxis assay*. ESSEN Bioscience.

# Curriculum Vitae

## Personal Details:

Name: **Bilal FAROOQ**  
Academic title: B.Sc. M.Sc. M.Phil. Physics  
Date and place of birth: 20<sup>th</sup> April 1984, Pakistan  
Address: 1210 Vienna, Austria  
E-Mail: bf\_bilal\_farooq@yahoo.com

## Academic Qualification:

03/2014 - 12/2016 **Master's degree** in Biomedical Engineering  
Technical University of Vienna, Austria  
**Thesis:** Characterization of Laser Scattering Detection System for Microfluidic 3D Cell Cultures

09/2008 - 10/2010 **Master of Philosophy** in Physics  
Quaid-i-Azam University, Islamabad, Pakistan  
**Thesis:** Information Transmission through an Unmodulated Spin Chain Channel

01/2006 - 01/2008 **Master of Science** in Physics  
Quaid-i-Azam University, Islamabad, Pakistan

07/2003 - 07/2005 **Bachelor of Science** in Mathematics & Physics  
Punjab University, Lahore, Pakistan

## Professional Experience:

06/2016 - 11/2016 **Researcher** - Technical University of Vienna, Austria  
**Project:** Establishing a microfluidics system for assessment of light scattering in cells

05/2015 - 12/2016 **Researcher** - Ludwig Boltzmann Institute for Experimental and Clinical Traumatology, Vienna, Austria  
**Project:** Preparation of cartilage samples with CO<sub>2</sub> laser

07/2015 - 09/2015 **Research Internee** - Nuclear Medicine, Oncology and Radiotherapy Institute, Islamabad, Pakistan  
**Project:** Radioactive treatment and diagnostics

10/2014 - 03/2015 **Research Internee** - Institute for Applied Physics, Technical University of Vienna, Austria  
**Master project:** Influence of femtosecond laser pulses on the porosity of gelatine

07/2013 - 03/2014 **Research Internee** - AKH, Centre for Medical Physics and Biomedical Engineering, Vienna, Austria

04/2011 - 06/2013	<b>Project:</b> Optical coherence tomography <b>Research Associate</b> - Department of Physics, COMSATS University, Islamabad, Pakistan <b>Project:</b> Autler-Townes quadruplet spectroscopy & Tripartite entanglement generation using cavity-QED
07/2009 - 07/2010	<b>Research Associate</b> - Quaid-i-Azam University, Islamabad, Pakistan
07/2009 - 07/2010	<b>Research Internee</b> - National Physical and Standard Laboratory (PCSIR), Islamabad, Pakistan <b>Project:</b> Temperature and pressure calibration
09/2005 - 03/2006	<b>Physics and Mathematics Teacher</b> - House of Secondary Education, Islamabad, Pakistan
06/2005 - 09/2005	<b>Internee:</b> Department of Customer Service - MOBILINK- Pakistan Mobile Company

### **Publications:**

1. Nathala C.S.R., Ajami A., Husinsky W., **Farooq B.**, Kudryashov S.I., Daskalova A., Bliznakova I., Assion A., **(2016)**, Ultrashort laser pulse ablation of copper, silicon and gelatin: effect of the pulse duration on the ablation thresholds and the incubation coefficients, *Applied Physics A, Materials Science and Processing*.
2. Leitgeb R.A., Blatter C., Grajciar B., **Farooq B.**, **(2014)**, Reliable Orientation Independent Pulsatile Retinal Flow Assessment with Doppler OCT, *The Association for Research in Vision and Ophthalmology*.
3. **Farooq B.**, **(2013)**, Autler-Townes quadruplet spectroscopy, *Canadian Journal of Physics*, 91(10).
4. **Farooq B.**, Tahira R., Ikram M., **(2012)**, Tripartite entanglement generation using cavity-QED and its dynamics in dissipative environments, *Journal of Modern Optics*, 59(11).

### **Special Skills:**

Languages:	<b>German</b> - basic <b>English</b> - written and spoken <b>Urdu</b> - Native language
PC/ EDV:	Advanced user (MS-Office, AutoCAD, Matlab, GraphPad, Origin, Datalab, Mathematica, ScientificWorkplace) Certificate in Graphic Designing